OUKA
Osaka University Knowledge Archive

Title	Ligand-Field Theoretical Studies on Magnetic Properties of Manganese and Cobalt Mononuclear Complexes
Author(s)	Baba, Haruyuki
Citation	大阪大学, 2012, 博士論文
Version Type	VoR
URL	https://hdl.handle.net/11094/26862
rights	
Note	

Osaka University Knowledge Archive : OUKA

https://ir.library.osaka-u.ac.jp/

Osaka University

博 15736

Ligand-Field Theoretical Studies on Magnetic Properties of Manganese and Cobalt Mononuclear Complexes

HARUYUKI BABA

Division of Applied Chemistry

Graduate School of Engineering

Osaka University

2011

Ligand-Field Theoretical Studies on Magnetic Properties of Manganese and Cobalt Mononuclear Complexes

(マンガンおよびコバルト単核錯体の磁性の配位子場理論による研究)

HARUYUKI BABA

Division of Applied Chemistry

Graduate School of Engineering

Osaka University

2011

Preface

The study presented in this dissertation was carried out under the guidance of Associate Professor Motohiro Nakano at Division of Applied Chemistry, Graduate School of Engineering, Osaka University.

The objective of the present study is to fully analyze the physical properties of a series of mononuclear manganese(III) and cobalt(II) complexes on the basis of ligand-field theory aiming to provide a way to regulate electronic states of single metal centers as functional synthons in construction of higher assembled systems, *e.g.* nanomagnets. The author hopes that these results and findings contribute to the rational design of the paramagnetic polynuclear complexes.

Haruyuki Baba

Division of Applied Chemistry

Graduate School of Engineering

Osaka University

2-1 Yamadaoka, Suita, Osaka, 565-0871, JAPAN

March 2012

Contents

Part III. Magnetic and Spectroscopic Characterizations of Cobalt(II/III) Complexes Consisting of Soft-Scorpionate Ligands

Part I. General Introduction

Chapter 1. Background

Self-assembled metal complexes and their functionalities have been extensively studied during the past decades and new field of metal-organic framework (MOF) is now opening practical applications of nanopore space as functional adsorbents, hydrogen-storage materials, specific catalysts, guest-dependent magnets, and so on [1]. In order to develop and improve functionalities of metal-assembled systems, it is essential to get better understanding of single-metal centers as functional elements. In the present dissertation, single-metal centers for assembling nanomagnets including single-molecule magnets (SMMs) and single-chain magnets (SCMs) were closely investigated so as to give criteria in rational design of magnetic anisotropy and electronic states via chemical modification of coordination environments.

Single-molecule magnets are discrete molecules, which behave as molecular-size permanent magnets at low temperature, and most of them belong to a class of paramagnetic polynuclear complexes [2]. Potential huge capacity of magnetic information storage attracts a lot of attention and SMM is expected to bring about nanodevice applications such as quantum computer and molecular memory [3]. The origin of SMM behavior is the combination of large magnetic anisotropy and giant spin quantum number. Among SMMs consisting of first-row transition metal ions, manganese(III) and cobalt(II) ions are most commonly used owing to their magnetic anisotropy. The first SMM was a dodecanuclear manganese acetate complex discovered at the beginning of the 1990s [4]. The polynuclear manganese-based SMMs are most popular and the magnetic anisotropy is attributable to the Jahn-Teller stretched octahedral manganese(III) centers of high-spin $(3d)^4$ configuration. On the other hand, the first cobalt-based SMM was reported in 2002 and consists of four cobalt(II) ions which possess octahedral coordination environment with high-spin $(3d)^7$ electron configuration [5].

The orbital angular momentum in an octahedral cobalt(II) ion is not fully quenched and causes large magnetic anisotropy. In this manner, there are many factors affecting magnetic anisotropy in single metal ions [6], and it is worthwhile to elucidate the electric structure of mononuclear complexes and the associated magnetic anisotropies in order to grasp the character of synthons for SMMs [7].

In the next chapter, theoretical prerequisites including outline of ligand-field theory and its AOM (angular-overlap model) formulation are summarized, followed by a short chapter on the objective and composition of the dissertation.

Chapter 2. Fundamentals of Electronic States of Transition-Metal Complexes

In order to understand magnetic properties of transition metal complex, it is necessary to obtain the wavefuntions and energies by solution of following Schrödinger equation:

$$\hat{\boldsymbol{H}}\psi = \mathrm{E}\psi \tag{I-1}$$

Then, the complete Hamiltonian operator is expressed as:

$$\hat{\boldsymbol{H}} = \sum_{i=1}^{n}\left[-\frac{\hbar^2}{2m}\nabla^2 - \frac{Ze^2}{4\pi\varepsilon_0 r_i}\right] + \sum_{i<j}^{n}\frac{e^2}{r_{ij}} + \sum_{i=1}^{n}\zeta(r_i)\boldsymbol{l}_i\cdot\boldsymbol{s}_i + \boldsymbol{V}_{\mathrm{cf}} + \boldsymbol{\mu}\cdot\boldsymbol{H} \tag{I-2}$$

where, the first term is free ion Hamiltonian including the kinetic energy of electrons and electrostatic interaction of the electrons with nuclei, the second term is interelectronic repulsion, the third term is spin-orbit coupling, the fourth term is ligand-field potential, and the fifth and last terms are interaction of electron and magnetic field. Here $\hbar = h/2\pi$, h is Planck constant, m is electron mass, Z is charge of the nucleus, e is elementary charge, and ε_0 is vacuum permittivity. It is very complicated problem to solve the equation. Now, perturbation method is employed to the approximate solution. As first step, the unperturbed Hamiltonian operator for free ions is featured. Next, the spin-orbit coupling, crystal field potential, spin-orbit coupling, and the effect of magnetic field as small perturbation are treated. Then, related phenomena, theory, and methods are introduced sequentially.

2.1. Genaral Hamiltonian for Free Ions [8]

The unperturbed Hamiltonian for free ions is expressed as:

$$\hat{\boldsymbol{H}} = \sum_{i=1}^{n}\left[-\frac{\hbar^2}{2m}\nabla^2 - \frac{Ze^2}{4\pi\varepsilon_0 r_i}\right] \tag{I-3}$$

using spherical polar coordinates, the wavefunctions are expressed as:

$$\Psi_{nlm} = R_{nl}(r)Y_l^m(\theta,\varphi) \tag{I-4}$$

where, $R_{nl}(r)$ is the radial distribution function and $Y_l^m(\theta, \varphi)$ the spherical harmonics. Here, n is the principal quantum number, l the quantum number of orbital angular momentum of the electron, and m the magnetic quantum number. n is a positive integer, l takes on integral value from 0 to n-1, and m takes on integral value from $-l$ to l. the orbital multiplicity for $3d$ orbitals is $2l+1 = 5$, and therefore angular dependent part, spherical harmonic $Y_l^m(\theta, \varphi)$ corresponding to this multiplicity is:

$$\begin{aligned} Y_2^0(\theta,\varphi) &= \sqrt{\frac{1}{2\pi}}\cdot\sqrt{\frac{5}{8}}\left(3\cos^2\theta - 1\right) \\ Y_2^{\pm1}(\theta,\varphi) &= \sqrt{\frac{1}{2\pi}}\cdot\sqrt{\frac{15}{4}}\sin\theta\cos\theta\cdot e^{\pm\varphi} \\ Y_2^{\pm2}(\theta,\varphi) &= \sqrt{\frac{1}{2\pi}}\cdot\sqrt{\frac{15}{16}}\sin^2\theta\cdot e^{\pm i2\varphi} \end{aligned} \tag{I-5}$$

From Next section, the further behavior of multielectron system is explained and the splitting of $3d$-orbitals in the case of transition ion placed in a crystal field described later.

2.2. Russell-Saunders Coupling in Free Ions [8]

The energy levels for free ion of n electron system are determined by the total orbital angular momentum quantum number L and total spin angular quantum number S. L is the largest sum of orbital angular momentum m_l of individual electrons, and zero or a positive integer. S is the largest sum of spin angular momentum m_l of individual electrons, and zero or a positive integer or half-integer. The values M_L and M_S, which are allowed for L and S, respectively, are:

$$\begin{aligned} M_L &= L,(L-1),\cdots,-L \\ M_s &= S,(S-1),\cdots,-S \end{aligned}$$

A state for specific L and S is defined as term $^{(2S+1)}$X, where X corresponds to L as follows:

L	0	1	2	3	4	5	⋯
X	S	P	D	F	G	H	⋯

The quantity $(2S+1)$ is multiplicity of the term. Here, it is necessary to explain the stability of the term when the energies levels for each term are ordered. Thus, the energy for interelectronic repulsion is considered.

2.3. Interelectronic Repulsion [9-10]

In order to solve interelectronic interactions for two electrons, matrix elements of following type are evaluated:

$$\langle ab|\frac{e^2}{r_{12}}|cd\rangle \tag{I-6}$$

Here, a, b, c, and d refer to each population of d-orbitals. Thus, $1 / r_{12}$ is:

$$\frac{1}{r_{12}} = \sum_{n=0}^{\infty}\sum_{m=-n}^{n}\frac{4\pi}{2n+1}\cdot\frac{r_<^n}{r_>^{n+1}}\cdot Y_n^m(\theta_1,\varphi_1)\cdot Y_n^{m*}(\theta_2,\varphi_2) \tag{I-7}$$

where $r_>$ denotes the shorter distance from the origin to the points i and j. The spherical harmonic is expanded as:

$$Y_l^m(\theta,\varphi) = \sqrt{\frac{1}{2\pi}}P_l^m(\cos\theta)e^{im\varphi} \tag{I-8}$$

Here, $P_l^m(\cos\theta)$ is associated Legendre function, and the two functions for two electron system are defined as:

$$\begin{aligned} c^n(lm_l,l'm_l') &= \sqrt{\frac{4\pi}{2n+1}}\int_0^{\infty}P_n^{m_l-m_l'}(\cos\theta)P_n^{m_l}(\cos\theta)P_n^{m_l'}(\cos\theta)\sin\theta d\theta \\ R^n(abcd) &= e^2\int_0^{\infty}\int_0^{\infty}\frac{r_<^n}{r_>^{n+1}}R_a^1R_b^2R_c^1R_d^2r_1^2r_2^2dr_1dr_2 \end{aligned} \tag{I-9}$$

Using these functions the matrix elements for interelectronic repulsion is expressed as:

$$\begin{aligned} \langle ab|\frac{e^2}{r_{12}}|cd\rangle = {} & \delta(m_s^a,m_s^c)\delta(m_s^b,m_s^d)\delta(m_s^a,m_s^c)\delta(m_l^a+m_l^b,m_l^c+m_l^d) \\ & \sum_{n=0}^{\infty}c^n(l^am_l^a,l^cm_l^c)c^n(l^bm_l^d,l^bm_l^d)R^n(abcd) \end{aligned} \tag{I-10}$$

Because the direct products of two d-orbitals do not have fifth or more rotational symmetry, the sum

over the fifth or more n is zero and reduced to $n = 0, 2, 4$.

When $ab = cd$, the matrix element include two important functions:

$$\langle ab|\frac{e^2}{r_{12}}|ab\rangle = \langle a(1)b(2)|\frac{e^2}{r_{12}}|a(1)b(2)\rangle - \langle a(1)b(2)|\frac{e^2}{r_{12}}|b(1)a(2)\rangle = J(a,b) - K(a,b) \tag{I-11}$$

where $J(a, b)$ is a Coulomb integral and $K(a, b)$ is an exchange integral. Using these integrals total energy of an n electron determinant is expressed as:

$$E(\Psi) = \sum_n h_n + \sum_{m<n} J_{m,n} - \sum_{m<n} K_{m,n}\delta(s_m, s_n) \tag{I-12}$$

Where h_n is one electron energy and the second and third terms correspond to the energy of interelectronic repulsion. In order to evaluate these two integrals, they are regarded as radial parameters and the term of radial function is replaced as:

$$F^n = R^n(abcd) \tag{I-13}$$

Furthermore these parameters are expressed as:

$$\begin{aligned} &F_0 = F^0, F_2 = F^2/49, F_4 = F^4/441 \\ &A = F_0 - 49F_4, B = F_2 - 5F_4, C = 35F_4 \end{aligned} \tag{I-14}$$

Here, F_0, F_2 and F_4 are Condon-Shortley parameters and A, B, and C are Racah parameters. Racah parameters are most useful because the energy level separation between the same spin multiplicities for d-electron configuration is expressed as a function of the parameter B alone.

In the case of two or more d-electrons, it is necessary to derive resultant angular momentum for all electrons. For this, following couplings are considered:

$$\boldsymbol{s}_i \cdot \boldsymbol{s}_j, \quad \boldsymbol{l}_i \cdot \boldsymbol{l}_j, \quad \boldsymbol{s}_i \cdot \boldsymbol{l}_i$$

When the coupling of spin angular momenta above is the largest value, the term is most stable and each spin becomes parallel (Hund's first rule). When the coupling of orbital angular momenta above is the largest value, the term is also most stable and the orbital vectors become parallel (Hund's second rule). The spin-orbit coupling above explained later. Here total angular momentum quantum number J about $(3d)^n$ electron configuration is expressed as the vector sum of L and S and this

coupling is called Russell-Saunders coupling or *LS* coupling. In the case of Russell-Saunders coupling, these resultant angular momenta are determined under relative magnitude:

$$\boldsymbol{s}_i \cdot \boldsymbol{s}_j > \boldsymbol{l}_i \cdot \boldsymbol{l}_j > \boldsymbol{s}_i \cdot \boldsymbol{l}_i$$

According to these procedure and Pauli exclusion principle, the several terms of free ion are determined.

2.4. Spin-Orbit Coupling [8,11]

In order to describe energy level of spin-orbit coupling for one-electron system, a new quantum number j is defined as:

$$\boldsymbol{j} = \boldsymbol{s} + \boldsymbol{l} \tag{I-15}$$

The operator of spin-orbit coupling for one electron system is expressed as:

$$\zeta(r_i)\boldsymbol{l}_i \cdot \boldsymbol{s}_i$$

where $\zeta(r_i)$ is the radial component of the wavefunction. The energy $E(n, l, s, j)$ of spin-orbit coupling is described as:

$$E(n,l,s,j) = \frac{\zeta}{2}\left[j(j+1) - l(l+1) - s(s+1)\right] \tag{I-16}$$

where ζ is spin-orbit coupling constant for one electron and a positive value. The operator of spin-orbit coupling for multielectron system is given by the sum of operator for one-electron system:

$$\hat{\boldsymbol{H}} = \sum_{i=1}^{n} \zeta(r_i)\hat{\boldsymbol{l}}_i \cdot \hat{\boldsymbol{s}}_i \tag{I-17}$$

The energy $E(J, L, S)$ of spin-orbit coupling for muiltielectron system is described as:

$$E(J,L,S) = \frac{\zeta}{2}\left[J(J+1) - L(L+1) - S(S+1)\right] \tag{I-18}$$

where $J = L+S, L+S-1, \cdots, |L-S|$ and the energy separation between J and $(J+1)$ levels are given by $\lambda(J+1)$. λ and ζ are related :

$$\lambda = \pm\frac{\zeta}{2S} \tag{I-19}$$

ζ is positive value while the sign of λ changes depending on *d*-electron configuration. When *d*-electrons fill into the shells more than half full, λ is negative value. For this, the order of energy-level splitting for d^n configuration is inverted against d^{10-n} configuration.

2.5. Effect of Crystal Field [8,12]

Considering the crystal field of MX_6 type complexes, ligand X^- can be regarded as negative point charge, $-Z'e$. The electrons surrounding a central atom are subjected to V_{cf} electric field from the six point charges. The result given by:

$$V_{cf} = \sum_{i=1}^{6} v_i = \sum_{i=1}^{6} \frac{Z'e^2}{4\pi\varepsilon_0 r_{ij}} \tag{I-20}$$

Here, r_{ij} indicates the distance from the *i*-th charge to the point (x,y,z). This field V_{cf} is Coulomb field from surrounding ions in ionic crystal, and corresponds to the part of electron-nucleus or electron-electron interactions. In preceding section, the eigenfunctions of the unperturbed Hamiltonian for free ions were obtained. When this complex possesses octahedral structure, the crystal field is represented as V_{oct}. Then, the energy of the crystal field contributing *d*-orbitals is expanded as following spherical harmonic when it is regarded as perturbation to the free ions:

$$V_{oct} = \frac{Z'e^2}{4\pi\varepsilon_0} \sum_{n=0}^{\infty} \sum_{m=-n}^{n} \frac{4\pi}{2n+1} \cdot \frac{r_<^n}{r_>^{n+1}} \cdot Y_n^m(\theta_j,\varphi_j) \cdot Y_n^{m*}(\theta_i,\varphi_i) \tag{I-21}$$

where $r_>$ denotes the electron-nucleus distance and $r_<$ denotes electron-ligand distance. For simplicity the two distances $r_>$ and $r_<$ replaced to r and a, individually, and each spherical harmonics were expressed as:

$$q_{nm} = \sqrt{\frac{4\pi}{2n+1}} \frac{Z'e}{4\pi\varepsilon_0 a^{n+1}} Y_n^{m*}(\theta_i, \varphi_i)$$
$$C_m^n = \sqrt{\frac{4\pi}{2n+1}} Y_n^m(\theta, \varphi) \tag{I-22}$$

Thus Eq. I-21 is expressed as:

$$V_{\text{oct}} = \sum_{n=0}^{\infty} \sum_{m=-n}^{n} r^k q_{nm} C_m^n \tag{I-23}$$

The polar coordinates (θ_i, φ_i) of six charges are ($\pi/2$, 0), ($\pi/2$, $\pi/2$), (0, φ), ($\pi/2$, π), ($\pi/2$, $3\pi/2$), and (π, φ), individually. Because V_{oct} belongs to a_{1g} representation of O_h group, the spherical harmonics of expansion also belongs to a_{1g} and so n is zero or even. Furthermore, $Y_2^m(\theta, \varphi)$ with odd n is not a_{1g} representation. Thus, Eq. I-21 is:

$$V_{\text{oct}}(r,\theta,\varphi) = \frac{3Z'e^2}{2\pi\varepsilon_0 a} + \frac{7Z'e^2r^4}{8\pi\varepsilon_0 a}\left[C_0^4 + \sqrt{\frac{5}{14}}\left(C_4^4 + C_{-4}^4\right)\right] + \frac{3Z'e^2r^6}{16\pi\varepsilon_0 a}\left[C_0^6 + \sqrt{\frac{7}{2}}\left(C_4^6 + C_{-4}^6\right)\right] + \cdots \tag{I-24}$$

The first term increases all orbital energy for free ions and the second or later terms give the crystal-field splitting. Because the direct products of two d-orbitals do not have fifth or more rotational symmetry, the fifth or more integral of $\langle d|\hat{V}_{\text{oct}}|d\rangle$ is zero. For simplicity, the mixture of the wavefunctions which has distinct n each other is neglected, and the wavefunction in V_{oct} is expressed as a linear combination of $3d$ orbitals (φ_{32m}):

$$\varphi = \sum_{m=-2}^{2} a_m \varphi_{32m} \tag{I-25}$$

V_{oct} is regarded as perturbation for the Hamiltonian of Eq. I-3 and substituted to the following equation:

$$E = \langle \varphi | \hat{\boldsymbol{H}} + \hat{V}_{\text{oct}} | \varphi \rangle \tag{I-26}$$

With variation method about a_m, the following simultaneous equation is obtained:

$$(\varepsilon_3 - E)a_m + \sum_{m'=-2}^{2} \langle m|\hat{V}_{\text{oct}}|m'\rangle a_{m'} = 0 \tag{I-27}$$

In order to solve the determinant from this equation, the following elements are displaced:

$$\begin{aligned}
\langle 2|\hat{V}_{\text{oct}}|2\rangle &= \langle -2|\hat{V}_{\text{oct}}|-2\rangle = Dq \\
\langle 1|\hat{V}_{\text{oct}}|1\rangle &= \langle -1|\hat{V}_{\text{oct}}|-1\rangle = -4Dq \\
\langle 0|\hat{V}_{\text{oct}}|0\rangle &= 6Dq \\
\langle 2|\hat{V}_{\text{oct}}|-2\rangle &= \langle -2|\hat{V}_{\text{oct}}|2\rangle = 5Dq
\end{aligned} \tag{I-28}$$

Here,

$$\begin{aligned}
D &= \frac{35Z'e^2}{16\pi\varepsilon_0 a^5} \\
q &= \frac{2e^2\overline{r^4}}{105}
\end{aligned} \tag{I-29}$$

$\overline{r^4}$ is the mean fourth power radius for the $3d$ radial function $R_{3d}(r)$. The determinant from Eq. I-27 is expressed as:

$$\begin{vmatrix}
\varepsilon_3 + Dq - E' & 0 & 0 & 0 & 5\text{Dq} \\
0 & \varepsilon_3 - 4Dq - E' & 0 & 0 & 0 \\
0 & 0 & \varepsilon_3 + 6Dq - E' & 0 & 0 \\
0 & 0 & 0 & \varepsilon_3 - 4Dq - E' & 0 \\
5\text{Dq} & 0 & 0 & 0 & \varepsilon_3 + Dq - E'
\end{vmatrix} = 0 \tag{I-30}$$

Here,

$$E' = E - \frac{3Z'e^2}{2\pi\varepsilon_0 a} \tag{I-31}$$

This determinant can be easily reduced to a 2-by-2 determinant and three 1-by-1 determinants, and two eigenvalues $\varepsilon_3+\varepsilon_M+6\text{Dq}$ and $\varepsilon_3+\varepsilon_M-4\text{Dq}$ ($\varepsilon_M = 3Z'e^2/2\pi\varepsilon_0 a$) are obtained. The former eigenvalue is doubly degenerated and the latter is triply degenerated. As a result, the five d-orbitals which split into t_{2g} and e_g-orbitals ($10Dq$) are obtained:

$$
\begin{aligned}
e_g : d_{z^2} &= \varphi_{320} = R_{32}(r)\sqrt{\frac{5}{16\pi}}\left(3\cos^2\theta - 1\right) \\
d_{x^2-y^2} &= \frac{1}{\sqrt{2}}\left[\varphi_{322} + \varphi_{32-2}\right] = R_{32}(r)\sqrt{\frac{15}{16\pi}}\sin^2\theta\cos 2\varphi \\
t_{2g} : d_{yz} &= \frac{1}{\sqrt{2}i}\left[\varphi_{321} - \varphi_{32-1}\right] = R_{32}(r)\sqrt{\frac{15}{4\pi}}\sin\theta\cos\theta\sin\varphi \\
d_{xz} &= \frac{1}{\sqrt{2}}\left[\varphi_{321} + \varphi_{32-1}\right] = R_{32}(r)\sqrt{\frac{15}{4\pi}}\sin\theta\cos\theta\cos\varphi \\
d_{xy} &= \frac{1}{\sqrt{2}i}\left[\varphi_{322} - \varphi_{32-2}\right] = R_{32}(r)\sqrt{\frac{15}{4\pi}}\sin^2\theta\sin 2\varphi
\end{aligned}
\qquad \text{(I-32)}
$$

Furthermore, these wavefunctions on Cartesian coordinate are:

$$
\begin{aligned}
d_{z^2} &= R_{32}(r)\sqrt{\frac{5}{16\pi}}\frac{3z^2 - r^2}{r^2} \\
d_{x^2-y^2} &= R_{32}(r)\sqrt{\frac{15}{16\pi}}\frac{x^2 - y^2}{r^2} \\
d_{yz} &= R_{32}(r)\sqrt{\frac{15}{4\pi}}\frac{yz}{r^2} \\
d_{xz} &= R_{32}(r)\sqrt{\frac{15}{4\pi}}\frac{xz}{r^2} \\
d_{xy} &= R_{32}(r)\sqrt{\frac{15}{4\pi}}\frac{xy}{r^2}
\end{aligned}
\qquad \text{(I-33)}
$$

2.6. Ligand Field Theory [8,12]

According to crystal field theory, the splitting of *d*-orbitals into t_{2g} and e_g-orbitals ($10Dq$) are obtained. However, there are some experimental facts against crystal-field theory: CO ligand without negative charge affords large the energy-level separation and OH^- ligand affords lower than H_2O and so on. In order to explain these facts, it is necessary to develop from the theory to ligand-field theory based on molecular-orbital theory. The ligand-field splitting is also given as $10Dq$ and the magnitude is available from spectroscopic data and the series for each ligand is arranged in order of the measure of Dq:

$$CO > CN > NO_2 > NH_3 > H_2O > ONO > NCS > OH > F > Cl > Br > I$$

This alignment is known to spectrochemical series. By ligand-field theory, the interactions of *d*-orbitals in metal ion and ligand orbitals can be classified as σ-orbital and π-orbital interactions. The evaluation of these interactions is explained later.

2.7. Molecular Structure and Extended Hückel Method [13]

Extended Hückel method is one of the molecular orbital calculations which lead to powerful information about the electronic structure of metal complexes. As basic assumption, the Hamiltonian of one-molecular orbital φ_i does not correctly include electrostatic interaction and consists of only simple one-electron operator. Thus, the Hamiltonian of all electrons $\hat{\boldsymbol{H}}$ is expressed as:

$$\hat{\boldsymbol{H}} = \hat{\boldsymbol{h}}(1) + \hat{\boldsymbol{h}}(2) + \cdots \hat{\boldsymbol{h}}(N) \tag{I-34}$$

Because $\boldsymbol{h}(N)$ is the Hamiltonian which corresponds to the orbital energy obtained from N-th electron, $\hat{\boldsymbol{H}}$ is the sum of the Hamiltonian of $\boldsymbol{h}(N)$. This eigenfunction of Hamiltonian Ψ is expressed as Slater-type determinant:

$$\Psi = |\varphi_1(1)\varphi_1(2)\cdots\varphi_{n-1}(N-1)\varphi_n(N)| \tag{I-35}$$

The energy of total electrons E is afforded as the sum of occupied-orbital energy, but not reliable value compared with DFT or *ab initio* calculations because the Hamiltonian of one-molecular orbital φ_i does not correctly include electrostatic interaction. For this reason, Extended Hückel calculation is suitable to visualize the delocalized molecular orbitals on determined molecular structures at low calculation cost, but not to optimize molecular geometry. The energy of total electrons E was diagonalized according to the determination of the matrix elements of $\boldsymbol{h}(N)$ using the three following step:

1. Overlap integrals S_{pq} $(p \neq q)$ are calculated by LCAO-MO method using Slater-type orbital.

2. Coulomb integral α_q is evaluated as follows using valence state ionization potential I_q obtained experimentally:

$$\alpha_q = -I_q \tag{I-36}$$

3. Resonance integral β_{pq} $(p \neq q)$ is evaluated as following Wolfsberg-Helmholz equation:

$$\beta_{pq} = KS_{pq}(\alpha_p + \alpha_q)/2 \tag{I-37}$$

where, K is constant and usually adopted for 1.75.

Using atomic coordinates of complexes obtained from X-ray crystallography, specific energies of one-electron derived from *d*-orbitals can be determined. It enables to evaluate the strength of ligand-field by comparing this result to the ligand-field theory, perturbational phenomenology.

2.8. Angular Overlap Model and Ligand-Field Parameters [8,14]

Overlap integral can be expressed as cross product of the terms attributed to atomic distance and depending on angle (configuration). Angular-dependant terms are not influenced by the types of atoms because these terms are occupied by only relative configuration of atomic orbitals. Considering each atomic orbital on two atoms, the orbital energies E of one-electron which takes account of orbital overlap follow as:

$$\begin{aligned} E_1 &= \alpha_1 + (\beta_{12} - S_{12}\alpha_2)^2/(\alpha_1 - \alpha_2) \\ E_2 &= \alpha_2 + (\beta_{12} - S_{12}\alpha_1)^2/(\alpha_2 - \alpha_1) \end{aligned} \tag{I-38}$$

If β is approximated as $K = 2$, the energies are:

$$\begin{aligned} E_1 &= \alpha_1 + (S_{12}\alpha_2)^2/(\alpha_1 - \alpha_2) \\ E_2 &= \alpha_2 + (S_{12}\alpha_1)^2/(\alpha_2 - \alpha_1) \end{aligned} \tag{I-39}$$

These perturbation energies (difference of E_i and α_i) are allowed to be proportional to the squared overlap integral.

Angular overlap model (AOM) determines these angular-independent components of overlap integral as empirical parameters and expresses orbital interaction of general molecular structure without symmetry restriction. If a vector connecting the atoms has the length r, and direction θ, ϕ on the local coordinate system of two atoms, the overlap integral is expressed as the equation by separation of variables: $S_{12} = S(r)F_{12}(\theta, \phi)$. If the two atoms system regards as the coordination bond metal (M) - ligand (L), the energy shifts ($\Delta E_M \equiv E_M - \alpha_M$, $\Delta E_L \equiv E_L - \alpha_L$) of d-orbital and ligand orbital by the forming of coordinate bond are:

$$\begin{aligned} \Delta E_M &= (S_{ML}\alpha_L)^2/(\alpha_M - \alpha_L) = F_{ML}{}^2(\theta,\varphi)(S\alpha_L)^2/(\alpha_M - \alpha_L) \\ \Delta E_L &= (S_{ML}\alpha_M)^2/(\alpha_M - \alpha_L) = F_{ML}{}^2(\theta,\varphi)(S\alpha_M)^2/(\alpha_L - \alpha_M) \end{aligned} \tag{I-40}$$

When all angular independent terms are replaced with e_λ, these equations are expressed as:

$$\begin{aligned} \Delta E_M &= e_\lambda F_{ML}{}^2 \\ \Delta E_L &= e'_\lambda F_{ML}{}^2 \end{aligned} \tag{I-41}$$

These differences of energy become maximum when the configuration takes as maximum orbital overlap, $F_{ML}{}^2 = 1$. The parameters e_λ and e_λ' are interpreted as maximum stabilization or unstabilization parameters obtained by the maximum overlap. λ shows local symmetry about types of orbital overlap, σ, π, $\delta\cdots$. Appling these parameters to metal complexes, ligand-field parameters e_σ, e_π can be distinguishable if the types of d-orbital and ligand-orbital overlap take whether σ-symmetry or π-symmetry. By the estimation of these parameters, the influence of ligand field in the case of no high-symmetry complexes can be discussed generally.

2.9. Spin Hamiltonian [15]

The spin magnetic moment μ_S of electron is given by:

$$\mu_S = -g_e\left(\frac{e\hbar}{2mc}\right)\boldsymbol{S} \tag{I-42}$$

where g_e is electron g factor and c is speed of light in vacuum. Here, Bohr magneton μ_B is defined as:

$$\mu_B = \frac{e\hbar^2}{2mc} \tag{I-43}$$

The orbit magnetic moment $\boldsymbol{\mu}_L$ of electron is given by:

$$\boldsymbol{\mu}_L = -\left(\frac{e\hbar}{2mc}\right)\boldsymbol{L} \tag{I-44}$$

The energy E of electron in magnetic field $\boldsymbol{H}$ is written by:

$$E = -\boldsymbol{\mu}\cdot\boldsymbol{H} = \mu_B\left(g_e\boldsymbol{S}+\boldsymbol{L}\right)\cdot\boldsymbol{H} \tag{I-45}$$

Thus, the energy levels split into $(2S+1)$ and $(2L+1)$ levels. This is the first order Zeeman effect.

The magnetic properties of atom or ion depend on its ground state. Only Zeeman terms are not enough to describe the magnetic property because the complexes have spin-orbit coupling. The Hamiltonian is described as:

$$\hat{\boldsymbol{H}} = -\lambda\left(\boldsymbol{L}\cdot\boldsymbol{S}\right)+\mu_B\left(g_e\boldsymbol{S}+\boldsymbol{L}\right)\cdot\boldsymbol{H} \tag{I-46}$$

For further consideration, it is necessary to derive spin Hamiltonian. When $(2L+1)$ orbital states on lowest energy level of multiplicity split in crystal, the orbital wavefunctions are defined as ψ_0, $\psi_1,\cdots$, ψ_n in the order of increasing energy and $(2S+1)$ spin states as ϕ_{-s}, ϕ_{-s+1}, $\cdots$, ϕ_s in the same way. Here, the wavefunction Ψ for arbitrary level is expressed as:

$$\Psi = \sum_{n,m} a_{nm}\psi_n\phi_m \tag{I-47}$$

ψ_n is assumed to orthogonalize up to all ligand field on true Hamiltonian, and the Hamiltonian $\boldsymbol{W}_{LS} = \lambda\left(\hat{\boldsymbol{L}}\cdot\hat{\boldsymbol{S}}\right)$ for spin-orbit coupling and Zeeman energy $\boldsymbol{W}_0$ are regarded as perturbation. Thus, the Hamiltonian is expressed as:

$$\hat{\boldsymbol{H}}' = \boldsymbol{W}_{LS} + \boldsymbol{W}_0 \tag{I-48}$$

The Hamiltonian for ligand-field is defined as $\hat{\boldsymbol{H}}_c$ and total Schrödinger equation is:

$$\left(\hat{\boldsymbol{H}}_c + \hat{\boldsymbol{H}}'\right)\Psi = E\Psi \tag{I-49}$$

Here, the eigenenergies for $\hat{\boldsymbol{H}}_c$ are defined as E_0, $E_1,\cdots$, E_n in the order of increasing energy and:

$$\langle n|\hat{H}'|n'\rangle = E_n\delta_{nn'} \tag{I-50}$$

The Schrödinger equation above is multiplied by ψ_n and integrated as follows:

$$\sum_{n',m}\langle n|\hat{H}'|n'\rangle a_{n'm}\phi_m = (E-E_n)\sum_m a_{nm}\phi_m \tag{I-51}$$

Here, E is considered in the case of ϕ_0 ($n = 0$) and anything else ($n \neq 0$) separately. When $n = 0$, Eq. I-51 is written as:

$$\sum_{n',m}\langle 0|\hat{H}'|n'\rangle a_{n'm}\phi_m = (E-E_n)\sum_m a_{0m}\phi_m \tag{I-52}$$

Because the left-hand member also includes spin wavefunctions for any states but ground state, Eq. I-51 in the case of $n \neq 0$ is employed in order to rewrite the above equation. First, E in the case of $n = 0$ is approximated as E_0, because Zeeman energy is much less than (E-E_0). When the information of only ground state is considered (only $n' = 0$), Eq. I-52 is organized:

$$\sum_m a_{nm}\phi_m = \frac{\langle n|\hat{H}'|0\rangle}{E_0-E_n}\sum_m a_{0m}\phi_m \qquad (n>1) \tag{I-53}$$

n of Eq. I-53 is replaced n' and substituted to Eq. I-51. For simplicity, n' of calculated equation is replaced n again, and following equation is obtained:

$$\left[\langle 0|\hat{H}'|0\rangle + \sum_{n\neq 0}\frac{\langle 0|\hat{H}'|n\rangle\langle n|\hat{H}'|0\rangle}{E_0-E_n}\right]\sum_m a_{0m}\phi_m = (E_0-E_n)\sum_m a_{0m}\phi_m \tag{I-54}$$

Therefore, the effective Hamiltonian including up to second-order perturbation is defined as effective spin Hamiltonian $\tilde{H}$:

$$\tilde{H} = \langle 0|\hat{H}'|0\rangle + \sum_{n\neq 0}\frac{\langle 0|\hat{H}'|n\rangle\langle n|\hat{H}'|0\rangle}{E_0-E_n} \tag{I-55}$$

Here the spin wavefunction of ground state is:

$$\sum a_{0m}\phi_m = \Psi_{0s} \tag{I-56}$$

The Schrödinger equation including spin function alone is explained as:

$$\tilde{H}\Psi_{0s} = (E-E_0)\Psi_{0s} \tag{I-57}$$

The effective spin Hamiltonian $\tilde{H}$ gives Zeeman energy. Next section, the magnetic property of complex by contribution of spin Hamiltonian is explained.

2.10. Symmetry Lowering of Ligand Field and Zero-Field Splitting [8,11,15]

In order to evaluate spin Hamiltonian, Eq. I-46 is substituted to Eq. I-55 and following equation is obtained:

$$\tilde{\boldsymbol{H}} = g_e \mu_B \boldsymbol{S} g_e (1 - \lambda \Lambda) \boldsymbol{H} - \lambda^2 \boldsymbol{S} \Lambda \boldsymbol{S} - \mu_B^2 \boldsymbol{H} \Lambda \boldsymbol{H} \tag{I-58}$$

where Λ is a symmetric traceless tensor:

$$\Lambda_{\mu\nu} = \sum_{n \neq 0} \frac{\langle 0 | \boldsymbol{L}_\mu | n \rangle \langle n | \boldsymbol{L}_\nu | 0 \rangle}{E_0 - E_n} \qquad (\mu, \nu = x, y, z) \tag{I-59}$$

If $\lambda = 0$, the first term of Eq. I-58 is expressed as Zeeman energy for free ion. The second term is spin self-energy. The third term is neglected because the term gives little effect to spin energy.

Take for example of octahedral manganese(III) complexes, the symmetry reduction of the complexes occurs when different ligands coordinate to each sites. If axial ligand is different to equatorial ligand, the symmetry reduces from O_h to D_{4h}. Under this environment, a ${}^5E_{2g}$ ground state splits to ${}^5A_{1g}$ and ${}^5B_{1g}$. The ${}^5B_{1g}$ ground state, which is still magnetically isotropic, is admixed with excited states by spin-orbit coupling to occur the splitting of the ${}^5B_{1g}$ ground state. This splitting is phenomenologically described by the zero-field splitting because this splitting is prefer to some directions in the absence of an external field. This zero-field splitting can be expressed as the second term of Eq. I-58. For simplicity, the equation is:

$$\hat{\boldsymbol{H}}_{ZF} = \boldsymbol{S} \tilde{\boldsymbol{D}} \boldsymbol{S} \tag{I-60}$$

When the main axes of tensor are x, y, and z, this Hamiltonian can also be explicitly rewritten as:

$$\boldsymbol{S} \tilde{\boldsymbol{D}} \boldsymbol{S} = D[S_z - S(S+1)/3] + E\left(S_x^2 - S_y^2\right) \tag{I-61}$$

where D is uniaxial and E is rhombic zero-field splitting parameter, they are correlated with the main value of $\tilde{D}$; $D_{uu}(u = x, y, z)$ as follows:

$$D = -3D_{zz}/2$$
$$E = \left|D_{xx} - D_{yy}\right|/2 \qquad \text{(I-62)}$$

Since *trans*-ML_4X_2 type complexes are allowed to have axial distortion and no distortion to xy-direction, rhombic axis zero-field splitting parameter E is zero. The term of zero-field splitting identifies the splitting of states belonging to the same S multiplet and different value Ms, which leads to a preferential axis. Taking the example of low-spin *trans*-$Mn^{III}L_4X_2$ complex (S = 1), the splitting $|D|$ between Ms = ±1 and Ms = 0 levels occurs. On the other hand, high-spin *trans*-$Mn^{III}L_4X_2$ complex (S =2) gives the splitting $4|D|$ totally, which includes the energy gap of $3|D|$, and $|D|$ between Ms = ±2, Ms = ±1 and Ms = 0, respectively. For $D > 0$ the anisotropy is of easy-plane type and gives Ms = 0 ground state while $D < 0$ the anisotropy is of easy-axis type and gives Ms = ±S ground state.

In order to estimate the value of zero-field splitting parameter from the result of magnetic susceptibility, energy eigenvalue and eigenvector are determined from diagonalization of $\boldsymbol{H}_{ZF}$ with Zeeman term. Based on these eigenvalue and eigenvector, the simulation of magnetization curve is performed from the expectation, which is calculated by the statistical averaging and further powder averaging, of spin component to an external field direction. From this simulation, the model parameters D, g (Landé factor), and *TIP* (temperature-independent paramagnetism) are optimized and determined at once to fit the observed data. This optimization program *axfit.f* was put as Appendix I [16-21].

2.11 General Theory of Energy Calculation for a Given Electron Configuration

Molecular orbital of one-electron is not enough to describe *d*-electron states of metal complexes because the *d*-electron takes over the feature from free atom dominated by Hund's rule. Thus, interelectronic repulsion is essential to describe the *d*-electron of metal complexes. In the case of manganese(III) complexes which possess d^4 electron configurations, 210 electron configurations are adopted for basic functions. Then, the interelctronic repulsion (Racah parameter *B*, *C*), spin-orbit coupling ζ, and Zeeman interaction introduce into the Hamiltonian as one-electron operator of ligand-field splitting. The diagonalization of this Hamiltonian enables to determine the all spin-orbit levels and the magnetic dependency.

2.12 Nephelauxetic Effect [8,9]

Compared to free transition ion, the interelectronic repulsion of the complexes is reduced. The electron clouds of *d*-orbitals in transition metal ion expand when a transition metal forms complex. Then, the interelectric repulsion is weakened and this phenomenon is referred to as nephelauxetic (cloud-expanding) effect. When the interelectronic repulsion is weakened, the *d*-orbitals interact with ligand orbitals covalently and the *d*-electron and ligand electron delocalize. This effect is shown by the ratio β:

$$\beta = B / B_0 \tag{I-63}$$

Here B_0 is a Racah parameter of free ion. *B* is available from spectroscopic data and the series for each ligand is arranged in order of the measure of *B*:

$$F > H_2O > NH_3 > en \sim Ox > SCN > Cl > CN > Br > I$$

This series is independent of metal ion and the ligands which contribute to metal ion covalently are called soft ligands.

Chapter 3. Objective and Plan of the Present Study

In this dissertation, a series of mononuclear manganese(III) and cobalt(II) complexes were newly synthesized and their spectroscopic and magnetic properties were examined in detail. These physical properties were fully analyzed on the basis of ligand-field theory, aiming to provide a way to regulate electronic states of single metal centers as functional synthons in construction of higher assembled systems, *e.g.* nanomagnets.

The present dissertation is composed of the following two parts.

In Part II, a series of octahedral manganese(III) complexes were synthesized, of which axial ligands were chosen among a variety of monodentate ligands, while the equatorial ligand was kept to be tetradentate cyclam (1,4,8,11-tetraazacyclotetradecane) across the series. The magnetic measurements of them revealed that the electron configuration depends on the nature of axial ligands to be high-spin or low-spin complexes. The combined application of angular-overlap method (AOM) and extended Hückel molecular-orbital calculations indicated that the relationship between molecular structure and magnetic anisotropy of axially elongated high-spin manganese(III) complexes.

In Part III, several sulfur-coordinate cobalt(II/III) complexes of soft-scorpionate which bear sulfur donor tripodal ligand belonging to thioamide family were synthesized. These complexes can be grouped into $[Co^{II}S_6]$, $[Co^{III}S_6]$, and $[Co^{II}S_4]$ coordination centers and single-crystal X-ray analysis revealed that one of the cobalt(II) complexes has a $[Co^{II}S_6]$ center, which is a first case distinguished from already-known $[Co^{III}S_6]$ or $[Co^{II}S_4]$ soft-scorpionate complexes. X-ray photoelectron spectroscopic and magnetic measurements demonstrated that this complex has a high-spin cobalt(II) metal center of $[Co^{II}(L)]$-type electron configuration. Small ligand-field splitting and also small Racah's parameters determined from the electronic spectrum of the $[Co^{II}S_6]$ complex

were successfully transferred in the analysis of magnetic susceptibility. Remarkable delocalization of *d*-electron onto the ligand moieties was also suggested from the simulation of the magnetic behavior.

References for Part I

[1] (a) S. Kiatgawa, R. Kitaura, S. Noro, Angew. Chem. Int. Ed. 43 (2004) 2334;
(b) R. E. Morris, Paul. S. Wheatley, Angew. Chem. Int. Ed. 47 (2008) 4966;
(c) J. R. Long, O. M. Yaghi, Chem. Soc. Rev. 38 (2009) 1213;
(d) G. Férey, C. Serre, Chem. Soc. Rev. 38 (2009) 1380;
(e) J.-R. Li, R. J. Kuppler, H.-C. Zhou, Chem. Soc. Rev. 38 (2009) 1477;
(f) L. J. Murray, M. Dincă, J. R. Long, Chem. Soc. Rev. 38 (2009) 1294;
(g) L. Ma, C. Abney, W. Lin, Chem. Soc. Rev. 38 (2009) 1248;
(h) J. Lee, O. K. Farha, J. Roberts, K. A. Scheidt, S. T. Nguyen, J. T. Hupp, Chem. Soc. Rev. 38 (2009) 1450;
(i) Z. Wang, G. Chen, K. Ding, Chem. Rev. 109 (2009) 322;
(j) D. Maspoch, D. Ruiz-Molina, J. Veciana, Chem. Soc. Rev. 36 (2007) 770;
(k) P. Dechambenoit, J. R. Long, Chem. Soc. Rev. 40 (2011) 3249.

[2] (a) D. Gatteschi, R. Sessoli, J. Villain, Molecular Nanomagnets, Oxford University Press, Oxford, 2006;
(b) Single-Molecule Magnets and Related Phenomena, Structure and Bonding, Ed. R. Winpenny, Splinger, Berlin/Heidelberg, 2006, vol. 122.

[3] (a) M. N. Leuenberger, D. Loss, Nature 410 (2001) 789;
(b) L. Bogani, W. Wernsdorfer, Nat. Mater. 7 (2008) 179;
(c) M. Mannini, F. Pineider, P. Sainctavit, C. Danieli, E, Otero, C. Sciancalepore, A. M. Talarico, M.-A. Arrio, A. Cornia, D. Gatteschi, R. Sessoli, Nat. Mater. 8 (2009) 194;
(d) F. Troiani, M. Affronte, Chem. Soc. Rev. 40 (2011) 3119.

[4] R. Sessoli, H. L. Tsai, A. R. Schake, S. Wang, J. B. Vincent, K. Foliting, D. Gatteschi, G. Christou, D. N. Hendrickson, J. Am. Chem. Soc. 115 (1993) 1804.

[5] E.-C. Yang, D. N. Hendrickson, W. Wernsdorfer, M. Nakano, L. N. Zakharov, R. D. Sommer, A. L. Rheingold, M. Ledezma-Gairaud, G. Christou, J. Appl. Phys. 91 (2002) 7382.

[6] R. L. Carlin, Magnetochemistry, Splinger, Berlin/Heidelberg, 1986.

[7] M. Nakano, H. Oshio, Chem. Soc. Rev. 40 (2011) 3239.

[8] B. N. Figgis, M. A. Hitchman, Ligand Field Theory and its Application, Wiley-VCH, New York, 2000.

[9] E. U. Condon, G. H. Shotley, The Theory of Atomic Spectra, Cambridge University Press, Cambridge, 1935.

[10] A. B. P. Lever, Inorganic Electronic Spectroscopy, Elsevier, Amsterdam, 2nd edn., 1968.

[11] 大川尚士, 朝倉化学体系 9　磁性の化学, 朝倉書店, 2004.

[12] 山内清吾, 野崎浩一, 複合系の光機能研究会選書 1　配位化合物の電子状態と光物理, 朝倉書店, 2010.

[13] 大塚齊之助, 巽和行, 分子軌道法に基づく錯体の立体化学（上）, 講談社, 1986.

[14] 大野公一, 量子物理化学, 東京大学出版会, 1989.

[15] 伊達宗之, 新物理学シリーズ 20 電子スピン共鳴, 培風館, 1978.

[16] E. Anderson, Z. Bai, C. Bischof, L. S. Blackford, J. Demmel, J. Dongarra, J. Du Croz, A. Greenbaum, S. Hammarling, A. McKenney, D. Sorensen, LAPACK Users' Guide, Third Edition, Software, Environments and Tools Vol.9, Society for Industrial and Applied Mathematics, Philadelphia, 1999. URL: <http://www.netlib.org/lapack/>

[17] M. Edén, M. H. Levitt, J. Magn. Reson. 132 (1998) 220. URL: <http://www.mhl.soton.ac.uk/research/software/Orientations/>

[18] J. A. Nelder, R. Mead, Computer Journal 7 (1965) 308.

[19] J. M. Parkinson, D. Hutchinson, Numerical Methods for Non-linear Optimization, Pages 115-135, Ed. F.A. Lootsma, Academic Press, London, 1972.

[20] W. H. Press, S. A. Teukolsky, W. T. Vetterling, B. P. Flannery, Numerical Recipes, Cambridge University Press, Cambridge, 1986.

[21] C. T. Kelly, SIAM J. Optim. 10 (1999) 43.

Part II. Magnetostructural Examination of Manganese(III) Complexes $[Mn(cyclam)X_2]^+$ with Strong Axial Ligands

Chapter 4. Introduction of manganese(III) complexes $[Mn(cyclam)X_2]^+$

The magnetism of manganese(III) complexes receives much attentions recently because their large magnetic anisotropy serves useful pinning potentials for magnetization reversal in various nanomagnets [1] and their complicated d^4 electron configurations provide a potential for multiple bistabilities including spin crossover and the Jahn-Teller effects [2-5]. A lot of mononuclear hexacoordinate manganese(III) complexes take a high-spin electron configuration ($t_{2g}^3e_g^1$;^5E_g) as their ground states. The doubly-degenerate ^5E_g ground state is unstable against the tetragonal axial elongation or compression. This Jahn-Teller distortion is just the source of magnetic anisotropy, or strictly a zero-field splitting, in manganese(III) complexes. The contribution of a single metal center to the net magnetic anisotropy of a polynuclear metal assembly is mainly attributed to the zero-field splitting of each metal center rather than anisotropic superexchange interactions. Although high-spin ground states ^5E_g of mononuclear manganese(III) complexes are commonly found, low-spin ground states ^3T_g are rare and spin-crossover phenomena between these two ground states are uncommon [3-5].

A series of manganese(III) complexes, *trans*-$[Mn(cyclam)X_2]^+$ (cyclam = 1,4,8,11-tetraazacyclo-tetradecane, X^- = axial anionic ligand), has been extensively studied, focusing on the electronic structure and magnetic properties, which may take high-spin or low-spin electron configurations [8-13]. Throughout the series, only one low-spin species is known with X^- = CN^- [14], and no spin-crossover complexes are reported yet. The stronger side of a range of axial ligand field is interesting, and three novel complexes with X^- = $NCBH_3^-$ (**1**), $NCBPh_3^-$ (**2**), and $NCSe^-$ (**3**), were

obtained in order to explore the spin-crossover boundary on the interaction parameter space. The crystal structure of *trans*-[Mn(cyclam)($NCBH_3$)$_2$](CF_3SO_3) (**1**) and *trans*-[Mn(cyclam)($NCBPh_3$)$_2$] (CF_3SO_3) (**2**) were solved and reported in detail. Several known complexes [8,9,11] were also prepared along with novel ones and their magnetic susceptibilities were measured aiming to determine the magnetic anisotropy parameter (uniaxial zero-field splitting parameter D) as a guide scale of axial ligand field. By applying angular-overlap model and extended Hückel molecular-orbital calculations, the relation between magnetic anisotropy and electronic structure was discussed for a series of [Mn(cyclam)X_2] complexes.

Chapter 5. Experimental for $[Mn(cyclam)X_2]^+$

Commercially available solvents and chemicals were used without further purification. The reaction procedures of *trans*-[Mn(cyclam)$(NCBH_3)_2$](CF_3SO_3) (**1**), and *trans*-[Mn(cyclam)-$(NCBPh_3)_2$](CF_3SO_3) (**2**) (cyclam = 1,4,8,11-tetraazacyclotetradecane) were carried out in ambient atmosphere. The reaction procedure of *trans*-[Mn(cyclam)$(NCSe)_2$](CF_3SO_3) (**3**) was performed under an argon atmosphere using standard Schrenk technique. The complex *trans*-[Mn(cyclam)$(OH_2)_2$]$(CF_3SO_3)_3 \cdot H_2O$ was prepared according to the literature method [8]. *trans*-[Mn(cyclam)Cl_2]$Cl \cdot 4H_2O$ was prepared according to the literature method [12]. Elemental analyses were carried out at the Laboratory for Instrumental Analysis, Graduate School of Engineering, Osaka University. IR spectra were recorded on a JASCO FT/IR-300E spectrometer. Solid state magnetic measurements of **1**, **2**, *trans*-[Mn(cyclam)$(CN)_2$](CF_3SO_3) (**4**), *trans*-[Mn(cyclam)$(NCO)_2$](CF_3SO_3) (**5**), and *trans*-[Mn(cyclam)I_2]I (**6**) were carried out on a Quantum Design MPMS-XL5 SQUID magnetometer equipped with reciprocating sample option (RSO) at magnetic fields of 1.0 and 5.0 T. Solid state magnetic measurement of **3** was carried out on a Quantum Design MPMS-2 SQUID magnetometer at a field of 1.0 T. Polycrystalline samples were mounted in calibrated gelatin capsules held at the center of a polypropylene straw fixed to the end of the sample rod.

5.1. Synthesis of complexes

trans-[Mn(cyclam)$(NCBH_3)_2$](CF_3SO_3) (1)

To an aqueous solution (3 mL) of *trans*-[Mn(cyclam)$(OH_2)_2$]$(CF_3SO_3)_3 \cdot H_2O$ (378 mg, 0.5 mmol) was added an aqueous solution (2 mL) of $NaNCBH_3$ (62.9 mg, 1.0 mmol) at room temperature and the mixture was stirred. Sky-blue solid precipitated immediately was filtered off and dried in air

(yield 135 mg, 56%). Infrared spectrum (KBr disk, cm^{-1}): 2184 (ν{C≡N}), 2350 (ν{B-H}). *Anal.* Calc. for $C_{13}H_{30}B_2F_3MnN_6O_3S$: C, 32.26; H, 6.25; N, 17.36%. Found: C, 31.77; H, 6.18; N, 17.35%. For X-ray crystallographic analysis, an aqueous solution (1.5 mL) of $NaNCBH_3$ (13.1 mg, 0.21 mmol) was carefully layered on an aqueous solution (1 mL) of *trans*-[Mn(cyclam)$(OH_2)_2$]-$(CF_3SO_3)_3 \cdot H_2O$ (76.1 mg, 0.10 mmol) to yield sky-blue single crystals in 2 h.

trans-[Mn(cyclam)$(NCBPh_3)_2$](CF_3SO_3) (2)

A mixture of KCN (130 mg, 2.0 mmol) and BPh_3 (484 mg. 2.0 mmol) in ethanol (2.5 mL) at room temperature was stirred for 1 h to give a clear solution. To an aqueous solution (2 mL) of *trans*-[Mn(cyclam)$(OH_2)_2$]$(CF_3SO_3)_3 \cdot H_2O$ (756 mg, 1.0 mmol) was added the ethanolic solution and the mixture was stirred. Immediately yellowish green solid was precipitated and filtered off. The solid was washed by ethanol, and dried in air (yield 357 mg, 38%). Infrared spectrum (KBr disk, cm^{-1}): 2171 (ν{C≡N}). *Anal.* Calc. for $C_{49}H_{54}B_2F_3MnN_6O_3S$: C, 62.57; H, 5.79; N, 8.93%. Found: C, 62.30; H, 5.82; N, 8.98%. For X-ray crystallographic analysis, a yellowish green crystal was obtained from acetonitrile solution by vapor diffusion of diethylether.

trans-[Mn(cyclam)$(NCSe)_2$]$(CF_3SO_3) \cdot H_2O$ (3)

To a solution of KSeCN (143 mg, 0.99 mmol) in acetonitrile (10 mL) was added a solution of *trans*-[Mn(cyclam)$(OH_2)_2$]$(CF_3SO_3)_3 \cdot H_2O$ (376 mg, 0.50 mmol) in the same solvent (5 mL) at room temperature. The deep purple solution changed to a clear orange solution immediately after stirring. After 20 min, the solution was evaporated in vacuo. In a half volume of solvent evaporated a dark-orange solid started to precipitate. The solid was washed by ethanol and dried in vacuo (yield 86.7 mg, 28%). Infrared spectrum (KBr disk, cm^{-1}): 2055 (ν{C≡N}). *Anal.* Calc. for $C_{13}H_{26}F_3MnN_6O_4SSe_2$: C, 24.69; H, 4.14; N, 13.29%. Found: C, 24.68; H, 3.78; N, 13.23%.

trans-[Mn(cyclam)(CN)$_2$](CF$_3$SO$_3$) (4)

Complex **4** was prepared following the literature method [11]. To a solution of NaCN in water added a solution of *trans*-[Mn(cyclam)(OH$_2$)$_2$](CF$_3$SO$_3$)$_3$·H$_2$O in the same solvent at room temperature. Immediately yellow solid was precipitated and filtered off. The solid was immediately washed by ethanol, and dried in vacuo. *Anal.* Calc. for $C_{13}H_{24}F_3MnN_6O_3S$: C, 34.21; H, 5.30; N, 18.42%. Found: C, 34.18; H, 5.19; N, 18.41%.

trans-[Mn(cyclam)(NCO)$_2$](CF$_3$SO$_3$) (5)

Complex **5** was prepared following the literature method [6]. To a solution of KNCO in water added a solution of *trans*-[Mn(cyclam)(OH$_2$)$_2$](CF$_3$SO$_3$)$_3$·H$_2$O in the same solvent at room temperature. Immediately yellowish green solid was precipitated and filtered off. The solid was washed by ethanol, and dried in air. *Anal.* Calc. for $C_{13}H_{24}F_3MnN_6O_5S$: C, 31.97; H, 4.95; N, 17.21%. Found: C, 31.43; H, 4.76; N, 16.88%.

trans-[Mn(cyclam)I$_2$]I (6)

Complex **6** was prepared following the literature method [12]. To a solution of *trans*-[Mn(cyclam)Cl$_2$]Cl· 4H$_2$O in water added concentrated HI solution in the same solvent at room temperature. Immediately dark red solid was precipitated and filtered off. The solid was washed by dichrolomethane and ethanol, and dried in air. *Anal.* Calc. for $C_{10}H_{24}I_3MnN_4$: C, 18.89; H, 3.80; N, 8.77%. Found: C, 19.28; H, 3.66; N, 8.77%.

5.2. X-ray structure determination

Single-crystal structure determination was performed for the compounds **1** and **2** at 123 K using a Rigaku RAXIS RAPID imaging-plate area detector with graphite monochromated Mo-K_α radiation

(λ = 0.071073 nm). The structure of the compound **1** was solved by direct methods (SIR 92) [13] and expanded using Fourier techniques (DIRDIF99) [14]. The positions of all non-hydrogen atoms were refined anisotropically. Hydrogen atoms were included and their positions were refined using a riding model. All calculation of the compound **1** were performed using the CrystalStructure crystallographic software package [15,16]. The data collection, cell refinement, and absorption correction of **2** were performed using the CrystalStructure crystallographic software package. Data reduction by the the CrystalStructure crystallographic software package was applied. The structure was solved by direct methods and refined by full-matrix least squares method on F^2 with anisotropic thermal parameters for all non-hydrogen atoms using the SHELXTL-PC V 6.1 software package [17, 18]. Hydrogen atoms bound to a carbon atom were placed in calculated positions and refined isotropically with a riding model. Detail on the data collections and refinements are summarized in Table II-1.

Table II-1. Crystallographic data and structure refinements for *trans*-[Mn(cyclam)($NCBH_3$)$_2$](CF_3SO_3) and *trans*-[Mn(cyclam)($NCBPh_3$)$_2$](CF_3SO_3).

	[Mn(cyclam)($NCBH_3$)$_2$](CF_3SO_3)	[Mn(cyclam)($NCBPh_3$)$_2$](CF_3SO_3)
Emprical formula	$C_{13}H_{30}B_2F_3MnN_6O_3S$	$C_{49}H_{50}B_2F_3MnN_6O_3S$
Formula weight	484.03	940.60
Crystal system	Orthorhombic	Monoclinic
Space Group	$P2_12_12_1$	*C*2/c
a (Å)	8.6989(5)	18.892(4)
b (Å)	13.3506(8)	16.155(3)
c (Å)	19.3131(10)	16.811(3)
α (°)	90	90
β (°)	90	115.42(3)
γ (°)	90	90
V (Å^3)	2242.9(2)	4634.0(16)
Z	4	4
T (K)	123	123
D_{calc} (g cm^{-3})	1.433	1.348
Crystal Color, Habit	sky blue, prism	yellowish green, needle
Crystal Dimensions (mm)	0.15 × 0.10 × 0.10	0.45×0.30×0.10
F_{000}	1008.00	1968.00
μ(Mo Kα) (cm^{-1})	7.315	3.910
Total data	21475	9598
Unique data	5125	5244
R_{int}	0.126	0.043
R_1 [$I > 1.5\sigma(I)$]	0.0717	
wR_2 [$I > 1.5\sigma(I)$]	0.0823	
R_1 [$I > 2.0\sigma(I)$]		0.0656
wR_2 [$I > 2.0\sigma(I)$]		0.1548
Goodness of fit	1.070	1.214
Flack parameter [19]	0.49	

Chapter 6. Results and Discussion on $[Mn(cyclam)X_2]^+$

6.1. Molecular structure of complexes

Crystal structure was determined for *trans*-$[Mn(cyclam)(NCBH_3)_2](CF_3SO_3)$ (**1**) (cyclam = 1,4,8,11-tetraazacyclotetradecane) which crystallizes in the non-centrosymmetric space group $P2_12_12_1$. The molecular structure is depicted in Figure II-1. The counter anion $CF_3SO_3^-$ links neighboring complex cations via weak hydrogen bonds O---N forming a chain structure along *c* axis (Figure II-2).

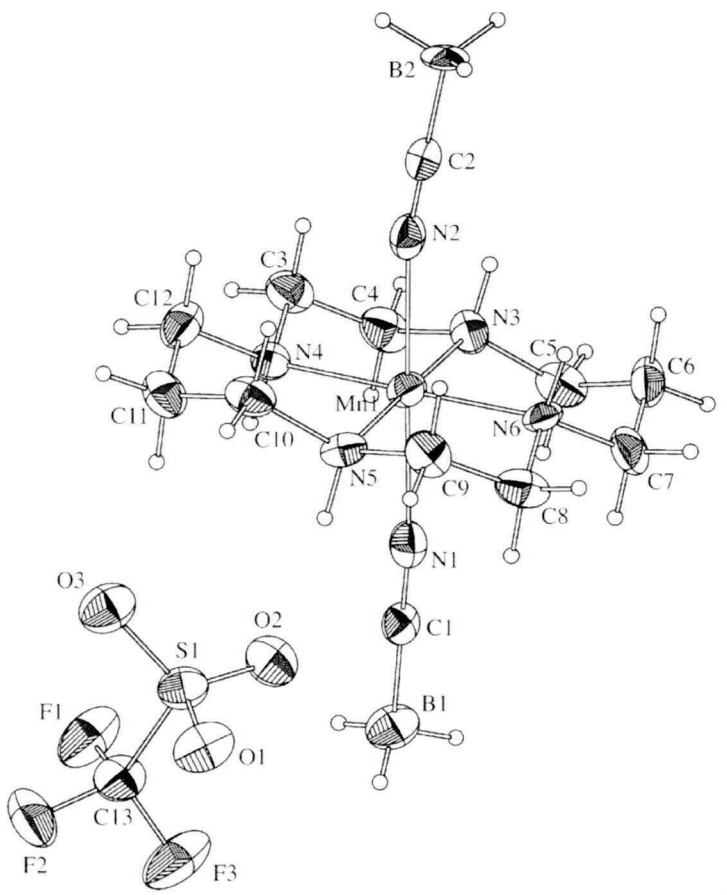

Figure II-1. Molecular structure of *trans*-[Mn(cyclam)-$(NCBH_3)_2](CF_3SO_3)$. All H atoms are shown as open circles, and thermal ellipsoids for heavier atoms are drawn at the 50% probability level.

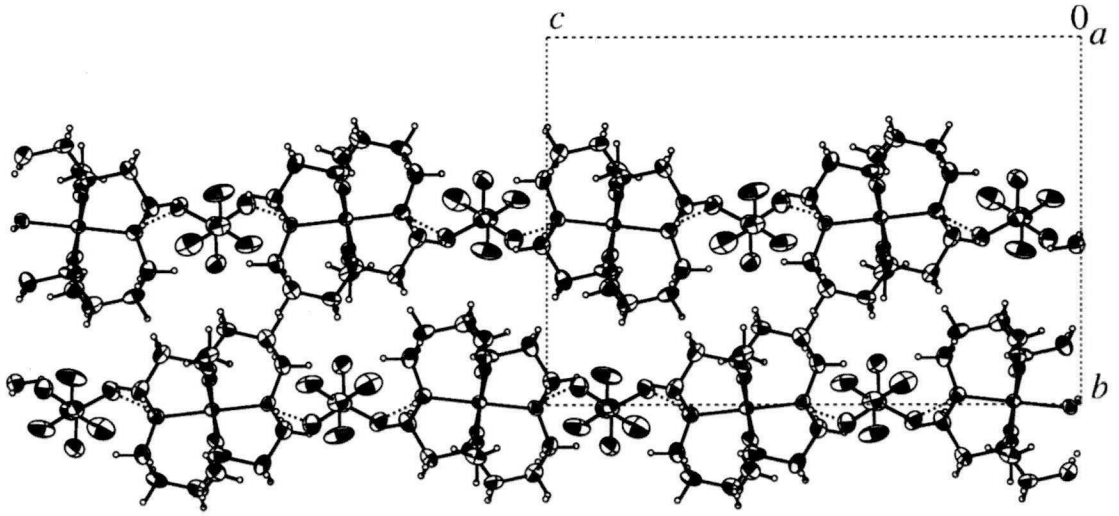

Figure II-2. Chain structure of *trans*-[Mn(cyclam)($NCBH_3$)$_2$](CF_3SO_3) with weak hydrogen bonds along *c* axis.

The coordination environment around manganese(III) is elongated-octahedron type. The equatorial Mn-N distances fall in a range of 2.004-2.034 Å. The axial Mn-N distances are significantly longer than them, being 2.209 and 2.215 Å. The Mn-N and N≡C bonds in Mn---$NCBH_3$ axial coordination are non-collinear with the Mn-N-C angle of 169.4-173.7°, which gives rise to a small deviation from tetragonal symmetry, while the axial Mn-N bond is almost normal to the equatorial N_4 plane with the tilt angle of 1.06° (Table II-2).

Table II-2. Comparison of structural data for *trans*-[Mn(cyclam)X_2]$^{+/3+}$ complexes.

axial ligand X	spin state	coordination. Sphere	average Mn-X distance / Å	average Mn-N_{cyclam} distance / Å	τ (°)[a]	references
I	HS	4N, 2I	2.9416(2)	2.028(2)	3.71	[8]
Br	HS	4N, 2Br	2.689(1)	2.029(6)	3.28	[6]
Cl	HS	4N, 2Cl	2.527(1)	2.035(3)	2.50	[6,7]
OH_2	HS	4N, 2O	2.187(8)	2.037(6)	7.80	[8]
ClO_4	HS	4N, 2O	2.1909(9)	2.0280(7)	8.71	[8]
NO_3	HS	4N, 2O	2.221(4)	2.036(7)	4.49	[6]
NO_2	HS	4N, 2O	2.188(12)	2.034(3)	5.90	[8]
N_3	HS	6N	2.175(3)	2.041(3)	3.76	[10]
NCS	HS	6N	2.166(17)	2.038(4)	1.48	[6]
$NCBH_3$	HS	6N	2.212(7)	2.020(9)	1.06	this work
$NCBPh_3$	HS	6N	2.237(3)	2.041(4)	10.47	this work
NCO	HS	6N	2.148(4)	2.043(4)	1.40	[9]
CN	LS	4N, 2C	2.007(4)	2.029(4)	1.30	[11]

[a] Tilt angle τ is defined as the angle between the normal to the equatorial MnN_4 plane and the Mn–X bond [8].

Crystal structure was determined for *trans*-[Mn(cyclam)($NCBPh_3$)$_2$](CF_3SO_3) **(2)** which crystallizes in the space group *C*2/c and the manganese(III) ion has a centrosymmetric octahedral N_6 coordination environment. The molecular structure is depicted in Figure II-3. The counter anion $CF_3SO_3^-$ does not link neighboring complex cations via no hydrogen bonds O---N forming a chain structure (Figure II-4).

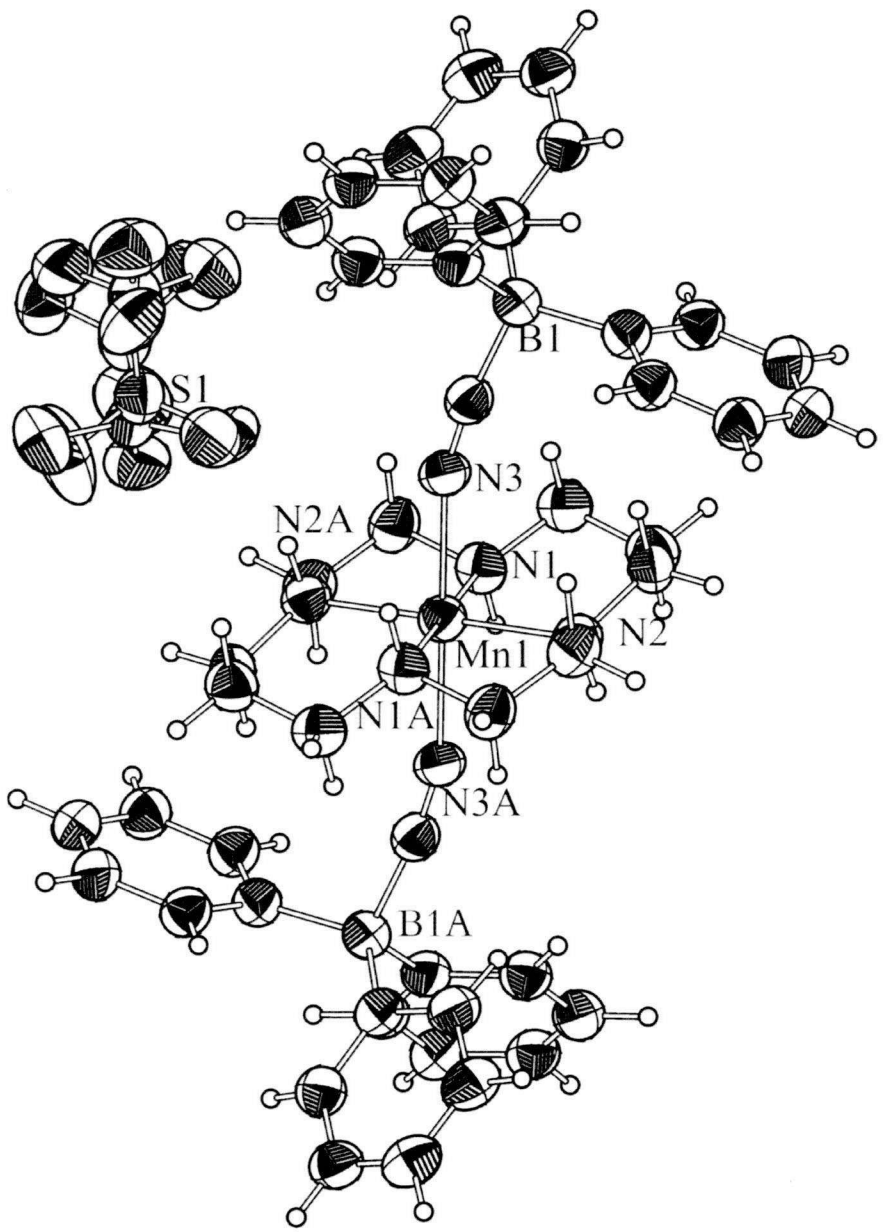

Figure II-3. Molecular structure of *trans*-[Mn(cyclam)($NCBPh_3$)$_2$](CF_3SO_3). All H atoms are shown as open circles, and thermal ellipsoids for heavier atoms are drawn at the 50% probability level.

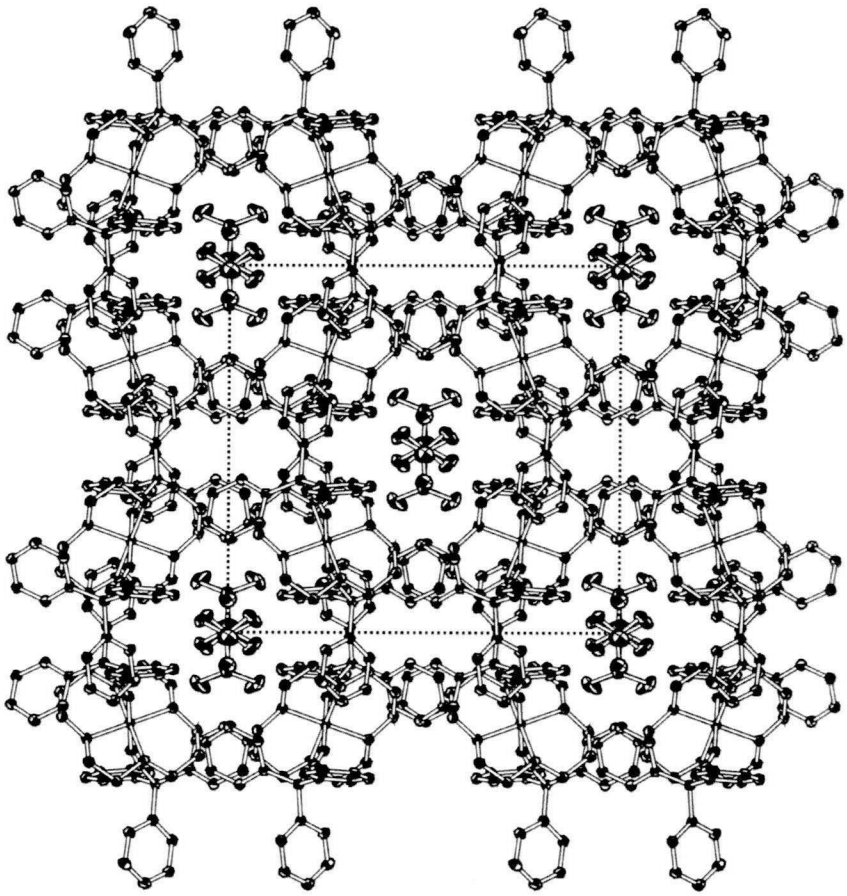

Figure II-4. Crystal structure of *trans*-[Mn(cyclam)($NCBPh_3$)$_2$](CF_3SO_3).

The coordination environment around manganese(III) is elongated-octahedron type. The counter anion is disordered at 123 K (Figure II-5). The equatorial Mn-N distances fall in a range of 2.035-2.044 Å. The axial Mn-N distances are significantly longer than them, being 2.237 Å. These values are the longest among axial Mn-N distances in the hitherto-reported [Mn(cyclam)X_2]$^+$ complexes [6-11]. The Mn-N and N≡C bonds in Mn---$NCBPh_3$ axial coordination are non-collinear with the Mn-N-C angle of 162.5°, which gives rise to a small deviation from tetragonal symmetry, while the axial Mn-N bond is almost normal to the equatorial N_4 plane with the tilt angle of 10.47° (Table II-2).

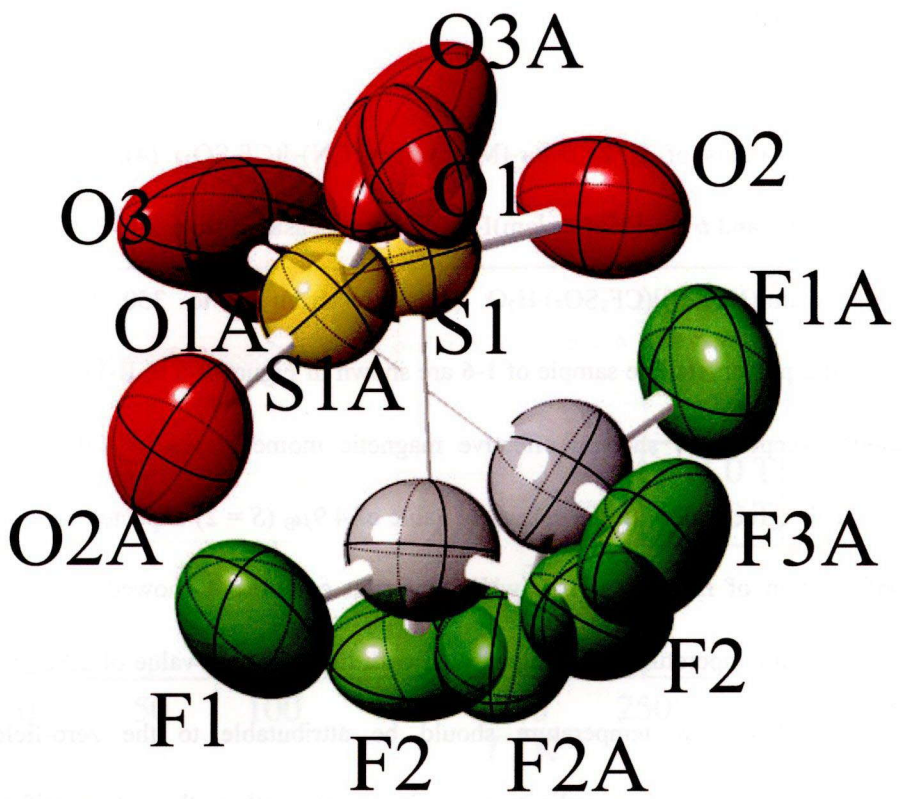

Figure II-5. Orientational disorder in the counter anion of *trans*-[Mn(cyclam)-$(NCBPh_3)_2$](CF_3SO_3).

6.2. Magnetic properties

Isofield magnetizations of **1**, **2**, *trans*-[Mn(cyclam)$(CN)_2$](CF_3SO_3) (**4**), *trans*-[Mn(cyclam)-$(NCO)_2$](CF_3SO_3) (**5**), and *trans*-[Mn(cyclam)I_2]I (**6**) were measured from 2 to 350 K, and the ones of *trans*-[Mn(cyclam)$(NCSe)_2$]$(CF_3SO_3)\cdot H_2O$ (**3**) were from 4 to 350 K. The magnetic susceptibilities of a polycrystalline sample of **1-6** are shown in Figure II-6 to II-11, respectively. All the compounds except for **4** showed effective magnetic moments μ_{eff} of 4.9-5.2 μ_B at room temperature, which agree well with the spin-only value of 4.9μ_B (S = 2) expected for a high spin d^4 electron configuration of manganese(III), while low-spin complex **4** showed effective magnetic moments μ_{eff} at room temperature which agree well with the spin-only value of 2.8μ_B (S = 1). The μ_{eff} drops observed at low temperature should be attributable to the zero-field splitting accompanying with tetragonal coordination environment, rather than to antiferromagnetic intermolecular interactions. The uniaxial zero-field splitting parameters D were estimated by assuming random orientation of crystallites (Table II-3).

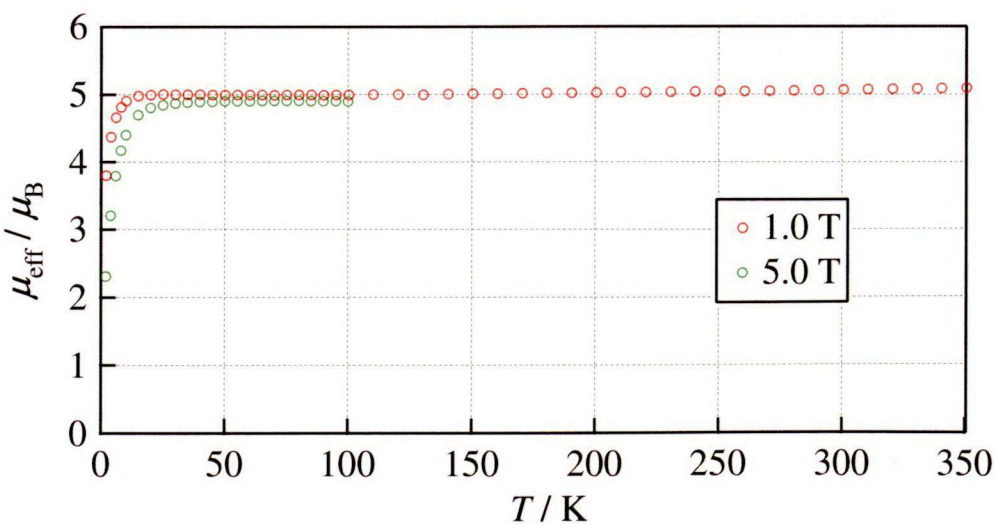

Figure II–6. The temperature dependence of effective magnetic moment of a polycrystalline sample of *trans*-[Mn(cyclam)$(NCBH_3)_2$](CF_3SO_3) from 2 K to 350 K.

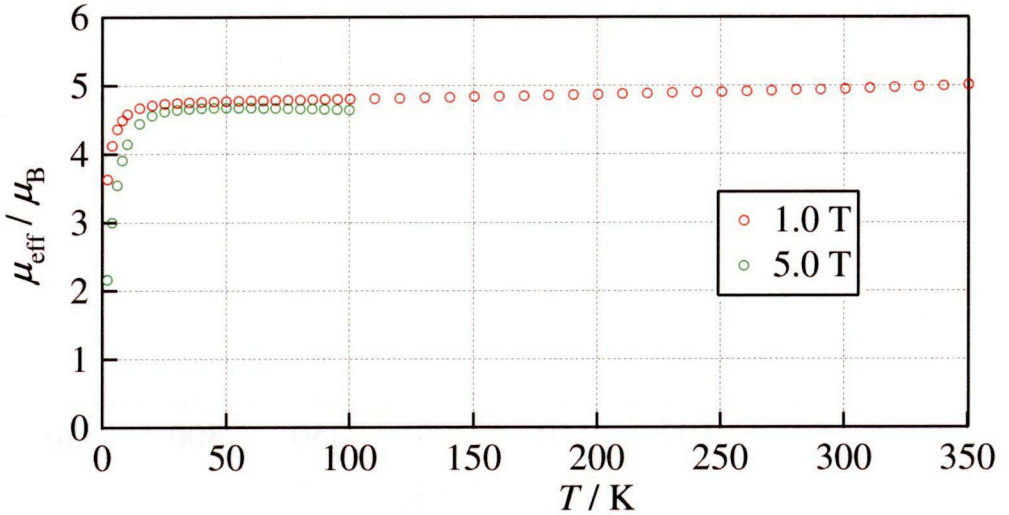

Figure II–7. The temperature dependence of effective magnetic moment of a polycrystalline sample of *trans*-[Mn(cyclam)($NCBPh_3$)$_2$](CF_3SO_3) from 2 K to 350 K.

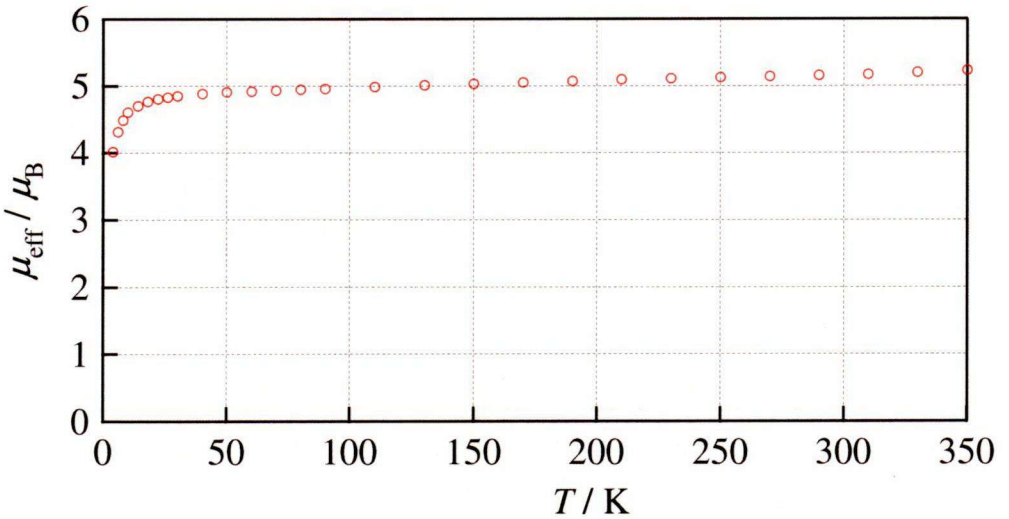

Figure II–8. The temperature dependence of effective magnetic moment of a polycrystalline sample of *trans*-[Mn(cyclam)($NCSe$)$_2$](CF_3SO_3)· H_2O from 4 K to 350 K.

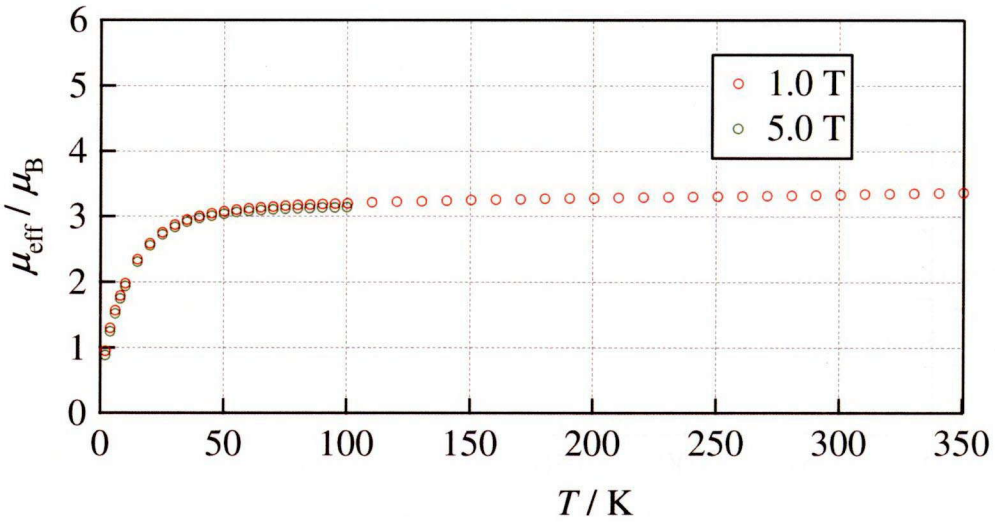

Figure II–9. The temperature dependence of effective magnetic moment of a polycrystalline sample of *trans*-[Mn(cyclam)$(CN)_2$](CF_3SO_3) from 2 K to 350 K.

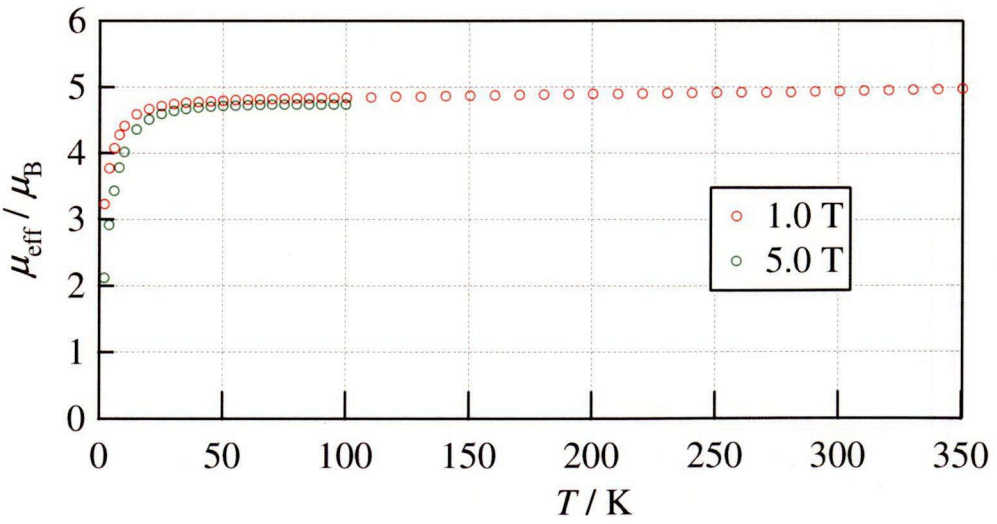

Figure II–10. The temperature dependence of effective magnetic moment of a polycrystalline sample of *trans*-[Mn(cyclam)$(NCO)_2$](CF_3SO_3) from 2 K to 350 K.

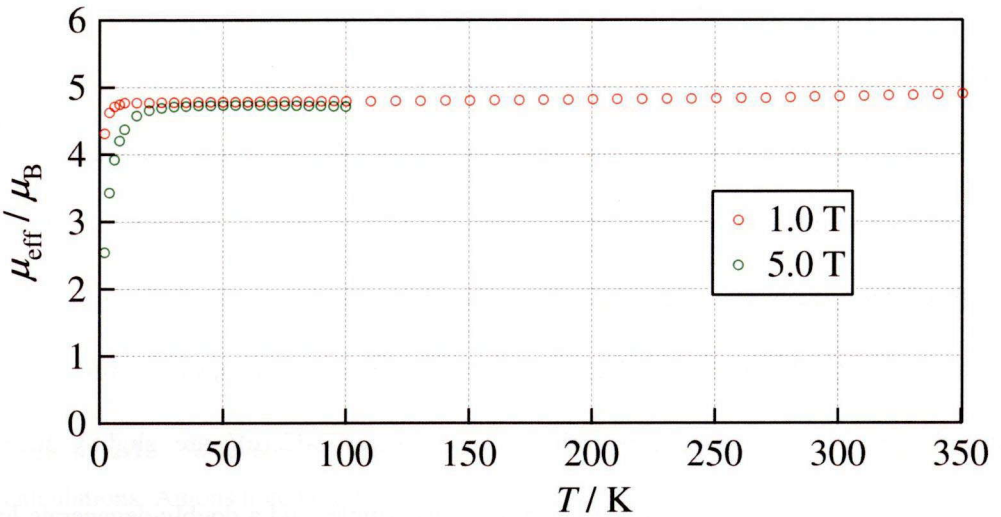

Figure II–11. The temperature dependence of effective magnetic moment of a polycrystalline sample of *trans*-[Mn(cyclam)I_2]I from 2 K to 350 K.

Table II-3. Uniaxial zero-field splitting parameter D of *trans*-[Mn(cyclam)X_2]$^+$ complexes.

axial ligand X	spin state	D / hc cm^{-1}	References
I	HS	0.82*	this work
Br	HS	-1.67	[20]
$NCBH_3$	HS	-4.65*	this work
$NCBPh_3$	HS	-5.76*	this work
NCSe	HS	-9.05*	this work
NCO	HS	-10.26*	this work

* Apparent value estimated by fitting of magnetic susceptibility data.

6.3. Magnetic anisotropy analysis on the basis of AOM

Ligand-field splitting based on extended Hückel calculations

Extended Hückel molecular-orbital calculations [21] were made to figure out one-electron orbital energies for the complexes with X^- = Cl^-, Br^-, I^-, $NCBH_3^-$, $NCBPh_3^-$, NCO^-, NCS^-, N_3^-, CN^-, ClO_4^-, NO_3^-, and NO_2^- using their crystallographic atomic coordinates [6-11]. The orbital energies of five *d*-character molecular orbitals are depicted in Figure II-12. It is obvious that the d_{z2} orbitals are strongly affected by σ-donor character of axial ligands, while the orbital energy of the d_{x2-y2} orbitals are dominated by the equatorial ligand cyclam and kept almost unchanged at around -8.2 eV throughout the series. Non-bonding t_{2g} orbitals found below -12 eV are slightly lifted by π-donor/acceptor character of the axial ligands, providing a single- and a doubly-degenerate levels. Further investigation of the splitting in t_{2g} orbitals was done, having the benefit of fragment molecular-orbital (FMO) analysis. Except for CN^- ligand, π-ligand orbitals on X^- interact with d_{yz} and d_{xz} orbitals of the manganese(III) ion, working as π-donor ligands. It is not the case in CN^- ligand, of which π-character ligand orbitals interact with d_{yz} and d_{xz} atomic orbaitals, thus working as π-acceptor ligand. The π-orbitals from N-donor and halide ligands are mixed with t_{2g} orbitals via π-overlap by over 15% contribution, while O-donor ligands have little contribution. On the other hand, the σ-orbitals of axial ligands and equatorial cyclam ligand interact with e_g orbitals by around 15% contribution, while the mixing ratio exceeds 50% in axial CN^- coordination showing very strong σ-donor character. In spite that the splitting in the t_{2g} orbitals are much smaller than that in e_g orbitals, this small splitting plays an essential role in the low-spin electronic configuration under a very strong ligand field, where the ordering of split levels (2:1 or 1:2) determines orbital degeneracy for the partially-lifted $(t_{2g})^4$ configuration.

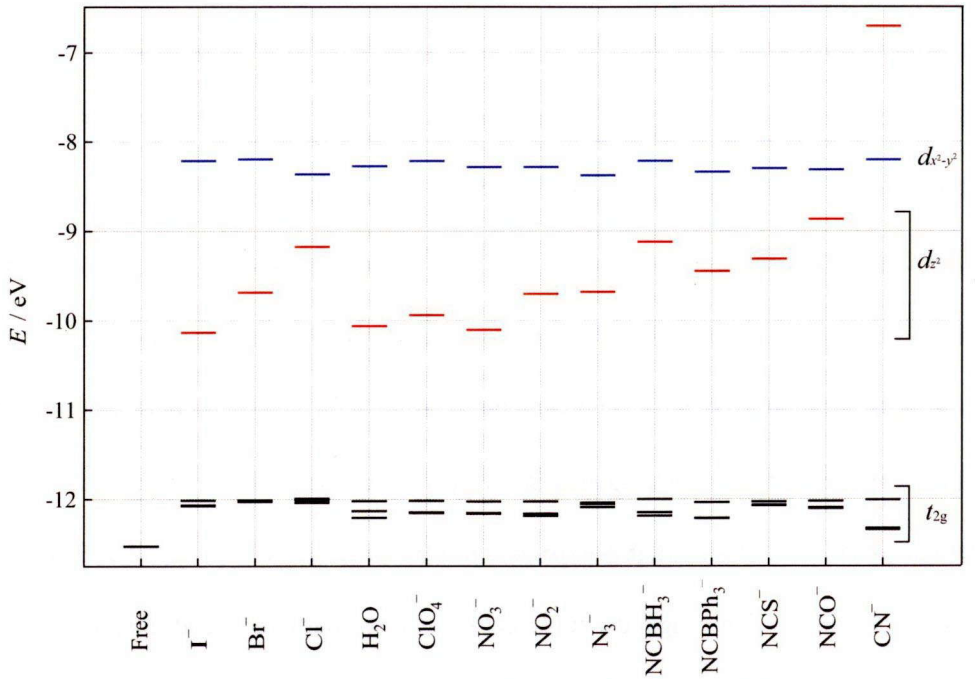

Figure II-12. 3*d*-levels for *trans*-$[Mn(cyclam)X_2]^{+/3+}$ estimated by extended Hückel calculations. Anions noted on the abscissa stand for the axial ligand X in the complex.

Estimation for ligand-field parameters of each axial ligand

One-electron orbital energies obtained from extended Hückel molecular orbital calculations are useful to estimate ligand-field parameters. The angular-overlap model (AOM), instead of a conventional cubic harmonics expansion, was adopted to describe the ligand fields in $[Mn(cyclam)X_2]^+$ complexes, since it is more convenient to attribute the effect of individual ligand to the AOM parameters representing localized σ- and π-donors (e_σ and e_π, respectively). For an octahedral complex *trans*-$[ML_4X_2]$ of D_{4h} symmetry, the orbital-energy relations:

$$E\left(x^2 - y^2\right) = 3e_\sigma(\mathrm{L})$$
$$E\left(z^2\right) = e_\sigma(\mathrm{L}) + 2e_\sigma(\mathrm{X})$$
$$E(yz) = E(zx) = 2e_\pi(\mathrm{L}) + 2e_\pi(\mathrm{X})$$
$$E(xy) = 4e_\pi(\mathrm{L}) \cong 0$$

are known for σ-donor equatorial ligand L and σ, π-donor axial ligand X, where $E(d)$ stands for the one-electron orbital energy of *d*-character orbital [22]. These relations were used to extract AOM

parameters which are compiled in Table II-4. If e (X) is smaller than e_π(L), *i.e.* $E(yz)$, $E(zx) < E(xy)$, the axial ligand behaves as a π-acceptor rather than a π-donor. In this case, the possible low-spin electronic configuration is orbitally-degenerate $\{(d_{yz})(d_{zx})\}^3(d_{xy})^1$, not $(d_{xy})^2(d_{yz})^1(d_{zx})^1$, which is subject to the Jahn-Teller instability. It is proposed to be responsible for the tilting of axial ligands observed in $X^- = CN^-$ [11]. The e_σ(X)'s for axial N-donor ligands are unexpectedly small because axially-elongated manganese(III) ion diminishes the overlap with ligand π-donor orbitals. Halide ligands, which are known to be weak ligands in the spectrochemical series, possess large e_σ(X) in our results. It is conceivable if remarkably expanded *p*-orbitals of halide ions are taken into account, in comparison to N- and O-donor ligands, sufficient orbital overlap is afforded in spite of the axial elongation.

Table II-4. AOM parameters of *trans*-$[Mn(cyclam)X_2]^{+/3+}$ extracted from extended Hückel energy levels.

axial ligand X	e_σ (X)/ *hc* cm^{-1}	e_π (X)/ *hc* cm^{-1}	e_σ (L)/ *hc* cm^{-1}
I	3860	800	11600
Br	5660	970	11650
Cl	7930	960	11200
OH_2	4220	420	11440
ClO_4	4640	490	11600
NO_3	4070	490	11410
NO_2	5700	410	11410
N_3	5900	860	11160
$NCBH_3$	7830	410	11820
$NCBPh_3$	7430	280	11270
NCS	7290	840	11340
NCO	9100	710	11330
CN	17660	-260	11640

Dependence of zero-field splitting on ligand-field splitting on manganese(III) complexes

Although there is a report that the magnetic anisotropy in the high-spin $[Mn(cyclam)I_2]^+$ complex may be dominated by MLCT excited states mixing into the high-spin $^5B_1$ ground state [23], the contribution of such low-energy MLCT excited states is very rare and reliably ignored in most of the $[Mn(cyclam)X_2]^+$ complexes. Thus, the magnetic anisotropies of them were examined taking only *d*-orbitals into account. Figure II-13 shows the zero-field splitting parameter (D) of $[Mn(cyclam)X_2]^+$ series mapped on an $e_\sigma(X)$–$e_\pi(X)$ plane, which was calculated by AOM in conjunction with typical values for manganese(III) electronic parameters: Racah's parameters B / hc = 1140 cm^{-1} and C/B = 4.3 [24]; spin-orbit coupling ζ / hc = 355 cm^{-1} [22]; Stevens' orbital reduction factor k = 0.8 [25]; the AOM parameter of equatorial cyclam ligands $e_\sigma(L) / hc$ = 10000 cm^{-1}. The red broken curve on the map is a spin-crossover boundary separating high-spin (S = 2) and low-spin (S = 1) region. On this map, $e_\sigma(X)$ and $e_\pi(X)$ values of several complexes summarized in Table II-4 are also plotted. This map suggested that zero-field splitting parameter D is usable as the indicator of ligand-field strength. On the contrary, the large zero-feild splitting parameter of high-spin $[Mn(cyclam)X_2]^+$ complexes can be obtained if an axial ligand gives strong ligand-field parameter which locates neighbor of spin-crossover boundary. Then, this map also suggested that the high-spin complexes **1** and **2** do not have enough strong ligand field to break Hund's rule, and the cyanohydroborate anion behaves as not a π-acceptor expected but a weak π-donor for manganese(III) ion. Given the comparison of D-value in Table II-3, complex **3** appears to be located between **1**, **2** and $[Mn(cyclam)(NCO)_2]^+$. Therefore, it is revealed that spin-crossover manganese(III) cyclam complexes should have stronger σ-donor and π-acceptor ligands.

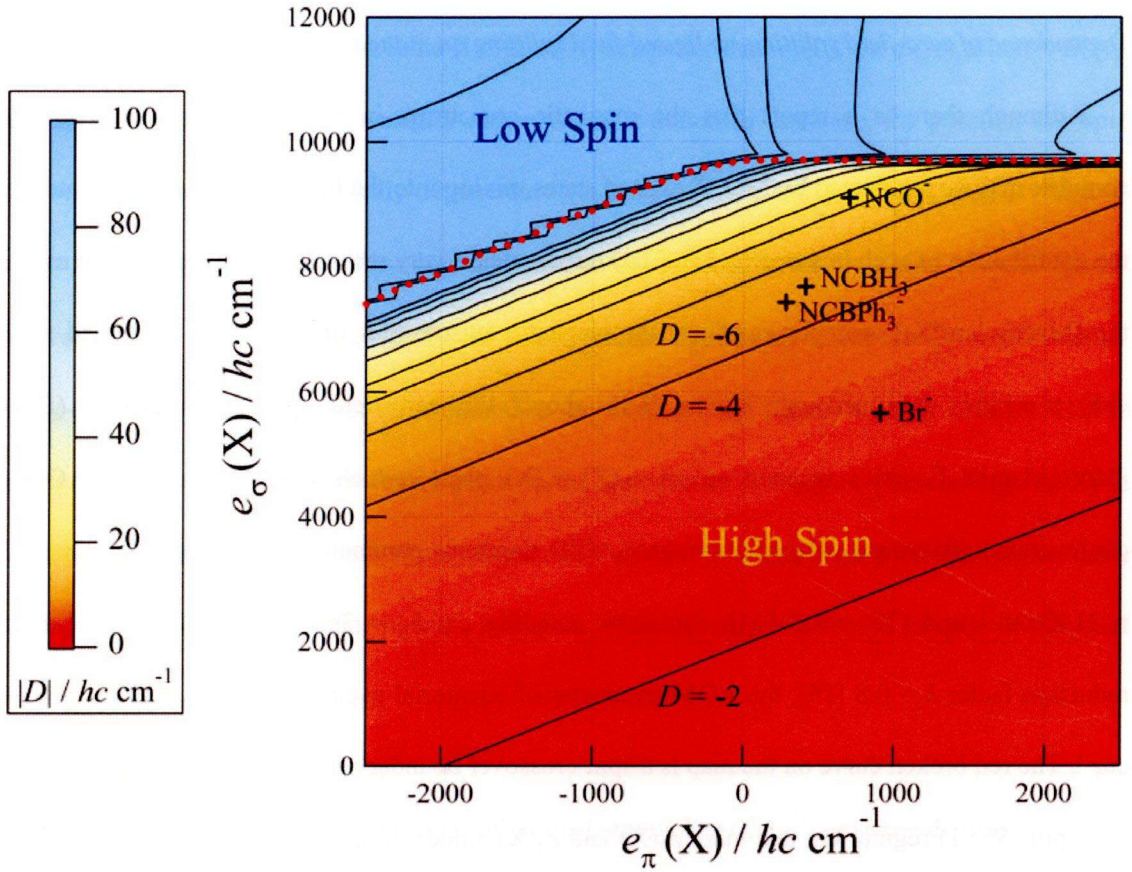

Figure II-13. Zero-field splitting parameter D of *trans*-[Mn(cyclam)X_2]$^+$ complexes as a function of axial ligand AOM parameters e_σ(X) and e_π(X).

Chapter 7. Conclusion of $[Mn(cyclam)X_2]^+$

The manganese(III) complexes *trans*-$[Mn(cyclam)(NCBH_3)_2](CF_3SO_3)$ (**1**) (cyclam = 1,4,8,11-tetraazacyclotetradecane), *trans*-$[Mn(cyclam)(NCBPh_3)_2](CF_3SO_3)$ (**2**), and *trans*-$[Mn(cyclam)(NCSe)_2](CF_3SO_3)$ (**3**) were newly prepared and found to be in the high-spin state. The magnetic measurements of them revealed very large uniaxial zero-field splittings D of **1-3**. The crystal structures of **1**, **2** and analogous complexes were utilized in extended Hückel and AOM calculations, providing two useful information of the ligand-field control for the large magnetic anisotropy, and the spin crossover boundary of $[Mn(cyclam)X_2]^+$.

References for Part II

[1] (a) R. Sessoli, D. Gatteschi, A. Caneschi, M. A. Novak, Nature 365 (1993) 141;

(b) R. Sessoli, H.-L. Tsai, A. R. Schake, S. Wang, J. B. Vincent, K. Folting, D. Gatteschi, G. Christou, D. N. Hendrickson, J. Am. Chem. Soc. 115 (1993) 1804;

(c) D. Gatteschi, A. Caneschi, L. Pardi, R. Sessoli, Science 265 (1994) 1054;

(d) H. J. Eppley, H.-L. Tsai, N. de Vries, K. Folting, G. Christou, D. N. Hendrickson, J. Am. Chem. Soc. 117 (1995) 301;

(e) L. Thomas, F. Lionti, R. Ballou, D. Gatteschi, R. Sessoli, B. Barbara, Nature 383 (1996) 145;

(f) J. Villain, F. Hartman-Boutron, R. Sessoli, A. Rettori, Europhys. Lett. 27 (1997) 159;

(g) S. L. Castro, Z. Sun, C. M. Grant, J. C. Bollinger, D. N. Hendrickson, G. Christou, J. Am. Chem. Soc.120 (1998) 2365;

(h) D. Ruiz, Z. Sun, B. Albela, K Folting, J. Ribas, G. Christou, D. N. Hendrickson, Angew. Chem. Int. Ed. 37 (1998) 300;

(i) Z. Sun, D. Ruiz, E. Rumberger, C. D. Incarvito, K. Folting, A. L. Rheingold, G. Christou, D. N. Hendrickson, Inorg. Chem. 37 (1998) 4758;

(j) W. Wernsdorfer, N. Aliaga-Alcalde, D. N. Hendrickson, G. Christou, Nature 416 (2002) 406;

(k) W. Wernsdorfer, S. Bhaduri, C. Boskovic, G. Christou, D. N. Hendrickson, Phys. Rev. B 65 (2002) 180403;

(l) S. Hill, E. S. Edwards, N. Aliaga-Alcalde, G. Christou, Science 302 (2003) 1015;

(m) D. Gatteschi, R. Sessoli, Angew. Chem. Int. Ed. 42 (2003) 268;

(n) M. Soler, W. Wernsdorfer, K. Folting, M. Pink, G Christou, J. Am. Chem. Soc. 126 (2004) 2156;

(o) M. Murugesu, M. Habrych, W. Wernsdorfer, K. A. Abboud, G. Christou, J. Am. Chem. Soc. 126 (2004) 4766;

(p) H. Oshio, N. Hoshino, T. Ito, M. Nakano, J. Am. Chem. Soc. 126 (2004) 8805;

(q) A. J. Tasiopoulos, A. Vinslava, W. Wernsdorfer, K. A. Abboud, G. Christou, Angew. Chem. Int. Ed. 43 (2004) 2117;

(r) A. K. Boudalis, B. Donnadieu, V. Nastopoulos, J. M. Clemente-Juan, A. Mari, Y. Sanakis, J.-P. Tuchagues, S. P. Perlepes, Angew. Chem. Int. Ed. 43 (2004) 2266;

(s) H. Miyasaka, R. Clérac, W. Wernsdorfer, L. Lecren, C. Bonhomme, K. Sugiura, M. Yamashita, Angew. Chem. Int. Ed. 43 (2004) 2801.

[2] Y. Garcia, P. Gütlich, Top. Curr. Chem. 234 (2004) 49.

[3] P. G. Sim, E. Sinn, J. Am. Chem. Soc. 103 (1981) 241.

[4] M. Nakano, G. Matsubayashi, T. Matsuo, Phys. Rev. B 65 (2002) 212412.

[5] G. G. Morgan, K. D. Murnaghan, H. Müller-Bunz, V. McKee, C. J. Harding, Angew. Chem. Int. Ed. 45 (2006) 7192.

[6] P. A. Daugherty, J. Glerup, P. A. Goodson, D. J. Hodgson, K. Michelsen, Acta Chem. Scand. 45 (1991) 244.

[7] P.-K. Chan, C.-K. Poon, J. Chem. Soc., Dalton Trans. (1976) 858.

[8] S. Mossin, H. O. Sørensen, H. Weihe, J. Glerup, I. Søtofte, Inorg. Chim. Acta 358 (2005) 1096.

[9] A. D. Rae, S. Mossin, H. O. Sørensen, Acta Crystallogr., Sect. B 61 (2004) 407.

[10] K. Meyer, J. Bendix, N. Meltzler-Norte, T. Weyhermüller, K. Wieghardt, J. Am. Chem. Soc. 120 (1998) 7260.

[11] S. Mossin, H. O. Sørensen, H. Weihe, Acta Crystallogr., Sect. C 58 (2002) m204.

[12] F. Létumier, G. Broeker, J. -M. Barbe, R. Guilard, D. Lucas, V. Dahaoui-Gindrey, C. Lecomte, L. Thouin, C. Amatore, J. Chem. Soc., Dalton Trans. (1998) 2233.

[13] SIR92: A. Altomare, G. Cascarano, C. Giacovazzo, A. Guagliardi, M. Burla, G. Polidori, M. Camalli, J. Appl. Cryst. 27 (1994) 435.

[14] DIRDIF99: P. T. Beurskens, G. Admiraal, G. Beurskens, W. P. Bosman, R. de Gelder, R. Israel, J. M. M. Smits, (1999). The DIRDIF-99 program system, Technical Report of the Crystallography Laboratory, University of Nijmegen, The Netherlands.

[15] CrystalStructure 3.8: Crystal Structure Analysis Package, Rigaku and Rigaku Americas (2000-2007). 9009 New Trails Dr., The Woodlands, TX 77381, USA.

[16] CRYSTALS Issue 11: J. R. Carruthers, J. S. Rollett, P. W. Betteridge, D. Kinna, L. Pearce, A. Larsen, E. Gabe, Chemical Crystallography Laboratory, Oxford, UK. 1999.

[17] G. M. Sheldrick (1997). SHELXS97. University of Göttingen, Germany.

[18] G. M. Sheldrick (1997). SHELXL97. University of Göttingen, Germany.

[19] H. D. Flack, Acta Crystallogr., Sect. A 39 (1983) 876.

[20] S. Mossin, M. Stefan, P. T. Heerdt, A. Bouwen, E. Goovaerts, H. Weihe, Appl. Magn. Reson. 21 (2001) 587.

[21] (a) M. Wolfsberg, L. J. Helmholz, J. Chem. Phys. 20 (1952) 837;
(b) R. Hoffmann, J. Chem. Phys. 39 (1963) 1397;
(c) R. Hoffmann, W. N. Lipscomb, J. Chem. Phys. 36 (1962) 2179; 3489;
(d) J. H. Ammeter, H.-B. Burgi, J. C. Thibeault, R. Hoffmann, J. Am. Chem. Soc. 100 (1978) 3686;
(e) C. Mealli, D. M. Proserpio, J. Chem. Educ. 67 (1990) 399.

[22] B. N. Figgis, M. A. Hitchman, Ligand Field Theory and Its Applications, Wiley-VCH, New York, 2000.

[23] S. Mossin, H. Weihe, A.-L. Barra, J. Am. Chem. Soc. 124 (2002) 8764.

[24] A. Bencini, I. Ciofini, M. G. Uytterhoeven, Inorg. Chim. Acta 274 (1998) 90.

[25] (a) J. J. Salzmann, H. H. Schmidtke, Inorg. Chim. Acta 3 (1969) 207;
(b) S. A. Cotton, Inorg. Nucl. Chem. Lett. 8 (1972) 371;
(c) N. Juranić , Spectrochim. Acta 36A (1980) 249.

Part III. Magnetic and Spectroscopic Characterizations of Cobalt(II/III) Complexes Consisting of Soft-Scorpionate Ligands

Chapter 8. Introduction to Cobalt(II/III) Complexes Consisting of Soft-Scorpionate Ligands

Sulfur-atom coordination to transition metal centers is fascinating in the research of electronic structures because of the polarizablity of sulfur ligands and associated nephelauxetic effect. Among sulfur ligands with weak σ-donor character preferring high-spin transition metal complexes, crown thioether ligands are known to give low-spin complexes due to their π-acceptor characters and remarkable nephelauxetic effects reducing interelectronic repulsions [1-7]. In the sharp contrast to it, thiolate and thioamide ligands work as π-donor ligands resulting in high-spin complexes [8-11].

High-spin octahedral cobalt(II/III) complexes are known as "T-term ions" with very strong magnetic anisotropy attributable to unquenched orbital angular momenta mixing to pure spins via spin-orbit coupling. In the last decade, this large magnetic anisotropy of cobalt(II) centers was successfully utilized to afford cobalt(II)-based single molecule magnets (SMMs) [12], but the use of high-spin cobalt(III) centers were not made because most of ligands yield low-spin complexes with diamagnetic low-spin $^1A_1$ ground states, not high-spin. Exceptional cases reported are the high-spin cobalt(III) complexes $[CoF_6]^{3-}$ [13] and $[CoF_3(H_2O)_3]$ [14]. It should be worthwhile if some weak and versatile ligands deliver a series of high-spin cobalt(III) complexes.

The sulfur ligands are also interesting for their coordination versatility toward paramagnetic cluster complexes.

Monodentate thiourea and bidentate dithiooxamide ligands are known to give high-spin cobalt(II) complexes, which have fully characterized by vibrational and electronic spectroscopies but X-ray crystal structure analysis [15-16]. There is a possibility of obtaining high-spin complexes even with cobalt(III) ions if weak enough sulfur ligands are adopted.

Soft-scorpionate ligands Tm^R [17] which bear three sulfur coordination sites on a molecule based on 1-alkylimidazol-2-ylthione donors belong to the thioamide family and a number of complexes were synthesized with focuses on not only metalloenzyme mimics but also industrial applications for sensors [18]. Among the soft-scorpionate cobalt complexes, the ocatahedral low-spin cobalt(III) complex $[Co^{III}(Tm^{Me})]^+$ [19] and the tetrahedral cobalt(II) complex $[Co^{II}(Tm^R)_2]$ (R = ^{t}Bu [20], Ph [21]) have been obtained. However, the nephelauxetic effects in them as soft donor ligands and detailed magnetochemical studies are not investigated yet. The soft scorpionate ligand based on 2-benzothiazolethione, NaTbz (Tbz^- = hydrotris(2-mercaptobenzothiazolyl)borate), is interesting because this ligand has a benzene-ring substructure on each pod, extending wider π-conjugation than in Tm^{R-} ligand [22].

In the Part III, the synthesis, molecular structure, magnetic property, and electronic spectrum of a novel cobalt(II) complex $[Co^{II}(Tbz)_2]$ were studied and the ligand-field splitting and nephelauxetic effect in the complex are discussed. Aiming to the high-spin ocatahedral configuration or spin-crossover phenomenon of cobalt(III) S_6 complex [23], $[Co^{III}(Tm^{Me})_2](Tm^{Me})$ was examined in terms of crystal structure, magnetic susceptibility and electronic spectrum. $[Co^{II}(Tm^{Me})_2]\cdot 4H_2O$ was obtained as a byproduct and examined in terms of crystal structure and magnetic susceptibility. The molecular structures and electronic structures of these complexes are compared.

Chapter 9. Experimental for $[Co^{II}(Tbz)_2]$ and $[Co^{II/III}(Tm^{Me})_2]^{0/+}$

Commercially available solvents and chemicals were used without further purification. The reaction procedure of ligand $^nBu_4NTbz$ (Tbz^- = hydrotris(2-mercaptobenzothiazolyl)borate) was performed under a nitrogen atmosphere. $Na(Tm^{Me})\cdot 4.5H_2O$ (Tm^{Me} = hydrotris(2-mercapto-1-methylimidazolyl)borate) was prepared according to the literature method [24-25]. All reaction procedures of complexes were carried out in ambient atmosphere. Elemental analyses (C, H, N) were carried out at the Laboratory for Instrumental Analysis, Graduate School of Engineering, Osaka University. Electronic spectrum of $[Co^{II}(Tbz)_2]$ (**1**) was measured on Jasco V-570 UV/Vis spectrophotometer equipped with a diffuse reflectance option at room temperature by using a powder sample sticking on a filter paper. Electronic spectrum of the acetonitrile solution in $[Co^{III}(Tm^{Me})_2](Tm^{Me})$ (**2**) was measured on the same spectrometer above. IR spectra were recorded on a Thermo Nicolet NEXUS 470 ESP FT-IR spectrometer. NMR spectrum was recorded on a JEOL JNM-EX270 spectrometer. Solid-state magnetic measurements of **1** was carried out on a Quantum Design MPMS-XL5 SQUID magnetometer equipped with reciprocating sample option (RSO) at magnetic fields of 1.0 T. Solid-state magnetic susceptibility measurements of **2** and $[Co^{II}(Tm^{Me})_2]\cdot 4H_2O$ (**3**) were performed on a Quantum Design MPMS-2 SQUID magnetometer in a field of 1.0 T. Polycrystalline samples were mounted in calibrated gelatin capsules held at the center of a polypropylene straw fixed to the end of the sample rod. X-ray photoelectron spectra were obtained by irradiating the complex with Mg–K_α X-rays (300 W) at 298 K using an ULVAC–PHI ESCA 5700 photoelectron spectrometer and calibrated with the carbon $1s_{1/2}$ photoelectron peak (285.0 eV).

9.1. Synthesis of a ligand and complexes

Tetrabutylammonium hydrotris(2-mercaptobenzothiazolyl)borate ($^nBu_4NTbz$)

Tetrabutylammonium tetrahydroborate, (2.06 g, 8 mmol) and 2-mercaptobenzothiazole, (5.35 g, 32 mmol) were mixed together in a 200 mL round-bottomed flask, which was fitted with an air jacket condenser. After the reaction vessel was flashed with nitrogen gas, the vessel was placed in an oil bath and the temperature was raised slowly to 170℃. The mixture started melting at approximately 120℃ (tetrabutylammonium tetrahydroborate; mp 124℃), whereupon the vigorous evolution of hydrogen gas began. Above 130℃ the reaction mixture changed to a suspension and then the evolution of hydrogen gas stopped. Upon reaching 170℃ (2-mercaptobenzothiazole; mp 168℃), the suspension completely melted to clearness and the evolution of hydrogen gas began again. The temperature should be kept under 180℃ to avoid decomposition. The reaction was allowed to proceed until the gas evolution stopped again. Once the reaction was complete the mixture was allowed to cool. In order to take the solid reaction mixture out of the flask, the yellow solid was dissolved in THF. Then solution was partially evaporated and the half-dry solid was extracted with hot toluene to isolate the product from excess 2-mercaptobenzothiazole and yellow decomposition by product. Large volume of ethanol was added to the grey-colored solid mass with vigorous stirring until white powder was suspended. The powder was filtered, washed with diethyl ether, and dried in vacuo, yield 3.30 g (55%). Calc. for $C_{37}H_{49}BN_4S_6$: C, 59.02; H, 6.56; N, 7.44%. Found: C, 59.09; H, 6.36; N, 7.40%. δ_H (270.05 MHz; solvent $CDCl_3$) 0.88 (t, 12H, $^+N(CH_2CH_2CH_2C\mathit{H}_3)_4$), 1.28 (sextet, 8H, $^+N(CH_2CH_2C\mathit{H}_2CH_3)_4$), 1.55 (quintet, 8H, $^+N(CH_2C\mathit{H}_2CH_2CH_3)_4$), 3.13 (t, 8H, $^+N(C\mathit{H}_2CH_2CH_2CH_3)_4$), 7.05 (br, 6H, benzothiazole *H*), 7.27 (br, 6H, benzothiazole *H*), B*H* not observed; Infrared spectrum (KBr disk, cm^{-1}): 2478 (ν{B-H}, w), 736 (ν{C=S}, m).

$[Co^{II}(Tbz)_2]$ (1)

An 20 mL acetone solution of $Co(NO_3)_2 \cdot 6H_2O$ (291 mg, 1 mmol) was added under stirring to an acetone solution (60 mL) of $^nBu_4NTbz$ (1.50 g, 2 mmol) at room temperature. Yellow solid

immediately precipitated. After 5 minutes, the solid was filtered off and washed with acetone, ethanol and diethyl ether, and dried in air (yield 388 mg, 36%). Calc. for $C_{42}H_{26}B_2CoN_6S_{12}$: C, 46.71; H, 2.43; N, 7.78%. Found: C, 46.57; H, 2.53; N, 7.74%. Infrared spectrum (KBr disk, cm^{-1}): 2478 (ν{B-H}, w), 726 (ν{C=S}, m). To obtain single crystals, $Co^{II}(NO_3)_2 \cdot 6H_2O$ and 2 equiv of $^nBu_4NTbz$ were placed at each side of an H-shaped tube. Then, acetone and acetonitrile were carefully added to the cobalt salt and the ligand in the H-tube, respectively, up to the level of solution contact. Yellow single crystals were obtained by allowing slow diffusion of two solutions for two weeks. Two different polymorphs of $[Co^{II}(Tbz)_2]$ were obtained in the same crystallization batch. One is prism and another is rhombus in shape.

$[Co^{III}(Tm^{Me})_2](Tm^{Me})$ (2)

CoF_3 (463 mg, 4 mmol) was added under stirring to an aqueous solution (80 mL) of $Na(Tm^{Me}) \cdot 4.5H_2O$ (1.92 g, 4 mmol) at room temperature. Green solid immediately precipitated and subsequently turned to brown. After 5 minutes, the brown solid was filtered and extracted by acetone. Dark red solution was concentrated to minimal volume. The brown solid was collected by filtration from the concentrated solution, washed with minimal ethanol and diethyl ether, and dried in air (yield 1.40 g, 25%). For X-ray crystallographic analysis, a dark red crystal was obtained from acetonitrile solution by vapor diffusion of diethyl ether. Calcd. for $C_{36}H_{48}B_3CoN_{18}S_9$: C, 38.85; H, 4.35; N, 22.66%. Found: C, 38.83; H, 4.20; N, 22.66%. Infrared spectrum (KBr disk, cm^{-1}): 2468, 2437 (ν{B-H}).

$[Co^{II}(Tm^{Me})_2] \cdot 4H_2O$ (3)

Complex **3** was isolated from the same reaction condition of **2**. Green solid precipitated was filtered quickly before the solid color turned to brown. The solid was washed with copious ethanol.

The green solid was extracted by acetonitrile and the dark-green solution was concentrated to minimal volume and stood for a few hours. Dark green crystalline solid was deposited, collected by filtration, washed with minimal acetonitrile and diethyl ether, and dried in air (yield <2%). For X-ray crystallographic analysis, a dark green crystal was obtained from acetonitrile solution by vapor diffusion of diethyl ether. Calcd. for $C_{24}H_{32}B_2CoN_{12}S_6 \cdot 4.5H_2O$: C, 34.21; H, 4.90; N, 19.95%. Found: C, 33.90; H, 4.50; N, 19.78%. Infrared spectrum (KBr disk, cm^{-1}): 2375 (ν{B-H}).

9.2. X-ray structure determination

Single crystal structure determinations of compounds **1-3** were performed at 173 K (**1**) and 123 K (**2-3**). The yellow prism crystal of **1** was covered with Paraton N oil and scooped up in a cryo-loop. The dark-red crystal of **2** and the dark-green crystal of **3** were attached to the tip of a glass fiber. These crystals were mounted on a Rigaku RAXIS RAPID imaging-plate area detector with graphite monochromated Mo-K_α radiation (λ = 0.071073 nm). The structures were solved by direct methods [26] and expanded using Fourier techniques [27]. Some non-hydrogen atoms for **1** were refined anisotropically, while the rest were refined isotropically. All non-hydrogen atoms for **2** and **3** were refined anisotropically. Hydrogen atoms were refined using the riding model. All calculations were performed using the CrystalStructure crystallographic software package [28-29]. Detail on the data collections and refinements are summarized in Table III-1. On the other hand, the rhombus-shaped polymorph crystal of **1** has crystal solvent and effloresces immediately in air, so that the crystal structure could not be solved even in Paratone oil.

Table III-1. Crystallographic data and structure refinement for $[Co^{II}(Tbz)_2]$, $[Co^{III}(Tm^{Me})_2](Tm^{Me})$ and $[Co^{II}(Tm^{Me})_2]\cdot 4H_2O$

	$[Co^{II}(Tbz)_2]$	$[Co^{III}(Tm^{Me})_2](Tm^{Me})$	$[Co^{II}(Tm^{Me})_2]\cdot 4H_2O$
Emprical formula	$C_{42}H_{26}B_2CoN_6S_{12}$	$C_{36}H_{48}B_3CoN_{18}S_9$	$C_{24}H_{40}B_2CoN_{12}O_4S_6$
Formula weight	1079.98	1112.80	833.57
Crystal system	Monoclinic	Monoclinic	Monoclinic
Space group	*C*2/c	$P2_1/a$	$P2_1/n$
a (Å)	19.038(3)	19.1540(5)	14.143(1)
b (Å)	13.142(2)	13.5985(4)	18.089(2)
c (Å)	18.141(3)	20.5414(6)	15.282(1)
α (°)	90	90	90
β (°)	103.467(5)	112.945(1)	102.382(2)
γ (°)	90	90	90
V (Å^3)	4414(1)	4927.0(3)	3818.6(5)
Z	4	4	4
T (K)	173	123	123
D_{calc} (g cm^{-3})	1.625	1.500	1.450
Crystal color, habit	yellow, prism	dark red, prism	dark green, block
Crystal dimensions (mm)	0.6 × 0.1 × 0.1	0.70 × 0.45 × 0.45	0.45 × 0.25 × 0.15
F_{000}	2196	2304.00	1732.00
μ(Mo K_α) (cm^{-1})	9.999	7.806	8.257
Total data	11094	15033	35290
Unique data	4729	10041	8685
R_{int}	0.1871	0.0346	0.0880
R_1 [$I > 2.0\sigma(I)$]	0.0893	0.0379	
wR_2 [$I > 2.0\sigma(I)$]	0.0932	0.0408	
R_1 [$I > 4.0\sigma(I)$]			0.0944
wR_2 [$I > 4.0\sigma(I)$]			0.1141
Goodness of fit	1.135	1.082	1.262

Chapter 10. Results and Discussion on $[Co^{II}(Tbz)_2]$ and $[Co^{II/III}(Tm^{Me})_2]^{0/+}$

10.1. Syntheses

$[Co^{II}(Tbz)_2]$ (**1**) (Tbz^- = hydrotris(2-mercaptobenzothiazolyl)borate) was synthesized by the reaction of a cobalt(II) salt and $^nBu_4NTbz$ which is a good starting material with high solubility in polar organic solvents. The complex is insoluble in water and most of common organic solvents, while soluble in DMF to decompose rapidly.

Meanwhile the preparation of S_3F_3-coordination cobalt(III) complex, highly likely to show high-spin state, initially was attempted starting from CoF_3. Because CoF_3 is sensitive to water, the powder was added promptly to an aqueous solution of soft S_3 tripodal ligands Tbz^- or Tm^{Me-} (hydrotris(2-mercapto-1-methylimidazolyl)borate). In the case of Tbz^-, yellow solid immediately precipitated at this moment, while in that of Tm^{Me-}, green solid immediately precipitated at this moment and fully turned to brown a few minute later.

On dissolution of CoF_3 in water, cobalt(II) ion is known to be the dominant species presented in the solution owing to rapid decomposition. Thus it is assumed that the low-solubility cobalt(II) complex precipitates as yellow solid for Tbz^-.

Another syntheses of $[Co^{III}(Tbz)_2]^-$ from other cobalt(III) materials were also attempted but failed. It is possible that Tbz^- immediately reduces cobalt(III) ion to afford neutral $[Co^{II}(Tbz)_2]$. On the other hand, in the case of Tm^{Me-}, it is likely that the low-solubility cobalt(II) complex precipitates as green solid at first and the residual cobalt(II) complex in the solution is readily oxidized into cobalt(III) cation, $[Co^{III}(Tm^{Me})_2]^+$. Soon after the cobalt(III) cation forms, it captures one unreacted Tm^{Me-} anion and precipitates as brown solid of the Tm^{Me-} salt. As a result, stoichiometric product $[CoF_3(Tm^{Me})]^-$ was not obtained and complex **1** formed instead.

Though the green product is not fully identified, it provides the dark green complex

$[Co^{II}(Tm^{Me})_2]\cdot 4H_2O$ (**3**) by recrystallization from an acetonitrile solution.

10.2. Molecular structure of complexes

Single crystal X-ray structure was determined for the complexes **1-3**. Selected bond lengths and angles for **1** are listed in Table III-2. The space group of **1** is *C*2/c and the cobalt(II) ion has a centrosymmetric octahedral S_6 coordination environment. It is a first report of $[Co^{II}S_6]$ core in the soft-scorpionate chemistry (Figure III-1). All Co–S distances are 2.489–2.535 Å and much longer than that of octahedral low-spin octahedral cobalt(II) complexes with thioether ligands (Table III-3) [2-3, 30]. The ∠S-Co-S bite angles in a same Tbz^- moiety vary from 92.0 to 99.5°, while other ∠S-Co-S angles defined for two S atoms originating from different Tbz^- moieties are less than 90°. It means the coordination octahedron in $[Co^{II}(Tbz)_2]$ is slightly compressed along its pseudo-C_3 axis (Figure III-2).

Table III-2. Selected bond distances (Å) and angles (°) for $[Co^{II}(Tbz)_2]$.

Co1–S1	2.489(3)	S1–Co1–S2	99.5(1)
Co1–S2	2.535(3)	S2–Co1–S3	92.0(1)
Co1–S3	2.451(3)	S3–Co1–S1	95.8(1)

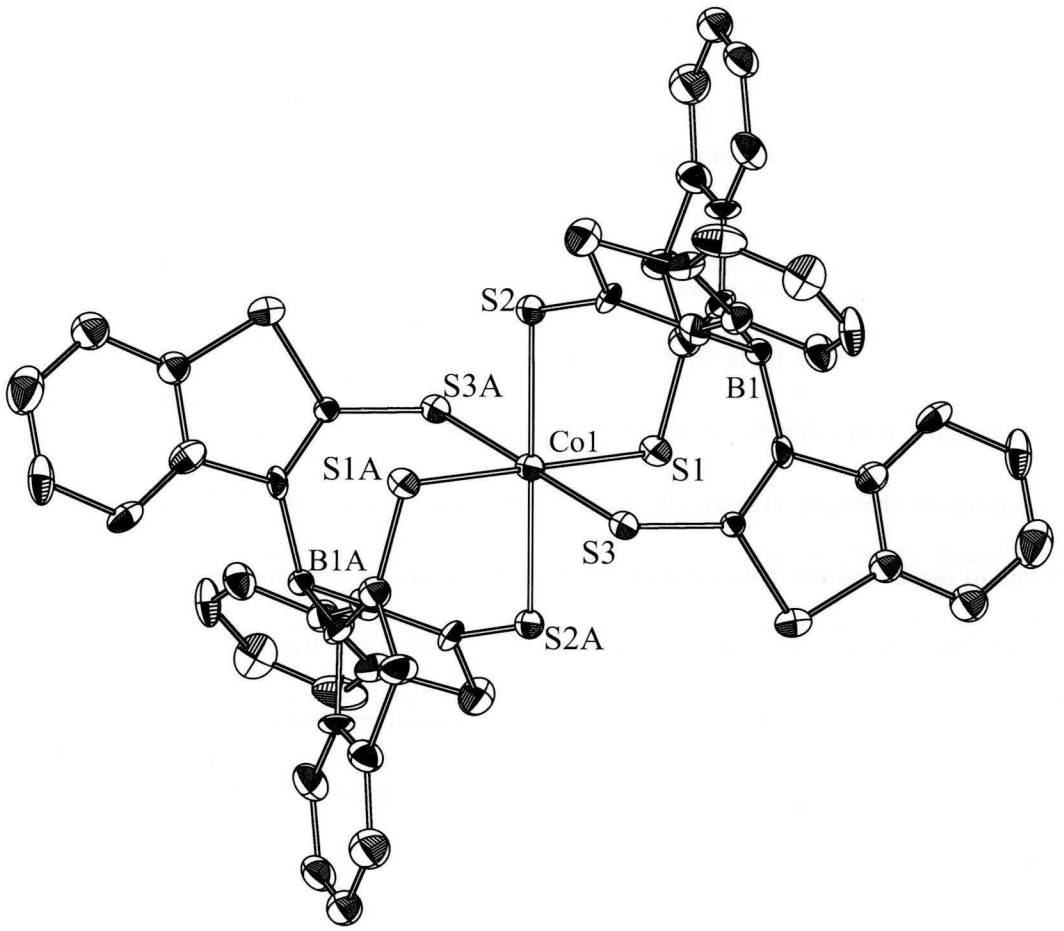

Figure III-1. Molecular structure of $[Co^{II}(Tbz)_2]$ with thermal ellipsoids drawn at 50% probability level. Hydrogen atoms are omitted for clarity.

Table III-3. Comparison of structural data for $[Co^{II}S_6]$ complexes.

complex	spin state	average Co-S / Å	references
$[Co^{II}(Tbz)_2]$	HS	2.492(3)	this work
$[Co^{II}(9S3)_2]^{2+}$ [a]	LS	2.321(5)	[5]
$[Co^{II}(10S3)]^{2+}$ [b]	LS	2.324(4)	[6]
$[Co^{II}(Ttn)_2]^{2+}$ [c]	LS	2.372(3)	[3]
$[Co^{II}(PhTt)_2]$ [d]	LS	2.383(1)	[30]

[a] 9S3 = 1,4,7-trithiacyclononane. [b] 10S3 =1,4,7- trithiacyclodecane.

[c] Ttn = 2,5,8-trithianonane. [d] PhTt = phenyltris((methylthio)methyl)borate.

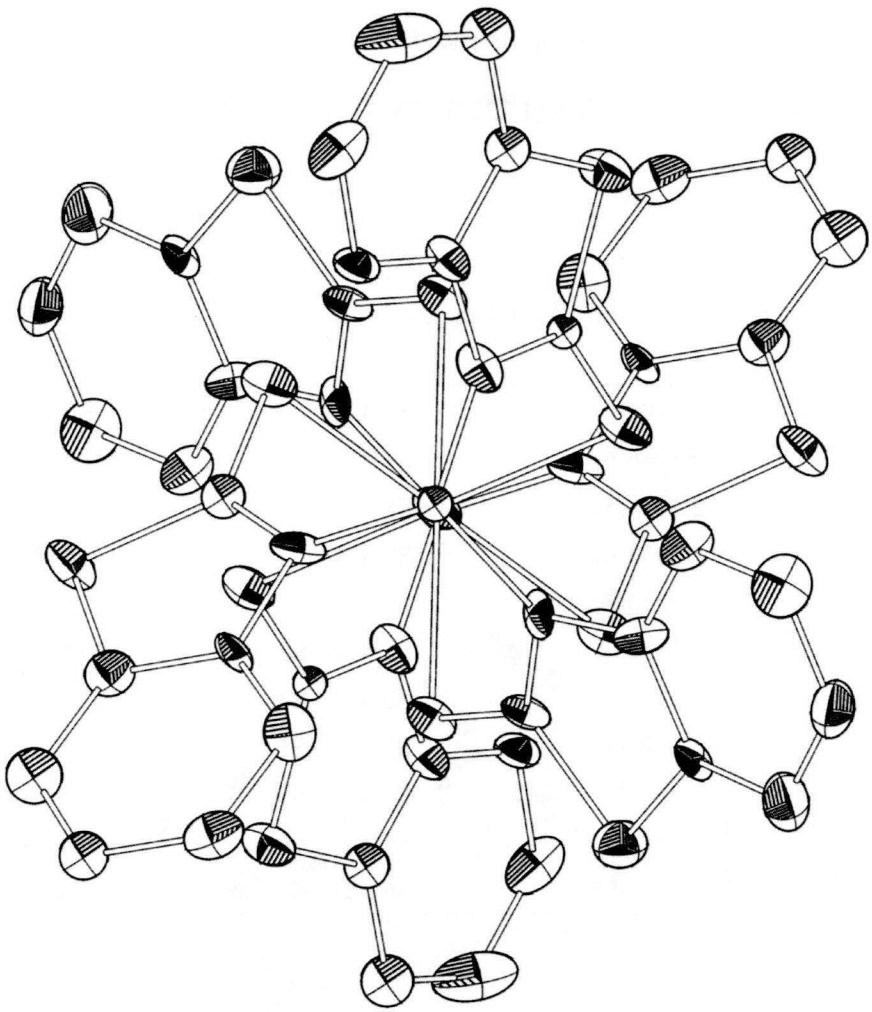

Figure III-2. Top view of $[Co^{II}(Tbz)_2]$ along B···Co···B direction.

Selected bond distances and angles for $[Co^{III}(Tm^{Me})_2](Tm^{Me})$ (**2**) are listed in Table III-4. The space group of **2** is $P2_1/a$. An imidazole ring in $[Co^{III}(Tm^{Me})_2]^+$ moiety and another ring in counter anion, Tm^{Me-} are mutually slant-stacked with the π-π distance of ~3.4 Å (Figure III-3). The cobalt(III) ion of **2** is hexacoordinate. Co–S distances fall in the range of 2.293–2.321 Å and are slightly shorter than that of other reported $[Co^{III}(Tm^{Me})_2]^+$ moiety (Table III-5) [19], while much shorter than that of $[Co^{II}(Tbz)_2]$. The ∠S–Co–S bite angles in which S-atoms come from a same Tm^{Me-} moiety vary from 93.09 to 97.26°, while all the ∠S–Co–S angles defined for two S atoms originating from different Tm^{Me-} moieties are less than 90°. It means the coordination octahedron in

complex **2** is slightly compressed along its pseudo-C_3 axis (Figure III-4). The C=S thione group bond lengths of $[Co^{III}(Tm^{Me})_2]^+$ moiety (1.722–1.738 Å) is longer than that of counter anion Tm^{Me-} (1.697–1.700 Å).

Table III-4. Selected bond distances (Å) and angles (°) for $[Co^{III}(Tm^{Me})_2](Tm^{Me})$.

Co1–S1	2.3109(6)	S6–C21	1.726(3)
Co1–S2	2.3066(6)	S7–C25	1.699(3)
Co1–S3	2.2934(5)	S8–C29	1.700(3)
Co1–S4	2.2934(6)	S9–C33	1.697(3)
Co1–S5	2.3213(5)		
Co1–S6	2.3111(6)	S1–Co1–S2	93.09(2)
S1–C1	1.732(3)	S2–Co1–S3	97.26(3)
S2–C5	1.722(3)	S3–Co1–S1	96.37(3)
S3–C9	1.731(3)	S4–Co1–S5	95.55(3)
S4–C13	1.728(3)	S5–Co1–S6	95.076(18)
S5–C17	1.738(3)	S6–Co1–S4	95.51(2)

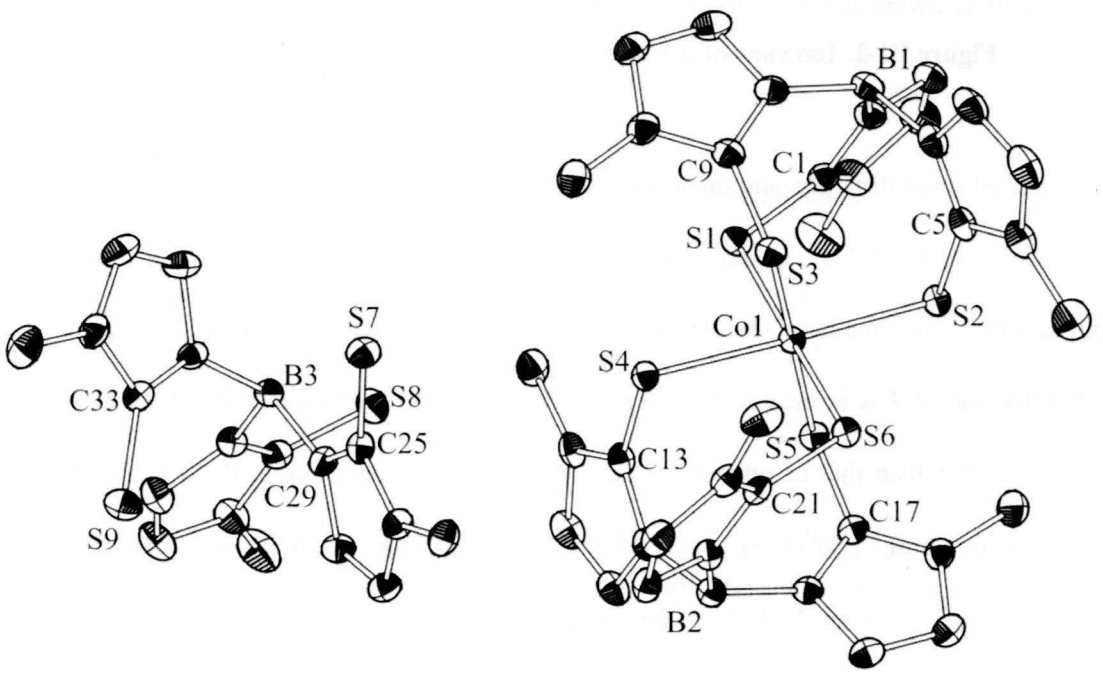

Figure III-3. Crystal structure of $[Co^{III}(Tm^{Me})_2](Tm^{Me})$ with thermal ellipsoids drawn at 50% probability level. Hydrogen atoms are omitted for clarity.

Table III-5. Comparison of Co–S bond distances (Å) for $[Co^{III}(Tm^{Me})_2]Y$.

$Y = Tm^{Me-}$	BF_4^-
2.3109	2.327
2.3066	2.326
2.2934	2.317
2.2934	2.311
2.3213	2.312
2.3111	2.304

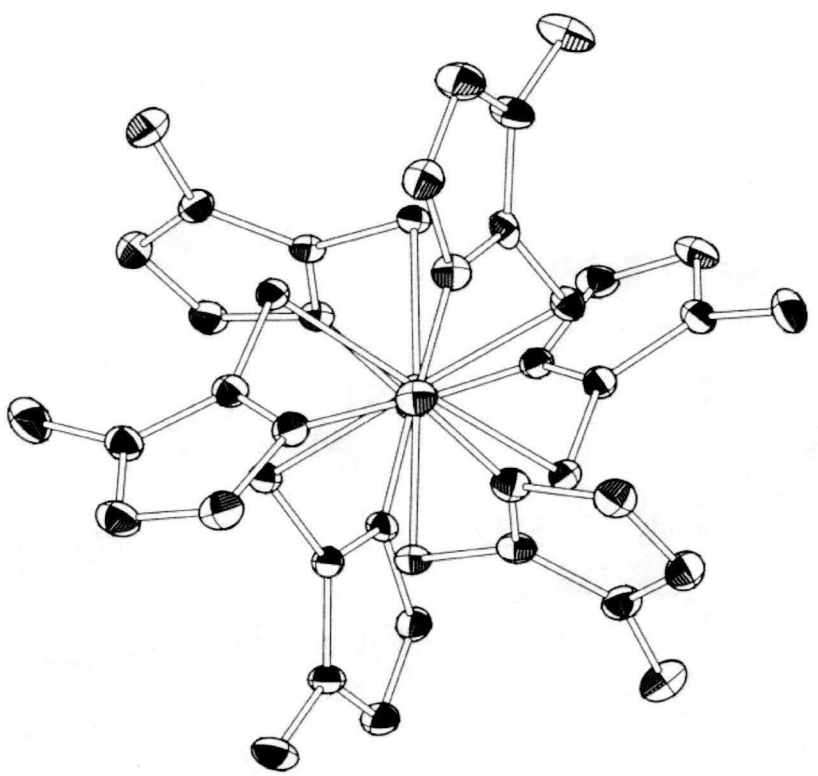

Figure III-4. Top view of $[Co^{III}(Tm^{Me})_2](Tm^{Me})$ along B···Co···B direction.

Complex **3** exhibits tetracoordinate tetrahedral structure and the space group is $P2_1/n$. The average Co–S bond distance is 2.36 Å (Table III-6) and shorter than that of $[Co^{II}(Tm^{Me})_2]$ analogue (Table III-7) [20-21] and fall between that of complex **1** and **2**. The ∠S–Co–S bite angles are 109.28° and 114.72°, so the tetrahedral structure of **3** is slightly distorted (Figure III-5).

Table III-6. Selected bond distances (Å) and angles (°) for $[Co^{II}(Tm^{Me})_2]\cdot 4H_2O$.

Co1–S1	2.375(2)	Co1–S2	2.391(3)
Co1–S4	2.345(3)	Co1–S5	2.3402(19)
S1–Co1–S2	114.72(8)	S4–Co1–S5	109.28(8)

Table III-7. Comparison of Co–S bond distances (Å) for tetrahedral soft tripodal cobalt(II) complexes.

$[Co^{II}(Tm^{Me})_2]$	$[Co^{II}(Tm^{tBu})_2]$[20]	$[Co^{II}(Tm^{Ph})_2]$[21]
2.375	2.3804	2.370
2.391	2.3607	2.372
2.345		
2.340		

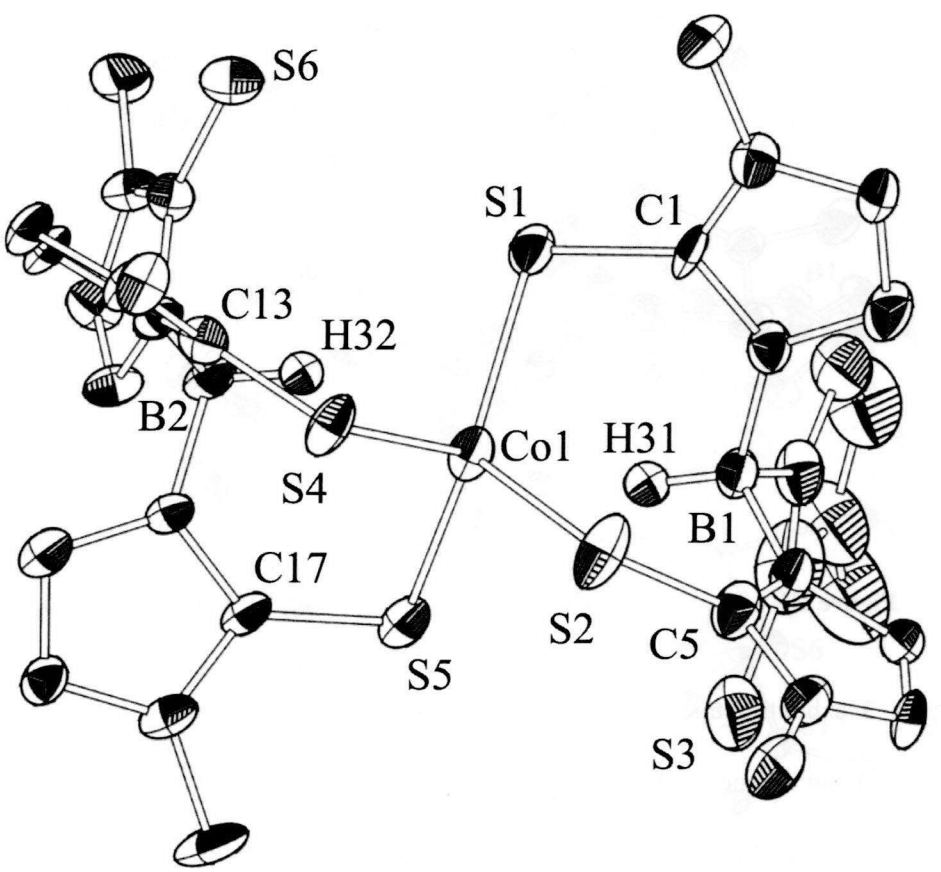

Figure III-5. Crystal structure of $[Co^{II}(Tm^{Me})_2]\cdot 4H_2O$ with thermal ellipsoids drawn at 50% probability level. Some of hydrogen atoms are omitted for clarity.

10.3. X-ray photoelectron spectra

The X-ray photoelectron spectra of complexes **1-3** were measured (Figure III-6).The spectrum of **1** showed Co(2p1/2) and Co(2p3/2) peaks at 795.5 and 780.0 eV, respectively, both of which are associated with shake-up satellites at higher binding energies characteristic to cobalt(II) compounds [26]. The Co(2p1/2)–Co(2p3/2) energy separation (spin-orbit splitting) was 15.5 eV, much larger than the cobalt(III) norm of 15.0 eV. The spin-orbit splitting of complex **3** was also 15.5 eV and again shake-up satellites were observed. On the other hand, the spin-orbit splitting of complex **2** was 15.0 eV and no satellite peaks were found. These results certify the valence state of complex **1** is +2 and reject the possibility of a valence tautomer [$Co^{III}(Tbz^{-})(Tbz^{\bullet 2-})$]. Taking into account the fact that the low-spin cobalt(II) compounds do not show remarkable satellites [31], it is consistent to conclude complex **1** to be a high-spin cobalt(II) complex.

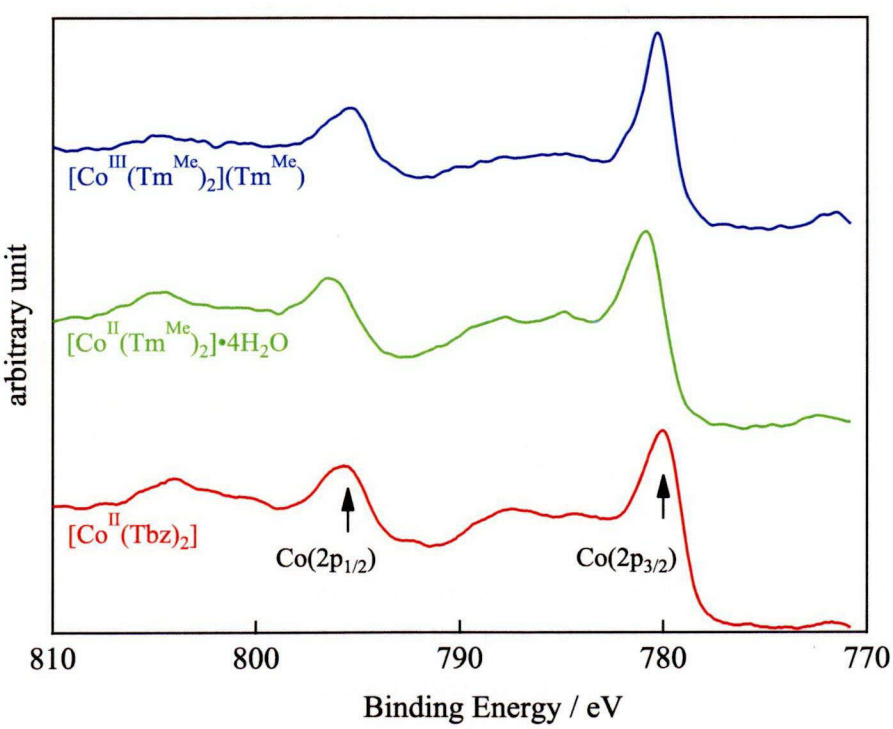

Figure III-6. The Co(2p) spectra of complexes $[Co^{II}(Tbz)_2]$, $[Co^{III}(Tm^{Me})_2](Tm^{Me})$, and $[Co^{II}(Tm^{Me})_2]\cdot 4H_2O$. These spectra were normalized at the $Co(2p_{3/2})$ peak.

10.4. Magnetic properties

Isofield magnetizations of complexes **1-3** were measured from 3 to 350 K (**1**) and from 4 to 330 K (**2-3**). The effective magnetic moments μ_{eff} of complex **1** increased gradually with heating to 4.8 μ_B at room temperature (Figure III-7), which is indicative of the high-spin electron configuration of cobalt(II) (S = 3/2). Over the range of measurement temperature, complex **2** indicated diamagnetic behavior, so complex **2** is typical low-spin cobalt(III) species. Complex **3** showed effective magnetic moments μ_{eff} of 4.4 μ_B at room temperature (Figure III-8), which was somewhat higher than the expected value 3.9 μ_B for a high-spin cobalt(II) (S = 3/2). This value is about the same as the analog of compound **3** [20]. This behavior may arise from mixing of low-energy excited states in tetrahedral complexes with small ligand-field splitting.

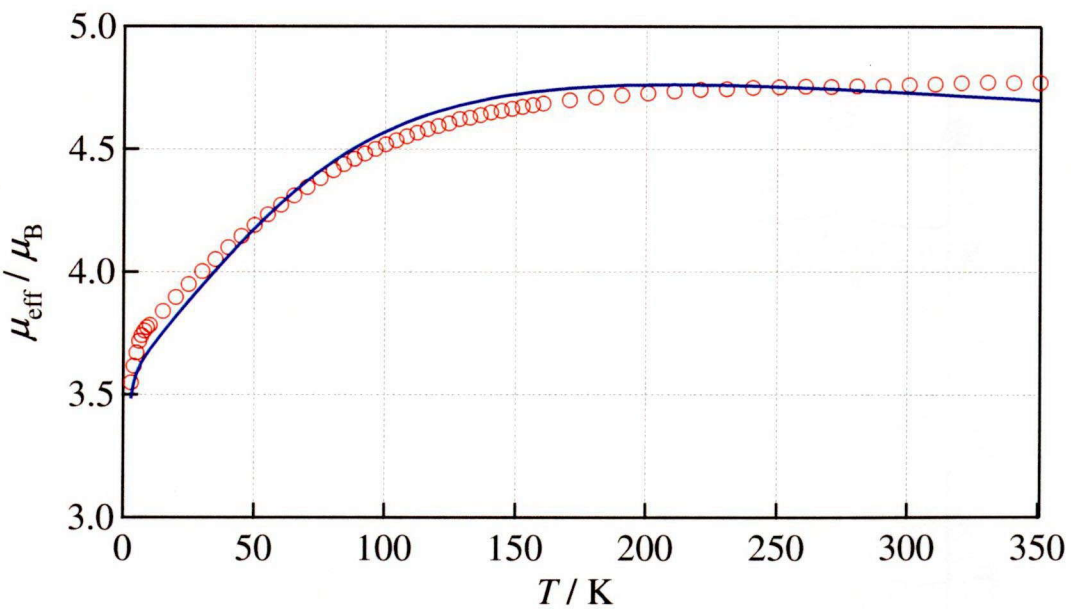

Figure III-7. The temperature dependence of effective magnetic moment of a polycrystalline [$Co^{II}(Tbz)_2$] recorded on a SQUID at 1.0 T. Open circles denote observed values and the solid curve is simulated by using parameters Δ_0 / hc = 8000 cm^{-1}, B / hc = 560 cm^{-1}, ζ / hc = 515 cm^{-1}, C / B = 3.1, and k = 0.74.

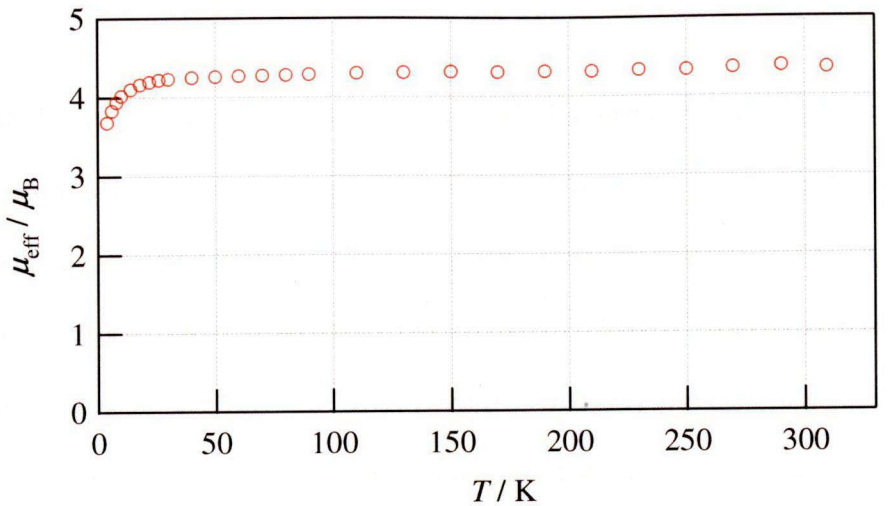

Figure III-8. The temperature dependence of effective magnetic moment of a polycrystalline $[Co^{II}(Tm^{Me})_2]\cdot 4H_2O$ recorded on a SQUID at 1.0 T.

For reference, the powder of $[Co^{II}(Tbz)_2]$ including impurity was obtained from the attempt of syntheses of $[Co^{III}(Tbz)_2]^-$. Isofield magnetization of this compound was measured from 2 to 300 K under applied high pressure 0.7 GPa (Figure III-9). Compared to ambient pressure 0.1 MPa, decrease of the effective magnetic moment below 150 K was observed. It is possible that pressure induced low-spin transition of $[Co^{II}(Tbz)_2]$ component occurs.

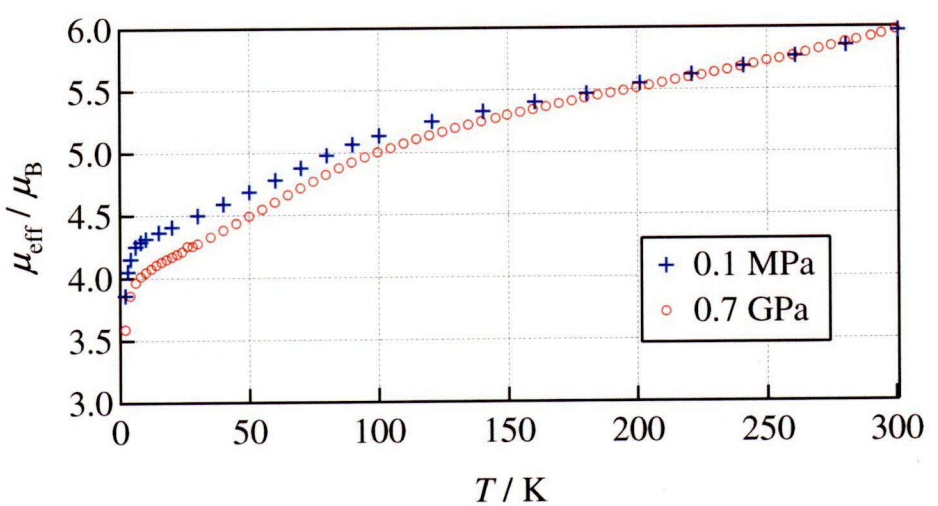

Figure III-9. The temperature dependence of effective magnetic moment of polycrystalline $[Co^{II}(Tbz)_2]$ including impurity recorded on a SQUID at 1.0 T under ambient pressure 0.1 MPa (+) and applied pressure 0.7 Gpa (○).

10.5. Electron absorption spectra

The electronic spectrum of complex **1** shows a strong absorption band at around 20000 cm^{-1} (ligand π-π*transition) and at 22000 cm^{-1} (MLCT). In addition, it has two weak *d-d* bands around 14700 cm^{-1} and 7140 cm^{-1} (Figure III-10). Assuming the O_h symmetry, the former can be assigned to $^4T_{1g} \rightarrow {}^4T_{1g}$(P) and the latter to $^4T_{1g} \rightarrow {}^4T_{2g}$(F). Similar *d-d* transitions were also reported in the diffuse reflectance spectrum of high-spin $[Co^{II}(DCTU)_6](NO_3)_2$ (DCTU = *N,N'*-dicyclohexylthiourea) [13]. Based on these *d-d* transitions, the ligand field splitting and the Racah's parameter were estimated as Δ_0 / hc = 8000 cm^{-1} and B / hc = 560 cm^{-1}, respectively [32]. The magnitude of Δ_0 is relatively low in comparison to that of hexaaqua cobalt(II) complex (8400 cm^{-1}) [33], and B is much smaller than the free ion value (B_0 / hc = 989 cm^{-1}) [34] and that reported for other thioamide complexes [13-14]. This value is even comparable to that of the thiacrown complex $[Co^{II}(18S6)]^{2+}$ with a low-spin $[Co^{II}S_6]$ center (B / hc = 580 cm^{-1}) attributable to large nepelauxetic effect [3,7]. These results suggest the complex **1** has also significantly covalent coordination bonds arising a remarkable nephelauxetic effect. By using these values of Δ_0 and B, ligand-field calculations were carried out to simulate the magnetic susceptibility curve. Non-linear least squares fittings to the magnetic susceptibility were performed with fixed parameters Δ_0 and B and adjustable parameters of the Racah's parameter C, spin-orbit coupling ζ, and Stevens' orbital reduction factor k. Optimized reduction factor k for given ζ and C / B ratio is mapped on a contour plot in Figure III-11. A cross on the map stands for a best-fitting parameter set (ζ / hc = 515 cm^{-1}, C / B = 3.1, k = 0.74) determined for the spin-orbit coupling fixed to the free-ion value [34], which yield a simulation curve in Figure III-12. The small k value also suggests intense delocalization of *d*-electrons over the ligands, weakening electron-electron repulsion on the cobalt ion.

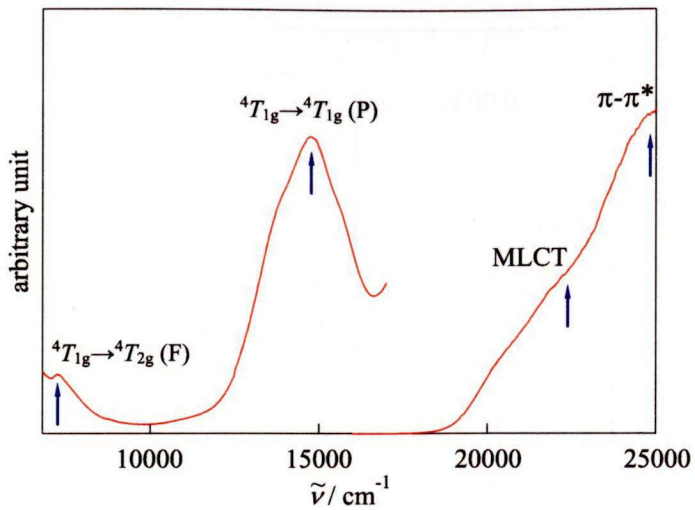

Figure III-10. Diffuse reflectance spectra of $[Co^{II}(Tbz)_2]$ recorded for a powder sample (left) and a KBr-diluted sample (right) at room temperature.

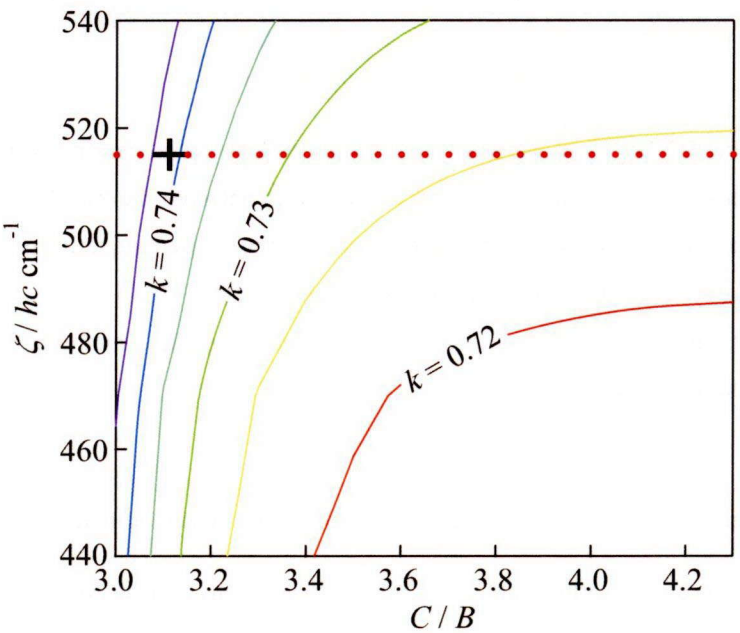

Figure III-11. Contour map of Stevens' orbital reduction factor k on a parameter plane of the spin-orbit coupling ζ and the ratio between the Racah's parameters C / B, determined by non-linear least-squares fitting to the magnetic susceptibility. A cross (+), placed at the point of ζ /hc = 498 cm^{-1}, C / B = 3.1, and k = 0.74, corresponds to the simulation curve in Figure III-7. The spin orbit-coupling for a free cobalt(II) ion is shown as a dotted line.

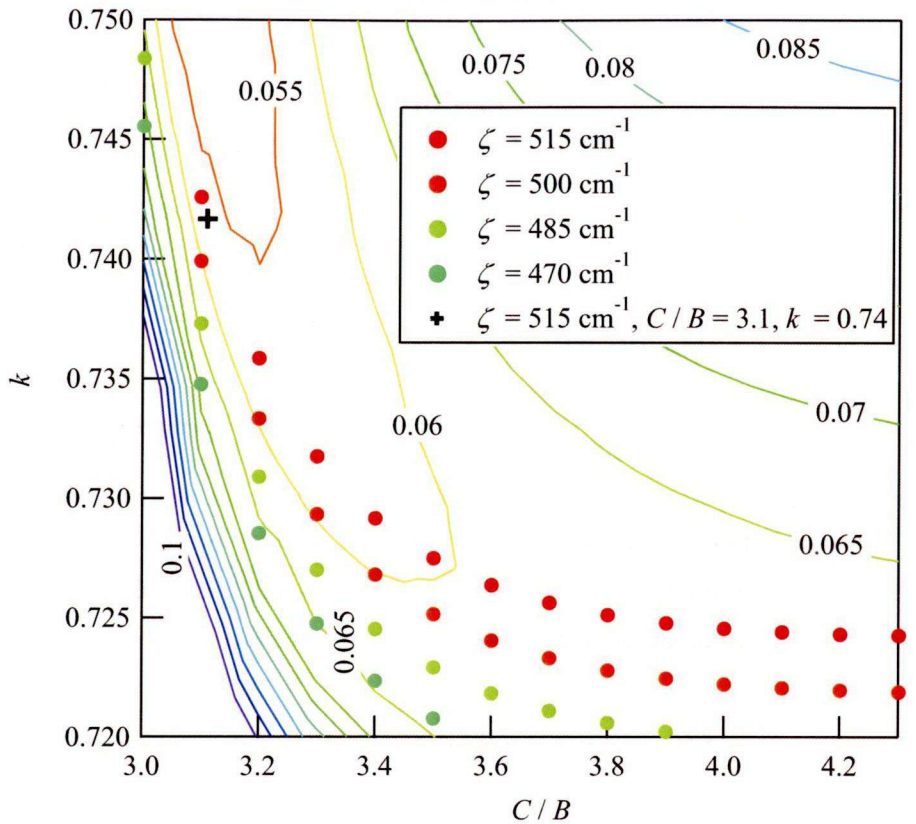

Figure III-12. Contour map of fitting residual on a parameter plane of the Stevens' orbital reduction factor k and the ratio between the Racah's parameters C / B, calculated by non-linear least-squares fitting to the magnetic susceptibility. A cross (+) stands for a best-fitting parameter set (ζ / hc = 515 cm^{-1}, C / B = 3.1, k = 0.74). Filled circles denote k values optimized for given ζ and C / B values using the magnetic data.

The electronic spectrum of complex **2** (3.1×10^{-5} M) in acetonitrile solution shows a strong absorption band at around 40000 cm^{-1} (ligand π-π*transition) and the splitting bands on MLCT at 25000 cm^{-1} (ε = 32800 mol^{-1} L cm^{-1}) and 21000 cm^{-1} (ε = 18700 mol^{-1} L cm^{-1}). In addition, it has weak *d-d* band around 12500 cm^{-1} (ε = 280 mol^{-1} L cm^{-1}) (Figure III-13). Assuming the O_h symmetry, the former can be assigned to $^1A_{1g}\rightarrow{}^1E_g$. Generally another *d-d* band assigned to $^1A_{1g}\rightarrow{}^1A_2$ for low-spin octahedral cobalt(III) complexes is observed but may be hidden by the presence of MLCT bands. Although the *d-d* band for $A_{1g}\rightarrow{}^1E_g$ is lower than that of hexaaqua cobalt(III) complex (16500

cm^{-1}) [35], complex **2** possess low-spin configuration. It is conceivable that the reason is the stabilization of low-spin configuration from large nephelauxetic effect for soft-scorpionate ligand Tm^{Me-}.

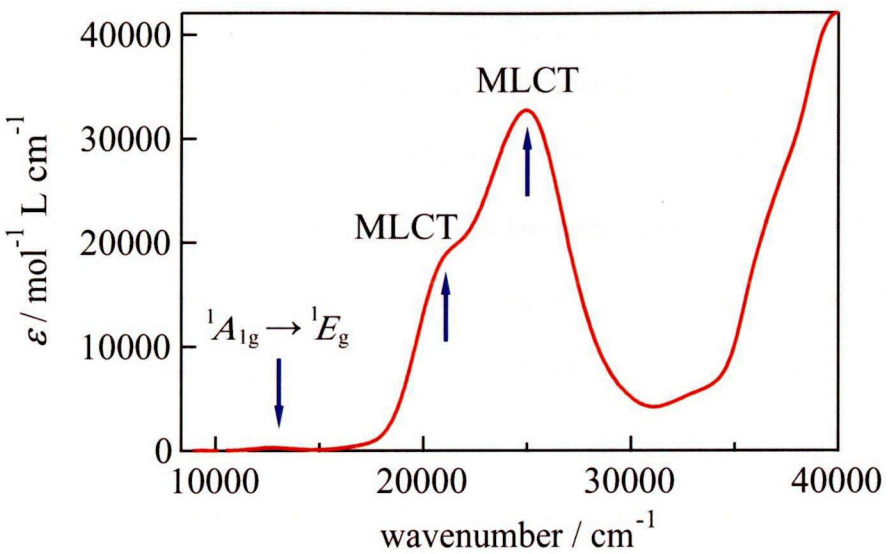

Figure III-13. Electron absorption spectrum of $[Co^{III}(Tm^{Me})_2](Tm^{Me})$, 3.1×10^{-5} M in CH_3CN.

Chapter 11. Conclusion of $[Co^{II}(Tbz)_2]$ and $[Co^{II/III}(Tm^{Me})_2]^{0/+}$

A novel cobalt(II) soft-scorpionate complex $[Co^{II}(Tbz)_2]$ (Tbz^- = hydrotris(2-mercaptobenzo-thiazolyl)borate) was synthesized. Single-crystal X-ray analysis revealed that this complex has a $[Co^{II}S_6]$ center, which is a first case distinguished from $[Co^{III}S_6]$ or $[Co^{II}S_4]$ soft-scorpionate complexes [19-21]. The diffuse reflectance spectrum of $[Co^{II}(Tbz)_2]$ and the electron absorption spectrum of $[Co^{III}(Tm^{Me})_2](Tm^{Me})$ (Tm^{Me-} = (hydrotris(2-mercapto-1-methylimidazolyl)borate) demonstrated that the soft-scorpionate Tbz^- and Tm^{Me-} ligand gives a small ligand-field splitting and a strong nephelauxetic effect. The ligand-field parameters derived from the electronic spectrum of $[Co^{II}(Tbz)_2]$ were successfully served in the analysis of magnetic susceptibility. Remarkable delocalization of *d*-electron onto the ligand moieties was also suggested from the simulation of the magnetic behavior. On tuning of these parameter, soft scorpionate ligands are expected to give paramagnetic cobalt(III) complexes and polynuclear cobalt(II) complexes which possess high-spin ground state.

References for Part III

[1] S. R. Cooper, Acc. Chem. Res. 21 (1988) 141.

[2] K. Wieghardt, H.-J. Küppers, J. Weiss, Inorg. Chem. 24 (1985) 3067.

[3] J. R. Hartman, E. J. Hintsa, S. R. Cooper, J. Am. Chem. Soc. 108 (1986) 1208.

[4] D. Sellmann, H.-P. Neuner, F. Knoch, Inorg. Chim. Acta 190 (1991) 61.

[5] W. N. Setzer, C. A. Ogle, G. S. Wilson, R. S. Glass, Inorg. Chem. 22 (1983) 266.

[6] W. N. Setzer, E. L. Cacioppo, Q. Guo, G. J. Grant, D. D. Kim, J. L. Hubbard, D. G. VanDerveer, Inorg. Chem. 29 (1990) 2672.

[7] G. J. Grant, C. G. Brandow, C. W. Bruce, M. A. Bryant, R. M. Kirk, S. D. Lee, K. R. Rickerd, L. F. Mehne, J. Hetrocycl. Chem. 38 (2001) 1281.

[8] K. Fukui, N. Kojima, H. Ohya-Nishiguchi, N. Hirota, Inorg. Chem. 31 (1992) 1338.

[9] M. T. Ashby, N. A. Sheshtawy, Organometallics 13 (1994) 236.

[10] P. A. Fox, M. A. Bruck, S. D. Grey, N. E. Gruhn, C. Grittini, D. E. Wigley, Organometallics 17 (1998) 2720.

[11] W. R. W. Welch, S. Harris, Inorg. Chim. Acta 361 (2008) 3012.

[12] (a) E.-C. Yang, D. N. Hendrickson, W. Wernsdorfer, M. Nakano, L. N. Zakharov, R. D. Sommer, A. L. Rheingold, M. Ledezma-Gairaud, G. Christou, J. Appl. Phys. 91 (2002) 7382.

(b) K. W. Galloway, A. M. Whyte, W. Wernsdorfer, J. Sanchez-Benitez, K. V. Kamenev, A. Perkin, R. D. Peacock, M. Murrie, Inorg. Chem. 47 (2008) 7438.

(c) D. Wu, D. Guo, Y. Song, W. Huang, C. Duan, Q. Meng, O. Sato, Inorg. Chem. 48 (2009) 7413.

(d) F. Klöwer, Y Lan, J. Nehrkorn, O. Waldmann, C. E. Anson, A. K. Powell, Chem. Eur. J. 15 (2009) 7413.

(e) M. Murrie, S. J. Teat, H. Stœckli-Evans, H. U. Güdel, Angew. Chem. Int. Ed. 42 (2003)

4653.

(f) Y.-Z. Zhang, W. Wernsdorfer, F. Pan, Z.-M. Wang, S. Gao, Chem. Commun. (2006) 3302.

(g) S. J. Langley, M. Helliwell, R. Sessoli, P. Rosa, W. Wernsdorfer, R. E. P. Winpenny, Chem. Commun. (2005) 5029.

(h) M.-H. Zeng, M.-X. Yao, H. Liang, W.-X. Zhang, X.-M. Chen, Angew. Chem. Int. Ed. 46 (2007) 1832.

(i) M. Marrie, Chem. Soc. Rev. 39 (2010) 1986.

[13] R. Hoppe, Recl. Trav. Chim. Pays-Bas 75 (1956) 569.

[14] H. C. Clark, B. Cox, A. G. Sharpe, J. Chem. Soc. (1957) 4132.

[15] G. Yagupsky, R. Levitus, Inorg. Chem. 4 (1965) 1589.

[16] G. Peyronel, G. C. Pellacani, A. Pignedoli, G. Benneti, Inorg. Chim. Acta 5 (1971) 263.

[17] M. Garner, J. Regrinski, I. Cassidy, M. D. Spicer, A. R. Kennedy, J. Chem. Soc., Chem. Commun. (1996) 1975.

[18] (a) L. Maria, A. Paulo, I. C. Santos, I. Santos, P. Kurz, B. Springer, R. Alberto, J. Am. Chem. Soc. 128 (2006) 14590.

(b) M. D. Spicer, J. Regrinski, Eur. J. Inorg. Chem. (2009) 1553.

(c) G. Dyson, A. Hamilton, B. Mitchell, G. R. Owen, Dalton Trans. (2009) 6120.

(d) R. Garcia, A. Paulo, I. Santos, Inorg. Chim. Acta 362 (2009) 4315.

[19] C. A. Dodds, M.-A. Lehmann, J. F. Ojo, J. Reglinski, M. D. Spicer, Inorg. Chem. 43 (2004) 4927.

[20] D. J. Mihalcik, J. L. White, J. M. Tanski, L. N. Zakharov, G. P. A. Yap, C. D. Incarvito, A. L. Rabinnovich, Dalton Trans. (2004) 1626.

[21] C. Kimblin, D. G. Churchill, B. M. Bridgewater, J. N. Girard, D. A. Quarless, G. Perkin, Polyhedron 20 (2001) 1891.

[22] J. F. Ojo, P. A. Slavin, J. Regrinski, M. Garner, M. D. Spicer, A. R. Kennedy, S. J. Teat, Inorg. Chim. Acta 313 (2001) 15.

[23] W. Kläui, J. Chem. Soc. Chem. Commun. (1979) 700.

[24] J. Reglinski, M. Garner, I. D. Cassidy, P. A. Slavin, M. D. Spicer, D. R. Armstrong, J. Chem. Soc., Dalton Trans. (1999) 2119.

[25] P. J. Bailey, D. J. Lorono-Gonzales, C. McCormack, S. Parsons, M. Price, Inorg. Chim. Acta 354 (2003) 61.

[26] SIR92: A. Altomare, G. Cascarano, C. Giacovazzo, A. Guagliardi, M. Burla, G. Polidori, M. Camalli, J. Appl. Cryst. 27 (1994) 435.

[27] DIRDIF99: P. T. Beurskens, G. Admiraal, G. Beurskens, W. P. Bosman, R. de Gelder, R. Israel, J. M. M. Smits, (1999). The DIRDIF-99 program system, Technical Report of the Crystallography Laboratory, University of Nijmegen, The Netherlands.

[28] CrystalStructure 4.0: Crystal Structure Analysis Package, Rigaku and Rigaku Americas (2000-2007). 9009 New Trails Dr., The Woodlands, TX 77381, USA.

[29] CRYSTALS Issue 11: J. R. Carruthers, J. S. Rollett, P. W. Betteridge, D. Kinna, L. Pearce, A. Larsen, E. Gabe, Chemical Crystallography Laboratory, Oxford, UK. 1999.

[30] C. Ohrenberg, P. Ge, P. J. Schebler, C. G. Riodan, G. P. A. Yap, A. L. Rheingold, Inorg. Chem. 35 (1996) 749.

[31] D. C. Frost, C. A. McDowell, I. S. Woolsey, Mol. Phys. 27 (1974) 1473.

[32] A. B. P. Lever, J. Chem. Educ. 45(1968) 711.

[33] D. A. Johnson, P. G. Nelson, Inorg. Chem. 34 (1995) 5666.

[34] B. N. Figgis, M. A. Hitchman, Ligand Field Theory and its Application, Wiley-VCH, New York, 2000.

[35] A. B. P. Lever, Inorganic Electronic Spectroscopy, Elsevier, Amsterdam, 2nd edn., 1968.

Summary

The present dissertation is intended to deliver some ideas on rational molecular design of paramagnetic polynuclear complexes through the theoretical analysis of magnetic and spectroscopic properties of mononuclear manganese(III) and cobalt(II) complexes. The contents are constructed in two Parts following a concise General Introduction in Part I.

In Part II, a series of octahedral manganese(III) complexes were synthesized, of which axial ligands were chosen among a variety of monodentate ligands, while the equatorial ligand was kept to be tetradentate cyclam (1,4,8,11-tetraazacyclotetradecane) across the series. The magnetic measurements of them revealed that the electron configuration depends on the nature of axial ligands to be high-spin or low-spin complexes. Axial ligands of cyanoborohidride derivatives exert a relatively strong ligand field, despite not enough to yield a low-spin complex, to invest a large easy-axis magnetic anisotropy. The combined application of angular-overlap method (AOM) and extended Hückel molecular-orbital calculations confirmed that stronger axial ligands, just neighboring to spin-crossover boundary, bring about larger magnetic anisotropy of axially elongated high-spin manganese(III) complexes.

In Part III, several sulfur-coordinate cobalt(II/III) complexes of soft-scorpionate ligands were synthesized, which can be grouped into $[Co^{II}S_6]$, $[Co^{III}S_6]$, and $[Co^{II}S_4]$ coordination centers. Single-crystal X-ray analysis revealed that one of the cobalt(II) complexes has a $[Co^{II}S_6]$ center, which is a first case distinguished from already-known $[Co^{III}S_6]$ or $[Co^{II}S_4]$ soft-scorpionate complexes. X-ray photoelectron spectroscopic and magnetic measurements demonstrated that this complex has a high-spin cobalt(II) metal center of $[Co^{II}(L)]$-type electron configuration and rejected

the possibility of valence tautomer [$Co^{III}(L^{\bullet-})$]. Small ligand-field splitting and also small Racah's parameters determined from the electronic spectrum of the [$Co^{II}S_6$] complex were successfully transferred in the analysis of magnetic susceptibility. Remarkable delocalization of *d*-electron onto the ligand moieties was also suggested from the simulation of the magnetic behavior.

These findings on high-spin [$Mn^{III}N_6$] and [$Co^{II}S_6$] cores presented how the electronic ground state of a mononuclear metal complex unit is controlled by chemical modification of coordination environment. In order to address engineering the magnetic anisotropy of nanomagnets, *e.g.* single moleclule magnets, these results should contribute to the rational design of the paramagnetic polynuclear complexes.

List of Publications

Part II.

1. Magnetostructural Examination of Mn(III) Complexes $[Mn(cyclam)X_2]^+$ with Strong Axial Ligands

   Haruyuki Baba and Motohiro Nakano

   Polyhedron 28 (2009) 2087.

Part III.

2. Magnetic Properties of Cobalt(II/III) Complexes with Sulfur-Scorpionate Ligands

   Haruyuki Baba and Motohiro Nakano

   Polyhedron 30 (2011) 3182.

3. Magnetic and Spectroscopic Characterizations of High-Spin Cobalt(II) Complex with Soft-Scorpionate Ligand

   Haruyuki Baba and Motohiro Nakano

   Inorganic Chemistry Communications 17 (2012) 177.

Acknowledgments

First of all, the author would like to express his most sincere gratitude to his Ph.D supervisor, Associate Professor Motohiro Nakano for his invaluable instructions, helpful suggestions, untiring patience, and hearty encouragement to the author. Without them, the author cannot complete this dissertation. The author would also like to express his gratefully appreciation to Professor Shu Seki for his insightful suggestions and comments, vital encouragements to the author, and reviewing this dissertation.

The author is deeply indebted to Professor Sensuke Ogoshi for reviewing this dissertation and providing relevant comments.

The author is also grateful to Assistant Professor Akinori Saeki for his valuable suggestions, generous encouragements to the author.

The author is grateful to Dr. Tetsusya Takeuchi at Low Temperature Center and Professor Takayoshi Kuroda-Sowa in Kinki University for magnetic measurements. The author also thanks so much Professor Yuko Hosokoshi in Osaka Prefecture University for magnetic measurement under applied pressure. The author would like to thank sincerely Dr. Nobuko Kanehisa for her useful suggestions and technical advices in X-ray crystal structure determinations.

Elemental analyses were carried out by Mr. Kunihiko Kamon and Mr. Masahiro Matsuoka, and X-ray photoelectron spectra were recorded by Dr. Seiji Watase in Osaka Municipal Technical Reserch Institute. The author expresses his sincere thanks to them, and hears with deep regret of the passing of Mr. Matsuoka.

The author acknowledges financial supports from the Ushio Foundation and the Japan Student Service Organization.

The author also expresses appreciation to Dr. Hiroaki Iguchi, Mr. Ryuta Ishikawa, Dr. Koichi

Kagesawa, Dr. Masaaki Omichi, Dr. Yoshiko Koizumi, Dr. Kazuyuki Enomoto, Dr. Vijayakumar Chakkooth, Dr. Bijitha Balan, and Dr. Prasankumar Seelam for their kind encouragements and advice.

The author also thanks Mr. Yoshihito Honsho, Mr. Shogo Watanabe, Mr. Masanori Kashine, Mr. Tadakazu Itoh, Ms. Shima Nakanishi, Mr. Sohei Enomoto, Mr. Atsushi Asano, Mr. Yuta Maeyoshi, Mr. Takahiro Fukumatsu, Mr. Masashi Tsuji, Mr. Takenori Fujiwara, Ms. Hiromi Marui, Mr. Yoshihiro Yasutani, Ms. Marina Ide, Ms. Tomoyo Miyakai, Mr. Sho Yamanaka, Ms. Saya Yoshikawa and Ms. Yuko Fujiie as well as all members of the Seki laboratory for their kind support and creating a pleasant atmosphere.

The author also thanks Mr. Naoto Matsuyama, Mr. Takashi Tamaki, Mr. Yusuke Ano, Mr. Tsuneaki Sakurai, Mr. Satoru Tsukada, Mr. Akira Sugahara, Mr. Kazuhiro Ohtsuka, Mr. Yoshiharu Hirano, Mr. Hideaki Nakamura, Mr. Hiroyuki Taka, and Dr. Jaursap Boonmak as well as all my friends for their unwavering encouragements and support.

Finally, the author would like to express his thanks to his parents, Kenzo Baba and Ikuko Baba and his brothers, Tomoyuki Baba and Masayuki Baba for their understanding of this study, continuous encouragements, and supporting spiritually and financially.

Appendix

Fitting Program for Magnetic Susceptibility

axfit.f

```
C  ///  MAGNETIZATION OF ANISOTROPIC SPIN UNDER FIELD  ///
C       ( UNIAXIAL, POWDER, GAUSSIAN QUADRATURE, LAPACK )
C                              CODED BY M. NAKANO (1998)
C                              REVISED 2002 / 04 / 03

      PROGRAM AXFIT
      IMPLICIT DOUBLE PRECISION (A-H, O-Z)
      IMPLICIT INTEGER (I-N)
      PARAMETER (NPMAX = 6, NAPEXMAX = NPMAX + 1)
      PARAMETER (NAV = 16, NAV0 = 2 * NAV + 1)

C     --- SPIN MULTIPLICITY
      PARAMETER (MSPIN = 5)
      PARAMETER (LWORK  = 3030000)

      DIMENSION E0(MSPIN), LE(MSPIN), A(MSPIN, MSPIN), A0(MSPIN, MSPIN)
      DIMENSION XMU(MSPIN), ZMU(MSPIN), WORK(LWORK)
      DIMENSION BASIS(MSPIN)
      DIMENSION P(NPMAX), DP(NPMAX), ALPHA(NAV0), BETA(NAV0)
      DIMENSION Q(NAV0), Z(NAV0), W(NAV0)
      COMMON /STATE/ SPIN, ZSPIN
      COMMON /MAGDATA/ OMAG(300, 100), CMAG(300, 100), OMU(300, 100),
     &  CMU(300, 100), FIELD(100), TEMP(300, 100), NTEMP(100), NFIELD
      COMMON /PHYSCONST/ AVOGADRO, BOHR, BOLTZMANN, C0
      COMMON /HAMILTONIAN/ G, D, E, O40, O44, TIP
      COMMON /CRITERIA/ FTOL, OTOL
      COMMON /SUBSPACE/ IOPT(NPMAX), NOPT
      COMMON /REV_COMM/ SIMPLEX(NAPEXMAX, NPMAX), Y(NAPEXMAX),
     &        PR(NPMAX), PBAR(NPMAX), YNEW, YPR, YAV,
     &        INDEX(NAPEXMAX), ICOMM1, ICOMM2, ITER, IHI, INHI, ILO


      SPIN = (MSPIN - 1) / 2.0D0
      AVOGADRO = 6.0221415D23
      BOHR = 9.27400949D-24
      BOLTZMANN = 1.3806505D-23
      C0 = BOHR / BOLTZMANN
      FTOL = 1.0D-10
      IF (FTOL .LT. D1MACH(3)) FTOL = D1MACH(4)

      READ (*, *) G,    IOPT(1)
      READ (*, *) D,    IOPT(2)
      READ (*, *) E,    IOPT(3)
      READ (*, *) O40, IOPT(4)
      READ (*, *) O44, IOPT(5)
      READ (*, *) TIP, IOPT(6)
      READ (*, *) NFIELD
      DO IB = 1, NFIELD
        READ (*, *) FIELD(IB), NTEMP(IB)
        DO IT = 1, NTEMP(IB)
          READ (*, *) T, EFF
          TEMP(IT, IB) = T
C         --- conversion from mu_eff to M / N mu_B
          OMU(IT, IB)  = EFF
          OMAG(IT, IB) = C0 * FIELD(IB) * EFF * EFF / (3.0D0 * T)
C         OMU(IT, IB)  = SQRT (3.0D0 * EFF * T / (C0 * FIELD(IB)))
C         OMAG(IT, IB) = EFF
        ENDDO
      ENDDO
      NOPT = 0
      DO I = 1, NPMAX
        IF (IOPT(I) .NE. 0) THEN
          NOPT = NOPT + 1
          IOPT(NOPT) = I
        ENDIF
      ENDDO
      NAPEX = NOPT + 1
      DO I = 1, MSPIN
        BASIS(I) = (I - 1) - SPIN
      ENDDO

      CALL DRECUR (NAV0, 1, 0.0D0, 0.0D0, ALPHA, BETA, IERR)
      IF (IERR .GT. 0) PRINT *, 'DRECUR:IERR=', IERR
      CALL DGAUSS (NAV0, ALPHA, BETA, D1MACH(3), Z, W, IERR, Q)
      IF (IERR .GT. 0) PRINT *, 'DGAUSS:IERR=', IERR
      W(NAV + 1) = W(NAV + 1) / 2.0D0

      ICOMM1 = 0
      CALL SET_PARAMETER (P, 1)
      CALL PARAMETER_CONTROL (P)
      DO WHILE (ICOMM1 .GT. 0)
        CALL SET_PARAMETER (P, -1)
        CALL MATRIXCLEAR (A0, MSPIN)
        CALL D_TERM (D, A0, BASIS, MSPIN)
C       CALL E_TERM (E, A0, BASIS, MSPIN)
        CALL ORDER4 (O40, O44, A0, BASIS, MSPIN)
        DO IB = 1, NFIELD
          B = FIELD(IB)
          CDIA = 10.0D0 * TIP * B / (AVOGADRO * BOHR)
          DO IT = 1, NTEMP(IB)
            CMAG(IT, IB) = CDIA
          ENDDO
          DO ITHETA = 1, NAV + 1
            COS_T = Z(ITHETA)
            SIN_T = SQRT(1.0D0 - COS_T * COS_T)
            CALL COPYMATRIX (A0, A, MSPIN)
            CALL ZEEMAN_X (G, B * SIN_T, A, BASIS, MSPIN)
            CALL ZEEMAN_Z (G, B * COS_T, A, BASIS, MSPIN)

C           --- LAPACK diagonalization routine
            CALL DSYEV  ('V', 'U', MSPIN, A, MSPIN, E0, WORK, LWORK,
     &      INFO)
            IF (INFO .NE. 0)  PRINT *, 'INFO =', INFO
            CALL SORT (E0, LE, MSPIN, MSPIN)

            CALL MOMENT_X (XMU, A, BASIS, MSPIN)
            CALL MOMENT_Z (ZMU, A, BASIS, MSPIN)
            DO IT = 1, NTEMP(IB)
              T = TEMP(IT, IB)
              F = SIN_T * THERM_AV (T, E0, XMU, LE, MSPIN)
     &          + COS_T * THERM_AV (T, E0, ZMU, LE, MSPIN)
              CMAG(IT, IB) = CMAG(IT, IB) - G * F * W(ITHETA)
            ENDDO
          ENDDO
          DO IT = 1, NTEMP(IB)
            T = TEMP(IT, IB)
            CMU(IT, IB) = SQRT (3.0D0 * CMAG(IT, IB) * T / (C0 * B))
          ENDDO
        ENDDO
        YNEW = DEVIATION ()
        CALL PARAMETER_CONTROL (P)
      ENDDO

      PRINT *
      VX = 0.5D0 * SQRT (Y(ILO) / FTOL)
      DO J = 1, NOPT
        PMIN = SIMPLEX(1, J)
        PMAX = PMIN
        DO IAPEX = 2, NAPEX
          IF (PMIN .GT. SIMPLEX(IAPEX, J)) PMIN = SIMPLEX(IAPEX, J)
          IF (PMAX .LT. SIMPLEX(IAPEX, J)) PMAX = SIMPLEX(IAPEX, J)
        ENDDO
        DP(J) = VX * (PMAX - PMIN)
        P(J) = SIMPLEX(ILO, J)
      ENDDO
      CALL SET_PARAMETER (P, -1)

      PRINT *
      PRINT *, 'g         = ', G
      PRINT *, 'D   / kB = ', D, 'K'
      PRINT *, 'E   / kB = ', E, 'K'
      PRINT *, 'O40 / kB = ', O40, 'K'
      PRINT *, 'O44 / kB = ', O44, 'K'
      PRINT *, 'TIP       = ', TIP
      PRINT *
      PRINT *, 'DEV(final)   = ', Y(ILO)
      PRINT *
      DO J = 1, NOPT
        PRINT *, 'P(', J, ') = ', P(J), " +/- ", DP(J)
      ENDDO
```

```
      PRINT *
      PRINT *, '     B/T            T/K',
     &         '          mu_obs          mu_calc'
      DO IB = 1, NFIELD
        B = FIELD(IB)
        DO IT = 1, NTEMP(IB)
          T = TEMP(IT, IB)
          WRITE (*, 10) B, T, OMU(IT, IB), CMU(IT, IB)
        ENDDO
      ENDDO

      PRINT *
      PRINT *, '     B/T            T/K',
     &         '          M_obs           M_calc'
      DO IB = 1, NFIELD
        B = FIELD(IB)
        DO IT = 1, NTEMP(IB)
          T = TEMP(IT, IB)
          WRITE (*, 10) B, T, OMAG(IT, IB), CMAG(IT, IB)
        ENDDO
      ENDDO
   10 FORMAT(1X, 4E15.5)
      END



      DOUBLE PRECISION FUNCTION DEVIATION ()
      IMPLICIT DOUBLE PRECISION (A-H, O-Z)
      COMMON /MAGDATA/ OMAG(300, 100), CMAG(300, 100), OMU(300, 100),
     &  CMU(300, 100), FIELD(100), TEMP(300, 100), NTEMP(100), NFIELD
      N = 0
      SUM = 0.0D0
      W = 1.0D0
      DO IB = 1, NFIELD
        DO IT = 1, NTEMP(IB)
          N = N + 1
C         SUM = SUM + (OMAG(IT, IB) - CMAG(IT, IB)) ** 2.0D0
          SUM = SUM + W * (OMU(IT, IB) - CMU(IT, IB)) ** 2.0D0
C         SUM = SUM + (1.0D0 - OMU(IT, IB) / CMU(IT, IB)) ** 2.0D0
        ENDDO
      ENDDO
      DEVIATION = SQRT(SUM / (N - 1))
      END

      SUBROUTINE MATRIXCLEAR (A, N)
      DOUBLE PRECISION A(N, N)
      DO J = 1, N
      DO I = 1, N
        A(I, J) = 0.0D0
      ENDDO
      ENDDO
      END

      SUBROUTINE COPYMATRIX (A, B, N)
      DOUBLE PRECISION A(N, N), B(N, N)
      DO J = 1, N
      DO I = 1, N
        B(I, J) = A(I, J)
      ENDDO
      ENDDO
      END

      DOUBLE PRECISION FUNCTION UP ()
      IMPLICIT DOUBLE PRECISION (A-H, O-Z)
      COMMON /STATE/ SPIN, ZSPIN
      IF (ZSPIN .GE. SPIN) THEN
        UP = 0.0D0
      ELSE
        UP = SQRT((SPIN - ZSPIN) * (SPIN + ZSPIN + 1.0D0))
        ZSPIN = ZSPIN + 1.0D0
      ENDIF
      END

      DOUBLE PRECISION FUNCTION DOWN ()
      IMPLICIT DOUBLE PRECISION (A-H, O-Z)
      COMMON /STATE/ SPIN, ZSPIN
      IF (ZSPIN .LE. -SPIN) THEN
        DOWN = 0.0D0
      ELSE
        DOWN = SQRT((SPIN + ZSPIN) * (SPIN - ZSPIN + 1.0D0))
        ZSPIN = ZSPIN - 1.0D0
      ENDIF
      END

      INTEGER FUNCTION IROW ()
      IMPLICIT DOUBLE PRECISION (A-H, O-Z)
      COMMON /STATE/ SPIN, ZSPIN
      IROW = INT(SPIN + ZSPIN + 1.0D0)
      END

      SUBROUTINE D_TERM (D, A, BASIS, NSPIN)
      IMPLICIT DOUBLE PRECISION (A-H, O-Z)
      COMMON /STATE/ SPIN, ZSPIN
      DIMENSION A(NSPIN, NSPIN), BASIS(NSPIN)
      DO IBASIS = 1, NSPIN
        Z = BASIS(IBASIS)
        S = SPIN
        ELEMENT = D * (Z * Z - S * (S + 1.0D0) / 3.0D0)
        A(IBASIS, IBASIS) = A(IBASIS, IBASIS) + ELEMENT
      ENDDO
      END

      SUBROUTINE E_TERM (E, A, BASIS, NSPIN)
      IMPLICIT DOUBLE PRECISION (A-H, O-Z)
      COMMON /STATE/ SPIN, ZSPIN
      DIMENSION A(NSPIN, NSPIN), BASIS(NSPIN)
      DO IBASIS = 1, NSPIN
        ZSPIN = BASIS(IBASIS)
        ELEMENT = 0.5D0 * E
        ELEMENT = ELEMENT * UP ()
        ELEMENT = ELEMENT * UP ()
        IOFFD = IROW ()
        A(IOFFD, IBASIS) = A(IOFFD, IBASIS) + ELEMENT
      ENDDO
      DO IBASIS = 1, NSPIN
        ZSPIN = BASIS(IBASIS)
        ELEMENT = 0.5D0 * E
        ELEMENT = ELEMENT * DOWN ()
        ELEMENT = ELEMENT * DOWN ()
        IOFFD = IROW ()
        A(IOFFD, IBASIS) = A(IOFFD, IBASIS) + ELEMENT
      ENDDO
      END

      SUBROUTINE ORDER4 (O40, O44, A, BASIS, NSPIN)
C     --- O40 * (SZ)^4 + O44 * [ (S+)^4 + (S-)^4 ]
      IMPLICIT DOUBLE PRECISION(A-H, O-Z)
      COMMON /STATE/ SPIN, ZSPIN
      DIMENSION A(NSPIN, NSPIN), BASIS(NSPIN)
      DO IBASIS = 1, NSPIN
        ZSPIN = BASIS(IBASIS)
        ELEMENT = O40 * ZSPIN * ZSPIN * ZSPIN * ZSPIN
        A(IBASIS, IBASIS) = A(IBASIS, IBASIS) + ELEMENT
      ENDDO
      DO IBASIS = 1, NSPIN
        ZSPIN = BASIS(IBASIS)
        ELEMENT = O44
        ELEMENT = ELEMENT * UP ()
        ELEMENT = ELEMENT * UP ()
        ELEMENT = ELEMENT * UP ()
        ELEMENT = ELEMENT * UP ()
        IOFFD = IROW ()
        A(IOFFD, IBASIS) = A(IOFFD, IBASIS) + ELEMENT
      ENDDO
      DO IBASIS = 1, NSPIN
        ZSPIN = BASIS(IBASIS)
        ELEMENT = O44
        ELEMENT = ELEMENT * DOWN ()
```

```
  ELEMENT = ELEMENT * DOWN ()
  ELEMENT = ELEMENT * DOWN ()
  ELEMENT = ELEMENT * DOWN ()
  IOFFD = IROW ()
  A(IOFFD, IBASIS) = A(IOFFD, IBASIS) + ELEMENT
ENDDO
END

SUBROUTINE ZEEMAN_X (G, FIELD, A, BASIS, NSPIN)
IMPLICIT DOUBLE PRECISION (A-H, O-Z)
COMMON /STATE/ SPIN, ZSPIN
COMMON /PHYSCONST/ AVOGADRO, BOHR, BOLTZMANN, C0
DIMENSION A(NSPIN, NSPIN), BASIS(NSPIN)
DO IBASIS = 1, NSPIN
  ZSPIN = BASIS(IBASIS)
  ELEMENT = 0.5D0 * G * C0 * FIELD * UP ()
  IOFFD = IROW ()
  A(IOFFD, IBASIS) = A(IOFFD, IBASIS) + ELEMENT
ENDDO
DO IBASIS = 1, NSPIN
  ZSPIN = BASIS(IBASIS)
  ELEMENT = 0.5D0 * G * C0 * FIELD * DOWN ()
  IOFFD = IROW ()
  A(IOFFD, IBASIS) = A(IOFFD, IBASIS) + ELEMENT
ENDDO
END

SUBROUTINE ZEEMAN_Z (G, FIELD, A, BASIS, NSPIN)
IMPLICIT DOUBLE PRECISION (A-H, O-Z)
COMMON /PHYSCONST/ AVOGADRO, BOHR, BOLTZMANN, C0
DIMENSION A(NSPIN, NSPIN), BASIS(NSPIN)
DO IBASIS = 1, NSPIN
  ELEMENT = G * C0 * FIELD * BASIS(IBASIS)
  A(IBASIS, IBASIS) = A(IBASIS, IBASIS) + ELEMENT
ENDDO
END

SUBROUTINE MOMENT_X (XMU, V, BASIS, NSPIN)
IMPLICIT DOUBLE PRECISION (A-H, O-Z)
COMMON /STATE/ SPIN, ZSPIN
DIMENSION XMU(NSPIN), BASIS(NSPIN)
DIMENSION V(NSPIN, NSPIN)
DO IVEC = 1, NSPIN
  SUM = 0.0D0
  DO IBASIS = 1, NSPIN
    ZSPIN = BASIS(IBASIS)
    U1 = V(IBASIS, IVEC)
    P  = 0.5D0 * UP ()
    U2 = V(IROW (), IVEC)
    SUM = SUM + U2 * P * U1
  ENDDO
  DO IBASIS = 1, NSPIN
    ZSPIN = BASIS(IBASIS)
    U1 = V(IBASIS, IVEC)
    P  = 0.5D0 * DOWN ()
    U2 = V(IROW (), IVEC)
    SUM = SUM + U2 * P * U1
  ENDDO
  XMU(IVEC) = SUM
ENDDO
END

SUBROUTINE MOMENT_Z (ZMU, V, BASIS, NSPIN)
IMPLICIT DOUBLE PRECISION (A-H, O-Z)
DIMENSION ZMU(NSPIN), BASIS(NSPIN)
DIMENSION V(NSPIN, NSPIN)
DO IVEC = 1, NSPIN
  SUM = 0.0D0
  DO IBASIS = 1, NSPIN
    V2 = V(IBASIS, IVEC) * V(IBASIS, IVEC)
    SUM = SUM + V2 * BASIS(IBASIS)
  ENDDO
  ZMU(IVEC) = SUM
ENDDO
END
```

```
      SUBROUTINE SORT (E, IORDER, N, NMAX)
      IMPLICIT DOUBLE PRECISION (A-H, O-Z)
      DIMENSION E(NMAX), IORDER(NMAX)
      LOGICAL SORTED
      DO I = 1, N
        IORDER(I) = I
      ENDDO
      DO I = N + 1, NMAX
        IORDER(I) = 0
      ENDDO
      K = N
      SORTED = .FALSE.
      DO WHILE (.NOT. SORTED)
        IF (K .LE. 1) THEN
          SORTED = .TRUE.
        ELSE
          K = K - 1
          SORTED = .TRUE.
          DO I = 1, K
            IF (E(IORDER(I)) .LT. E(IORDER(I + 1))) THEN
              ITEMP = IORDER(I)
              IORDER(I) = IORDER(I + 1)
              IORDER(I + 1) = ITEMP
              SORTED = .FALSE.
            ENDIF
          ENDDO
        ENDIF
      ENDDO
C     EMIN = E(IORDER(N))
C     DO I = 1, N
C       E(I) = E(I) - EMIN
C       WRITE (*, 10) E(I)
C 10    FORMAT(1X, F15.5)
C     ENDDO
      END

      DOUBLE PRECISION FUNCTION THERM_AV (T, E, A, LE, N)
      IMPLICIT DOUBLE PRECISION (A-H, O-Z)
      DIMENSION E(N), A(N), LE(N)
      EMIN = E(LE(N))
      SUM1 = 0.0D0
      SUM2 = 0.0D0
      DO I = 1, N
        J = LE(I)
        BF = EXP(-(E(J) - EMIN) / T)
        SUM1 = SUM1 + A(J) * BF
        SUM2 = SUM2 + BF
      ENDDO
      THERM_AV = SUM1 / SUM2
      END

      SUBROUTINE SET_PARAMETER (P, IBACK)
      IMPLICIT DOUBLE PRECISION (A-H, O-Z)
      PARAMETER (NPMAX = 6, NAPEXMAX = NPMAX + 1)
      COMMON /HAMILTONIAN/ G, D, E, O40, O44, TIP
      COMMON /SUBSPACE/ IOPT(NPMAX), NOPT
      DIMENSION P(NPMAX)
      IF (IBACK .GT. 0) THEN
        DO I = 1, NOPT
          IF (IOPT(I) .EQ. 1) P(I) = G
          IF (IOPT(I) .EQ. 2) P(I) = D
          IF (IOPT(I) .EQ. 3) P(I) = E
          IF (IOPT(I) .EQ. 4) P(I) = O40
          IF (IOPT(I) .EQ. 5) P(I) = O44
          IF (IOPT(I) .EQ. 6) P(I) = TIP
        ENDDO
      ELSE
        DO I = 1, NOPT
          IF (IOPT(I) .EQ. 1) G   = P(I)
          IF (IOPT(I) .EQ. 2) D   = P(I)
          IF (IOPT(I) .EQ. 3) E   = P(I)
          IF (IOPT(I) .EQ. 4) O40 = P(I)
          IF (IOPT(I) .EQ. 5) O44 = P(I)
          IF (IOPT(I) .EQ. 6) TIP = P(I)
```

```
      ENDDO
    ENDIF
    END

    SUBROUTINE PARAMETER_CONTROL (P)
C   /// Nelder-Mead Downhill Simplex Method ///
C     ICOMM1 = 0: Start/Terminate Iteration
C     ICOMM1 = 1: Simplex Initialization
C     ICOMM1 = 2: Convergence Check & Simplex Reflection
C     ICOMM1 = 3: Simplex Expansion
C     ICOMM1 = 4: Simplex Contraction
C     ICOMM1 = 5: Simplex Shrinkage
C     ICOMM1 = 10: No Optimization
    IMPLICIT DOUBLE PRECISION (A-H, O-Z)
    PARAMETER (NPMAX = 6, NAPEXMAX = NPMAX + 1)
    PARAMETER (ITMAX = 2000)
    PARAMETER (ALPHA = 1.0D0, BETA = 0.25D0, GAMMA = 2.5D0)
    DIMENSION P(NPMAX), SG(NPMAX)
    COMMON /CRITERIA/ FTOL, OTOL
    COMMON /SUBSPACE/ IOPT(NPMAX), NOPT
    COMMON /REV_COMM/ SIMPLEX(NAPEXMAX, NPMAX), Y(NAPEXMAX),
   &        PR(NPMAX), PBAR(NPMAX), YNEW, YPR, YAV,
   &        INDEX(NAPEXMAX), ICOMM1, ICOMM2, ITER, IHI, INHI, ILO
    LOGICAL ORS
    ORS = .TRUE.
C   ORS = .FALSE.

    IF (NOPT .EQ. 0) THEN
      ICOMM1 = 10 - ICOMM1
      ILO = 1
      Y(ILO) = YNEW
      RETURN
    ELSE
      NAPEX = NOPT + 1
    ENDIF

    IF (ICOMM1 .EQ. 0) THEN
C   --- STAGE 0 ---
C       CLEAR COMMUNICATION FLAG &
C       SIMPLEX INITIALIZATION (1/2)
      ICOMM1 = 1
      ICOMM2 = 1
      ITER = 0
      IHI = 0
      INHI = 0
      ILO = 0
      DO J = 1, NOPT
        SIMPLEX(1, J) = P(J)
      ENDDO
      DELTA = 0.05D0
      DO IAPEX = 2, NAPEX
        DO J = 1, NOPT
          FACTOR = 1.0D0
          IF (IAPEX .EQ. J + 1) FACTOR = 1.0D0 - DELTA
          SIMPLEX(IAPEX, J) = SIMPLEX(1, J) * FACTOR
        ENDDO
      ENDDO

      DO J = 1, NOPT
        P(J) = SIMPLEX(ICOMM2, J)
      ENDDO
      RETURN
      ENDIF

      IF (ICOMM1 .EQ. 1) THEN
C     --- STAGE 1 ---
C         SIMPLEX INITIALIZATION (2/2)
      Y(ICOMM2) = YNEW
      IF (ICOMM2 .GE. NAPEX) THEN
        ICOMM1 = 2
        ICOMM2 = 0
        YAV = 1.0D+100
        CALL SIMPLEX_CHECK (SG, SGN2, VMIN, VMAX, INFOX, NOPT)
        IF (INFOX .EQ. 0) OTOL = 1.0D-6 * VMAX / SQRT(SGN2)
        PRINT *, 'SGN2 = ', SGN2
        PRINT *, 'VMAX = ', VMAX
        PRINT *, 'OTOL = ', OTOL
        PRINT *, 'SG   = ', (SG(J), J = 1, NOPT)
      ELSE
        ICOMM2 = ICOMM2 + 1
        DO J = 1, NOPT
          P(J) = SIMPLEX(ICOMM2, J)
        ENDDO
        RETURN
      ENDIF
      ENDIF

      IF (ICOMM1 .EQ. 3) THEN
C     --- STAGE 3 ---
C         SIMPLEX EXPANSION
      IF (ICOMM2 .EQ. 0) THEN
        YPR = YNEW
        ICOMM2 = 1
        IF (YPR .LE. Y(ILO)) THEN
          DO J = 1, NOPT
            P(J) = GAMMA * PR(J) + (1.0D0 - GAMMA) * PBAR(J)
          ENDDO
          RETURN
        ELSE
          ICOMM1 = 4
          ICOMM2 = 0
        ENDIF
      ELSE
        IF (YNEW .LT. YPR) THEN
          DO J = 1, NOPT
            SIMPLEX(IHI, J) = P(J)
          ENDDO
          Y(IHI) = YNEW
        ELSE
          DO J = 1, NOPT
            SIMPLEX(IHI, J) = PR(J)
          ENDDO
          Y(IHI) = YPR
        ENDIF
        ICOMM1 = 2
        ICOMM2 = 0
      ENDIF
      ENDIF

      IF (ICOMM1 .EQ. 4) THEN
C     --- STAGE 4 ---
C         SIMPLEX CONTRACTION
      IF (ICOMM2 .EQ. 0) THEN
        ICOMM2 = 1
        IF (YPR .GT. Y(INHI)) THEN
          IF (YPR .LT. Y(IHI)) THEN
            DO J = 1, NOPT
              SIMPLEX(IHI, J) = PR(J)
            ENDDO
            Y(IHI) = YPR
          ENDIF
          DO J = 1, NOPT
            P(J) = BETA * SIMPLEX(IHI, J) + (1.0D0 - BETA) * PBAR(J)
          ENDDO
          RETURN
        ELSE
          DO J = 1, NOPT
            SIMPLEX(IHI, J) = PR(J)
          ENDDO
          Y(IHI) = YPR
          ICOMM1 = 2
          ICOMM2 = 0
        ENDIF
      ELSE
        IF (YNEW .LT. Y(IHI)) THEN
          DO J = 1, NOPT
            SIMPLEX(IHI, J) = P(J)
          ENDDO
          Y(IHI) = YNEW
          ICOMM1 = 2
```

```
          ICOMM2 = 0
        ELSE
          ICOMM1 = 5
          ICOMM2 = 0
        ENDIF
      ENDIF
      ENDIF

      IF (ICOMM1 .EQ. 5) THEN
C     --- STAGE 5 ---
C         SIMPLEX SHRINKAGE
      IF (ICOMM2 .EQ. 0) THEN
        I = 0
        DO J = 1, NAPEX
          IF (J .NE. ILO) THEN
            I = I + 1
            INDEX(I) = J
          ENDIF
        ENDDO
        ICOMM2 = 1
        I = INDEX(ICOMM2)
        DO J = 1, NOPT
          P(J) = 0.5D0 * (SIMPLEX(I, J) + SIMPLEX(ILO, J))
          SIMPLEX(I, J) = P(J)
        ENDDO
        RETURN
      ELSE
        Y(INDEX(ICOMM2)) = YNEW
        IF (ICOMM2 .GE. NAPEX - 1) THEN
          ICOMM1 = 2
          ICOMM2 = 0
        ELSE
          ICOMM2 = ICOMM2 + 1
          I = INDEX(ICOMM2)
          DO J = 1, NOPT
            P(J) = 0.5D0 * (SIMPLEX(I, J) + SIMPLEX(ILO, J))
            SIMPLEX(I, J) = P(J)
          ENDDO
          RETURN
        ENDIF
      ENDIF
      ENDIF

      IF (ICOMM1 .EQ. 2) THEN
C     --- STAGE 2 ---
C         CONVERGENCE CHECK & REFLECTION
      CALL SIMPLEX_CHECK (SG, SGN2, VMIN, VMAX, INFOX, NOPT)
      IF ((INFOX .EQ. 0) .AND. ORS) THEN
      YAV0 = 0.0D0
      DO I = 1, NAPEX
        YAV0 = YAV0 + Y(I)
      ENDDO
      YAV0 = YAV0 / NAPEX
      IF (YAV - YAV0 .LE. OTOL * SGN2) THEN
C     --- SIMPLEX ORIENTED RESTART ---
        PRINT *, 'ORIENTED RESTART !'
        DO J = 1, NOPT
          P(J) = SIMPLEX(ILO, J)
        ENDDO
        Y(1) = Y(ILO)
        DO IAPEX = 1, NAPEX
        DO J = 1, NOPT
          SIMPLEX(IAPEX, J) = P(J)
        ENDDO
        ENDDO
        DO IAPEX = 2, NAPEX
          J = IAPEX - 1
          FACTOR = 0.5D0 * VMIN
          IF (SG(J) .NE. 0.0D0) THEN
            FACTOR = FACTOR * DSIGN(1.0D0, SG(J))
          ENDIF
          SIMPLEX(IAPEX, J) = SIMPLEX(IAPEX, J) + FACTOR
        ENDDO
        ICOMM1 = 1
        ICOMM2 = 2
          DO J = 1, NOPT
            P(J) = SIMPLEX(ICOMM2, J)
          ENDDO
          RETURN
        ELSE
          YAV = YAV0
        ENDIF
        ENDIF

        ILO = 1
        IF (Y(1) .GT. Y(2)) THEN
          IHI = 1
          INHI = 2
        ELSE
          IHI = 2
          INHI = 1
        ENDIF
        DO I = 1, NAPEX
          IF (Y(I) .LT. Y(ILO)) ILO = I
          IF (Y(I) .GT. Y(IHI)) THEN
            INHI = IHI
            IHI = I
          ELSE
            IF (Y(I) .GT. Y(INHI)) THEN
            IF (I .NE. IHI) INHI = I
            ENDIF
          ENDIF
        ENDDO
        RTOL = 2.0D0 * ABS(Y(IHI) - Y(ILO))
        RTOL = RTOL / (ABS(Y(IHI)) + ABS(Y(ILO)))
        WRITE (*, 10) ITER, Y(ILO), RTOL,
       &              (SIMPLEX(ILO, J), J = 1, NOPT)
     10 FORMAT (1X, I4, 10(1X, E10.4))

        IF (RTOL .LT. FTOL) THEN
          ICOMM1 = 0
          RETURN
        ENDIF
        IF (ITER .EQ. ITMAX) THEN
          PRINT *, 'Amoeba exceeding max iterations.'
C         DO J = 1, NOPT
C           PRINT *, 'P(', J, ') = ', SIMPLEX(ILO, J)
C         ENDDO
C         STOP
          ICOMM1 = 0
          RETURN
        ENDIF
        DO J = 1, NOPT
          PBAR(J) = 0.0D0
        ENDDO
        DO I = 1, NAPEX
          IF (I .NE. IHI) THEN
          DO J = 1, NOPT
            PBAR(J) = PBAR(J) + SIMPLEX(I, J)
          ENDDO
          ENDIF
        ENDDO
        DO J = 1, NOPT
          PBAR(J) = PBAR(J) / NOPT
        ENDDO
        ITER = ITER + 1
        DO J = 1, NOPT
          P(J) = (1.0D0 + ALPHA) * PBAR(J) - ALPHA * SIMPLEX(IHI, J)
          PR(J) = P(J)
        ENDDO
        ICOMM1 = 3
        ICOMM2 = 0
        RETURN
        ENDIF

        PRINT *, 'STACK IN PARAMETER_CONTROL !'
        STOP
        END

        SUBROUTINE SIMPLEX_CHECK (SG, SGN2, VMIN, VMAX, INFO, NOPT)
```

```
C     Evaluation of Simplex Gradient and Diameters
C       Ref. C. T. Kelly, SIAM J. Optim. 10(1), 43-55 (1999).
      IMPLICIT DOUBLE PRECISION (A-H, O-Z)
      PARAMETER (NPMAX = 6, NAPEXMAX = NPMAX + 1)
      COMMON /REV_COMM/ SIMPLEX(NAPEXMAX, NPMAX), Y(NAPEXMAX),
     &         PR(NPMAX), PBAR(NPMAX), YNEW, YPR, YAV,
     &         INDEX(NAPEXMAX), ICOMM1, ICOMM2, ITER, IHI, INHI, ILO
      DIMENSION SG(NPMAX)
      DIMENSION V(NOPT, NOPT), VF(NOPT, NOPT), VNORM(NOPT)
      DIMENSION SGRAD(NOPT), DELF(NOPT), WORK(4 * NOPT), IWORK(NOPT)
      DIMENSION IPIV(NOPT), BERR(NOPT), DUMMY1(NOPT), DUMMY2(NOPT)
      CHARACTER EQUED
      VMIN = 1.0D+100
      VMAX = 0.0D0
      IVEC = 0
      DO I = 1, NOPT + 1
        IF (I .NE. ILO) THEN
          IVEC = IVEC + 1
          VNORM(IVEC) = 0.0D0
          DO J = 1, NOPT
            V(J, IVEC) = SIMPLEX(I, J) - SIMPLEX(ILO, J)
            VNORM(IVEC) = VNORM(IVEC) + V(J, IVEC) * V(J, IVEC)
          ENDDO
          VNORM(IVEC) = SQRT(VNORM(IVEC))
          IF (VMIN .GT. VNORM(IVEC)) VMIN = VNORM(IVEC)
          IF (VMAX .LT. VNORM(IVEC)) VMAX = VNORM(IVEC)
          DELF(IVEC) = Y(I) - Y(ILO)
        ENDIF
      ENDDO
      RCOND = 0.0D0
      FERR  = 0.0D0
      INFO  = 0
      CALL DGESVX ('N', 'T', NOPT, 1, V, NOPT, VF, NOPT, IPIV, EQUED,
     &             DUMMY1, DUMMY2, DELF, NOPT, SGRAD, NOPT, RCOND,
     &             FERR, BERR, WORK, IWORK, INFO)
      IF (INFO .NE. 0) PRINT *, 'DGESVX INFO:', INFO
      SGN2 = 0.0D0
      DO J = 1, NOPT
        SG(J) = SGRAD(J)
        SGN2 = SGN2 + SG(J) * SG(J)
      ENDDO
C     PRINT *, '  GRAD:', SQRT(SGN2), RCOND, VMAX
      END




C     ------------------------------------------------------------------
C     Following routines are a part of ORTHPOL.
C     Ref. Walter Gautschi, ACM Transactions on Mathematical
C          Software, Vol.20, No.1, Pages 21-62 (1994).

      subroutine dlob(n,dalpha,dbeta,dleft,dright,dzero,dweigh,
     *ierr,de,da,db)
c
c This is a double-precision version of the routine  lob.
c
      double precision dleft,dright,depsma,dp0l,dp0r,dpll,dplr,dpmll,
     *dpmlr,ddet,dalpha(*),dbeta(*),dzero(*),dweigh(*),de(*),da(*),
     *db(*),dlmach
c
c The arrays  dalpha,dbeta,dzero,dweigh,de,da,db  are assumed to have
c dimension  n+2.
c
      depsma=dlmach(3)
c
c depsma is the machine double precision.
c
      npl=n+1
      np2=n+2
      do 10 k=1,np2
        da(k)=dalpha(k)
        db(k)=dbeta(k)
   10 continue
      dp0l=0.d0
      dp0r=0.d0
      dpll=1.d0
      dplr=1.d0
      do 20 k=1,npl
        dpmll=dp0l
        dp0l=dpll
        dpmlr=dp0r
        dp0r=dplr
        dpll=(dleft-da(k))*dp0l-db(k)*dpmll
        dplr=(dright-da(k))*dp0r-db(k)*dpmlr
   20 continue
      ddet=dpll*dp0r-dplr*dp0l
      da(np2)=(dleft*dpll*dp0r-dright*dplr*dp0l)/ddet
      db(np2)=(dright-dleft)*dpll*dplr/ddet
      call dgauss(np2,da,db,depsma,dzero,dweigh,ierr,de)
      return
      END


      subroutine dgauss(n,dalpha,dbeta,deps,dzero,dweigh,ierr,de)
c
c This is a double-precision version of the routine  gauss.
c
      double precision dalpha,dbeta,deps,dzero,dweigh,de,dp,dg,dr,
     *ds,dc,df,db
      dimension dalpha(n),dbeta(n),dzero(n),dweigh(n),de(n)
      if(n.lt.1) then
        ierr=-1
        return
      end if
      ierr=0
      dzero(1)=dalpha(1)
      if(dbeta(1).lt.0.d0) then
        ierr=-2
        return
      end if
      dweigh(1)=dbeta(1)
      if (n.eq.1) return
      dweigh(1)=1.d0
      de(n)=0.d0
      do 100 k=2,n
        dzero(k)=dalpha(k)
        if(dbeta(k).lt.0.d0) then
          ierr=-2
          return
        end if
        de(k-1)=dsqrt(dbeta(k))
        dweigh(k)=0.d0
  100 continue
      do 240 l=1,n
        j=0
  105   do 110 m=l,n
          if(m.eq.n) goto 120
          if(dabs(de(m)).le.deps*(dabs(dzero(m))+dabs(dzero(m+1))))
     *      goto 120
  110   continue
  120   dp=dzero(l)
        if(m.eq.l) goto 240
        if(j.eq.30) goto 400
        j=j+1
        dg=(dzero(l+1)-dp)/(2.d0*de(l))
        dr=dsqrt(dg*dg+1.d0)
        dg=dzero(m)-dp+de(l)/(dg+dsign(dr,dg))
        ds=1.d0
        dc=1.d0
        dp=0.d0
        mml=m-l
        do 200 ii=1,mml
          i=m-ii
          df=ds*de(i)
          db=dc*de(i)
          if(dabs(df).lt.dabs(dg)) goto 150
          dc=dg/df
          dr=dsqrt(dc*dc+1.d0)
```

```
        de(i+1)=df*dr
        ds=1.d0/dr
        dc=dc*ds
        goto 160
  150   ds=df/dg
        dr=dsqrt(ds*ds+1.d0)
        de(i+1)=dg*dr
        dc=1.d0/dr
        ds=ds*dc
  160   dg=dzero(i+1)-dp
        dr=(dzero(i)-dg)*ds+2.d0*dc*db
        dp=ds*dr
        dzero(i+1)=dg+dp
        dg=dc*dr-db
        df=dweigh(i+1)
        dweigh(i+1)=ds*dweigh(i)+dc*df
        dweigh(i)=dc*dweigh(i)-ds*df
  200   continue
        dzero(1)=dzero(1)-dp
        de(1)=dg
        de(m)=0.d0
        goto 105
  240 continue
      do 300 ii=2,n
        i=ii-1
        k=i
        dp=dzero(i)
        do 260 j=ii,n
          if(dzero(j).ge.dp) goto 260
          k=j
          dp=dzero(j)
  260   continue
        if(k.eq.i) goto 300
        dzero(k)=dzero(i)
        dzero(i)=dp
        dp=dweigh(i)
        dweigh(i)=dweigh(k)
        dweigh(k)=dp
  300 continue
      do 310 k=1,n
        dweigh(k)=dbeta(1)*dweigh(k)*dweigh(k)
  310 continue
      return
  400 ierr=1
      return
      END


      subroutine drecur(n,ipoly,dal,dbe,da,db,iderr)
c
c This is a double-precision version of the routine  recur.
c
      external dgamma
      double precision dal,dbe,da,db,dlmach,dlmach,dkm1,dalpbe,dt,
     *dlga,dal2,dbe2,dgamma
      dimension da(n),db(n)
      if(n.lt.1) then
        iderr=3
        return
      end if
      dlmach=dlog(dlmach(2))
      iderr=0
      do 10 k=1,n
        da(k)=0.d0
   10 continue
      if(ipoly.eq.1) then
        db(1)=2.d0
        if (n.eq.1) return
        do 20 k=2,n
          dkm1=dble(k-1)
          db(k)=1.d0/(4.d0-1.d0/(dkm1*dkm1))
   20   continue
        return
      else if(ipoly.eq.2) then
        da(1)=.5d0
        db(1)=1.d0
        if(n.eq.1) return
        do 30 k=2,n
          da(k)=.5d0
          dkm1=dble(k-1)
          db(k)=.25d0/(4.d0-1.d0/(dkm1*dkm1))
   30   continue
        return
      else if(ipoly.eq.3) then
        db(1)=4.d0*datan(1.d0)
        if(n.eq.1) return
        db(2)=.5d0
        if(n.eq.2) return
        do 40 k=3,n
          db(k)=.25d0
   40   continue
        return
      else if(ipoly.eq.4) then
        db(1)=2.d0*datan(1.d0)
        if(n.eq.1) return
        do 50 k=2,n
          db(k)=.25d0
   50   continue
        return
      else if(ipoly.eq.5) then
        db(1)=4.d0*datan(1.d0)
        da(1)=.5d0
        if(n.eq.1) return
        do 60 k=2,n
          db(k)=.25d0
   60   continue
        return
      else if(ipoly.eq.6) then
        if(dal.le.-1.d0 .or. dbe.le.-1.d0) then
          iderr=1
          return
        else
          dalpbe=dal+dbe
          da(1)=(dbe-dal)/(dalpbe+2.d0)
          dt=(dalpbe+1.d0)*dlog(2.d0)+dlga(dal+1.d0)+dlga(dbe+1.d0)-
     *      dlga(dalpbe+2.d0)
          if(dt.gt.dlmach) then
            iderr=2
            db(1)=dlmach(2)
          else
            db(1)=dexp(dt)
          end if
          if(n.eq.1) return
          dal2=dal*dal
          dbe2=dbe*dbe
          da(2)=(dbe2-dal2)/((dalpbe+2.d0)*(dalpbe+4.d0))
          db(2)=4.d0*(dal+1.d0)*(dbe+1.d0)/((dalpbe+3.d0)*(dalpbe+
     *      2.d0)**2)
          if(n.eq.2) return
          do 70 k=3,n
            dkm1=dble(k-1)
            da(k)=.25d0*(dbe2-dal2)/(dkm1*dkm1*(1.d0+.5d0*dalpbe/dkm1)
     *        *(1.d0+.5d0*(dalpbe+2.d0)/dkm1))
            db(k)=.25d0*(1.d0+dal/dkm1)*(1.d0+dbe/dkm1)*(1.d0+dalpbe/
     *        dkm1)/((1.d0+.5d0*(dalpbe+1.d0)/dkm1)*(1.d0+.5d0*(dalpbe
     *      -1.d0)/dkm1)*(1.d0+.5d0*dalpbe/dkm1)**2)
   70     continue
          return
        end if
      else if(ipoly.eq.7) then
        if(dal.le.-1.d0) then
          iderr=1
          return
        else
          da(1)=dal+1.d0
          db(1)=dgamma(dal+1.d0,iderr)
          if(iderr.eq.2) db(1)=dlmach(2)
          if(n.eq.1) return
          do 80 k=2,n
            dkm1=dble(k-1)
```

```
            da(k)=2.d0*dkm1+dal+1.d0
            db(k)=dkm1*(dkm1+dal)
   80     continue
          return
        end if
      else if(ipoly.eq.8) then
        db(1)=dsqrt(4.d0*datan(1.d0))
        if(n.eq.1) return
        do 90 k=2,n
          db(k)=.5d0*dble(k-1)
   90   continue
        return
      else
        iderr=4
      end if
      RETURN
      END

      double precision function dlga(dx)
      double precision dbnum,dbden,dx,dlmach,dc,dp,dy,dt,ds
      dimension dbnum(8),dbden(8)
c
c This routine evaluates the logarithm of the gamma function by a
c combination of recurrence and asymptotic approximation.
c
c The entries in the next data statement are the numerators and
c denominators, respectively, of the quantities B[16]/(16*15),
c B[14]/(14*13),..., B[2]/(2*1), where B[2n] are the Bernoulli
c numbers.
c
      data dbnum/-3.617d3,1.d0,-6.91d2,1.d0,-1.d0,1.d0,-1.d0,1.d0/,
     *     dbden/1.224d5,1.56d2,3.6036d5,1.188d3,1.68d3,1.26d3,3.6d2,
     *1.2d1/
c
c The quantity  dprec  in the next statement is the number of decimal
c digits carried in double-precision floating-point arithmetic.
c
      dprec=-alog10(sngl(dlmach(3)))
      dc=.5d0*dlog(8.d0*datan(1.d0))
      dp=1.d0
      dy=dx
      y=sngl(dy)
c
c The quantity  y0  below is the threshold value beyond which asymptotic
c evaluation gives sufficient accuracy; see Eq. 6.1.42 in M. Abramowitz
c and I.A. Stegun,Handbook of Mathematical Functions''. The constants
c are .12118868... = ln(10)/19 and .05390522... = ln(|B[20]|/190)/19.
c
      y0=exp(.121189*dprec+.053905)
   10 if(y.gt.y0) goto 20
      dp=dy*dp
      dy=dy+1.d0
      y=sngl(dy)
      goto 10
   20 dt=1.d0/(dy*dy)
c
c The right-hand side of the next assignment statement is B[18]/(18*17).
c
      ds=4.3867d4/2.44188d5
      do 30 i=1,8
        ds=dt*ds+dbnum(i)/dbden(i)
   30 continue
      dlga=(dy-.5d0)*dlog(dy)-dy+dc+ds/dy-dlog(dp)
      return
      END


      double precision function dgamma(dx,iderr)
c
c This evaluates the gamma function for real positive  dx, using the
c function subroutine  dlga.
c
      double precision dx,dlmach,dlmach,dt,dlga
      dlmach=dlog(dlmach(2))
      iderr=0
      dt=dlga(dx)
      if(dt.ge.dlmach) then
        iderr=2
        dgamma=dlmach(2)
        return
      else
        dgamma=dexp(dt)
        return
      end if
      RETURN
      END

      DOUBLE PRECISION FUNCTION D1MACH(I)
      INTEGER I
C
C  DOUBLE-PRECISION MACHINE CONSTANTS
C  D1MACH( 1) = B**(EMIN-1), THE SMALLEST POSITIVE MAGNITUDE.
C  D1MACH( 2) = B**EMAX*(1 - B**(-T)), THE LARGEST MAGNITUDE.
C  D1MACH( 3) = B**(-T), THE SMALLEST RELATIVE SPACING.
C  D1MACH( 4) = B**(1-T), THE LARGEST RELATIVE SPACING.
C  D1MACH( 5) = LOG10(B)
C
      INTEGER SMALL(2)
      INTEGER LARGE(2)
      INTEGER RIGHT(2)
      INTEGER DIVER(2)
      INTEGER LOG10(2)
      INTEGER SC, CRAY1(38), J
      COMMON /D9MACH/ CRAY1
      SAVE SMALL, LARGE, RIGHT, DIVER, LOG10, SC
      DOUBLE PRECISION DMACH(5)
      EQUIVALENCE (DMACH(1),SMALL(1))
      EQUIVALENCE (DMACH(2),LARGE(1))
      EQUIVALENCE (DMACH(3),RIGHT(1))
      EQUIVALENCE (DMACH(4),DIVER(1))
      EQUIVALENCE (DMACH(5),LOG10(1))
C  THIS VERSION ADAPTS AUTOMATICALLY TO MOST CURRENT MACHINES.
C  R1MACH CAN HANDLE AUTO-DOUBLE COMPILING, BUT THIS VERSION OF
C  D1MACH DOES NOT, BECAUSE WE DO NOT HAVE QUAD CONSTANTS FOR
C  MANY MACHINES YET.
C  TO COMPILE ON OLDER MACHINES, ADD A C IN COLUMN 1
C  ON THE NEXT LINE
      DATA SC/0/
C  AND REMOVE THE C FROM COLUMN 1 IN ONE OF THE SECTIONS BELOW.
C  CONSTANTS FOR EVEN OLDER MACHINES CAN BE OBTAINED BY
C          mail netlib@research.bell-labs.com
C          send oldlmach from blas
C  PLEASE SEND CORRECTIONS TO dmg OR ehg@bell-labs.com.
C
C     MACHINE CONSTANTS FOR THE HONEYWELL DPS 8/70 SERIES.
C      DATA SMALL(1),SMALL(2) / O402400000000, O000000000000 /
C      DATA LARGE(1),LARGE(2) / O376777777777, O777777777777 /
C      DATA RIGHT(1),RIGHT(2) / O604400000000, O000000000000 /
C      DATA DIVER(1),DIVER(2) / O606400000000, O000000000000 /
C      DATA LOG10(1),LOG10(2) / O776464202324, O117571775714 /, SC/987/
C
C     MACHINE CONSTANTS FOR PDP-11 FORTRANS SUPPORTING
C     32-BIT INTEGERS.
C      DATA SMALL(1),SMALL(2) /    8388608,           0 /
C      DATA LARGE(1),LARGE(2) / 2147483647,          -1 /
C      DATA RIGHT(1),RIGHT(2) /  612368384,           0 /
C      DATA DIVER(1),DIVER(2) /  620756992,           0 /
C      DATA LOG10(1),LOG10(2) / 1067065498, -2063872008 /, SC/987/
C
C     MACHINE CONSTANTS FOR THE UNIVAC 1100 SERIES.
C      DATA SMALL(1),SMALL(2) / O000040000000, O000000000000 /
C      DATA LARGE(1),LARGE(2) / O377777777777, O777777777777 /
C      DATA RIGHT(1),RIGHT(2) / O170540000000, O000000000000 /
C      DATA DIVER(1),DIVER(2) / O170640000000, O000000000000 /
C      DATA LOG10(1),LOG10(2) / O177746420232, O411757177572 /, SC/987/
C
C     ON FIRST CALL, IF NO DATA UNCOMMENTED, TEST MACHINE TYPES.
      IF (SC .NE. 987) THEN
         DMACH(1) = 1.D13
         IF (      SMALL(1) .EQ. 1117925532
```

```
*       .AND. SMALL(2) .EQ. -448790528) THEN
*          *** IEEE BIG ENDIAN ***
           SMALL(1) = 1048576
           SMALL(2) = 0
           LARGE(1) = 2146435071
           LARGE(2) = -1
           RIGHT(1) = 1017118720
           RIGHT(2) = 0
           DIVER(1) = 1018167296
           DIVER(2) = 0
           LOG10(1) = 1070810131
           LOG10(2) = 1352628735
        ELSE IF ( SMALL(2) .EQ. 1117925532
*       .AND. SMALL(1) .EQ. -448790528) THEN
*          *** IEEE LITTLE ENDIAN ***
           SMALL(2) = 1048576
           SMALL(1) = 0
           LARGE(2) = 2146435071
           LARGE(1) = -1
           RIGHT(2) = 1017118720
           RIGHT(1) = 0
           DIVER(2) = 1018167296
           DIVER(1) = 0
           LOG10(2) = 1070810131
           LOG10(1) = 1352628735
        ELSE IF ( SMALL(1) .EQ. -2065213935
*       .AND. SMALL(2) .EQ. 10752) THEN
*             *** VAX WITH D_FLOATING ***
           SMALL(1) = 128
           SMALL(2) = 0
           LARGE(1) = -32769
           LARGE(2) = -1
           RIGHT(1) = 9344
           RIGHT(2) = 0
           DIVER(1) = 9472
           DIVER(2) = 0
           LOG10(1) = 546979738
           LOG10(2) = -805796613
        ELSE IF ( SMALL(1) .EQ. 1267827943
*       .AND. SMALL(2) .EQ. 704643072) THEN
*             *** IBM MAINFRAME ***
           SMALL(1) = 1048576
           SMALL(2) = 0
           LARGE(1) = 2147483647
           LARGE(2) = -1
           RIGHT(1) = 856686592
           RIGHT(2) = 0
           DIVER(1) = 873463808
           DIVER(2) = 0
           LOG10(1) = 1091781651
           LOG10(2) = 1352628735
        ELSE IF ( SMALL(1) .EQ. 1120022684
*       .AND. SMALL(2) .EQ. -448790528) THEN
*          *** CONVEX C-1 ***
           SMALL(1) = 1048576
           SMALL(2) = 0
           LARGE(1) = 2147483647
           LARGE(2) = -1
           RIGHT(1) = 1019215872
           RIGHT(2) = 0
           DIVER(1) = 1020264448
           DIVER(2) = 0
           LOG10(1) = 1072907283
           LOG10(2) = 1352628735
        ELSE IF ( SMALL(1) .EQ. 815547074
*       .AND. SMALL(2) .EQ. 58688) THEN
*          *** VAX G-FLOATING ***
           SMALL(1) = 16
           SMALL(2) = 0
           LARGE(1) = -32769
           LARGE(2) = -1
           RIGHT(1) = 15552
           RIGHT(2) = 0
           DIVER(1) = 15568
           DIVER(2) = 0
           LOG10(1) = 1142112243
           LOG10(2) = 2046775455
        ELSE
           DMACH(2) = 1.D27 + 1
           DMACH(3) = 1.D27
           LARGE(2) = LARGE(2) - RIGHT(2)
           IF (LARGE(2) .EQ. 64 .AND. SMALL(2) .EQ. 0) THEN
              CRAY1(1) = 67291416
              DO 10 J = 1, 20
                 CRAY1(J+1) = CRAY1(J) + CRAY1(J)
10            CONTINUE
              CRAY1(22) = CRAY1(21) + 321322
              DO 20 J = 22, 37
                 CRAY1(J+1) = CRAY1(J) + CRAY1(J)
20            CONTINUE
              IF (CRAY1(38) .EQ. SMALL(1)) THEN
*                *** CRAY ***
                 CALL I1MCRY(SMALL(1), J, 8285, 8388608, 0)
                 SMALL(2) = 0
                 CALL I1MCRY(LARGE(1), J, 24574, 16777215, 16777215)
                 CALL I1MCRY(LARGE(2), J, 0, 16777215, 16777214)
                 CALL I1MCRY(RIGHT(1), J, 16291, 8388608, 0)
                 RIGHT(2) = 0
                 CALL I1MCRY(DIVER(1), J, 16292, 8388608, 0)
                 DIVER(2) = 0
                 CALL I1MCRY(LOG10(1), J, 16383, 10100890, 8715215)
                 CALL I1MCRY(LOG10(2), J, 0, 16226447, 9001388)
              ELSE
                 WRITE(*,9000)
                 STOP 779
                 END IF
           ELSE
              WRITE(*,9000)
              STOP 779
              END IF
           END IF
        SC = 987
        END IF
*    SANITY CHECK
      IF (DMACH(4) .GE. 1.0D0) STOP 778
      IF (I .LT. 1 .OR. I .GT. 5) THEN
         WRITE(*,*) 'D1MACH(I): I =',I,' is out of bounds.'
         STOP
         END IF
      D1MACH = DMACH(I)
      RETURN
 9000 FORMAT(/' Adjust D1MACH by uncommenting data statements'/
     *' appropriate for your machine.')
* /* Standard C source for D1MACH -- remove the * in column 1 */
*#include <stdio.h>
*#include <float.h>
*#include <math.h>
*double d1mach_(long *i)
*{
*       switch(*i){
*         case 1: return DBL_MIN;
*         case 2: return DBL_MAX;
*         case 3: return DBL_EPSILON/FLT_RADIX;
*         case 4: return DBL_EPSILON;
*         case 5: return log10(FLT_RADIX);
*         }
*       fprintf(stderr, "invalid argument: d1mach(%ld)\n", *i);
*       exit(1); return 0; /* some compilers demand return values */
*}
*     RETURN
      END
      SUBROUTINE I1MCRY(A, A1, B, C, D)
**** SPECIAL COMPUTATION FOR OLD CRAY MACHINES ****
      INTEGER A, A1, B, C, D
      A1 = 16777216*B + C
      A = 16777216*A1 + D
      RETURN
      END
```